1975

The synthesis and characterization of metal-metal bonded dimers of tantalum and tungsten

Joseph Leslie Templeton
Iowa State University

The synthesis and characterization of metal-metal bonded dimers of tantalum and tungsten

by

Joseph Leslie Templeton

A Dissertation Submitted to the
Graduate Faculty in Partial Fulfillment of
The Requirements for the Degree of
DOCTOR OF PHILOSOPHY

Department: Chemistry
Major: Inorganic Chemistry

Approved:

Signature was redacted for privacy.

In Charge of Major Work

Signature was redacted for privacy.

For the Major Department

Signature was redacted for privacy.

For the Graduate College

Iowa State University
Ames, Iowa

1975

TABLE OF CONTENTS

	Page
INTRODUCTION	1
PART I. SYNTHESIS AND CHARACTERIZATION OF $Ta_2X_6(SC_4H_8)_3$ (X = Cl, Br)	9
REVIEW OF RELATED WORK	10
Reduction of Niobium(V) in Aqueous Solution	10
Descriptive Chemistry of Tantalum(IV)	11
Niobium(III) and Tantalum(III)	19
Hexanuclear Tantalum Clusters	23
Organometallic Tantalum(III)	25
$Nb_2X_6(SC_4H_8)_3$, (X = Cl, Br, I)	28
EXPERIMENTAL	30
Materials	30
Analytical Procedures	31
Synthesis	32
Physical Measurements	37
RESULTS AND DISCUSSION	42
Synthesis	42
Proton Magnetic Resonance	46
Magnetic Susceptibility	54
Electronic Spectra	57
Nuclear Quadrupole Resonance	61
Infrared Spectra	70
X-ray Structural Determination of $Ta_2Br_6(SC_4H_8)_3$	75

	Page
PART II. SYNTHESIS AND CHARACTERIZATION OF $[(CH_3CH_2CH_2)_4N]_2[W_2Br_9]$	107
REVIEW OF RELATED WORK	108
A Brief Overview of the Descriptive Chemistry of Tungsten	108
Group VI $M_2X_9^{n-}$ Anions	110
Group VI Metal Carbonyl Halide Reactants	119
EXPERIMENTAL	126
Materials	126
Analytical Procedures	127
Synthesis	128
Physical Measurements	131
RESULTS AND DISCUSSION	136
Synthesis	136
X-ray Powder Pattern Data	144
Temperature Dependent Magnetic Susceptibility Measurements	144
Electronic Spectrum	148
Infrared Spectra	150
X-ray Structural Determination of $[(n\text{-}C_3H_7)_4N]_2[W_2Br_9]$	153
SUMMARY	182
BIBLIOGRAPHY	185
APPENDIX	193

LIST OF TABLES

		Page
Table 1.	Proton magnetic resonance data for $Ta_2X_6(SC_4H_8)_3$	55
Table 2.	Magnetic susceptibility data	56
Table 3.	Electronic absorption band parameters	58
Table 4.	Nuclear quadrupole resonance data for $Ta_2Cl_6(SC_4H_8)_3$ and $Ta_2Br_6(SC_4H_8)_3$	64
Table 5.	Comparison of halogen nqr frequencies in Ta(III) and Ta(V) compounds	69
Table 6.	Tetrahydrothiophene infrared frequencies (700-1400 cm^{-1})	71
Table 7.	Low frequency infrared data for $Ta_2Cl_6(SC_4H_8)_3$ and $Ta_2Br_6(SC_4H_8)_3$ (100-700 cm^{-1})	73
Table 8.	Bond distances in $Ta_2Br_6(SC_4H_8)_3$, Å	80
Table 9.	Nonbonded distances in $Ta_2Br_6(SC_4H_8)_3$, Å	81
Table 10.	Angles (degrees) within $Ta_2Br_6(SC_4H_8)_3$	82
Table 11.	X-ray powder pattern data for $[(n\text{-}C_3H_7)_4N]_2[W_2Br_9]$	145
Table 12.	Electronic absorption band parameters for $[(n\text{-}C_3H_7)_4N]_2[W_2Br_9]$	149
Table 13.	Tetrapropylammonium infrared frequencies (700-1400 cm^{-1})	149
Table 14.	Low frequency metal-halogen vibrations in $M_2X_9^{n-}$ anions	151
Table 15.	Bond distances in $W_2Br_9^{2-}$, Å	161
Table 16.	Nonbonded distances in $W_2Br_9^{2-}$, Å	161
Table 17.	Angles (degrees) within $W_2Br_9^{2-}$	162
Table 18.	Selected confacial bioctahedral structural comparisons	163

Table 19.	Final positional parameters for $Ta_2Br_6(SC_4H_8)_3$	194
Table 20.	Final thermal parameters ($x10^4$) for $Ta_2Br_6(SC_4H_8)_3$	195
Table 21.	Observed and calculated structure factors for $Ta_2Br_6(SC_4H_8)_3$	196
Table 22.	Bond distances in the tetrapropylammonium cations of $[(n\text{-}C_3H_7)_4N]_2[W_2Br_9]$, Å	199
Table 23.	Final positional parameters for $[(n\text{-}C_3H_7)_4N]_2[W_2Br_9]$	200
Table 24.	Final thermal parameters ($x10^3$) for $[(n\text{-}C_3H_7)_4N]_2[W_2Br_9]$	202
Table 25.	Observed and calculated structure factors for $[(n\text{-}C_3H_7)_4N]_2[W_2Br_9]$	204

LIST OF FIGURES

		Page
Figure 1.	Modified reaction vessel for preparing $Ta_2X_6(SC_4H_8)_3$	36
Figure 2.	^1H nmr spectrum of SC_4H_8 in benzene solution	47
Figure 3.	^1H nmr spectrum of a saturated solution of $Ta_2Cl_6(SC_4H_8)_3$ in benzene	49
Figure 4.	^1H nmr spectrum of a saturated solution of $Nb_2Cl_6(SC_4H_8)_3$ in benzene	53
Figure 5.	A perspective view of the 50% probability thermal ellipsoids of the $Ta_2Br_6(SC_4H_8)_3$ molecular unit	79
Figure 6.	A general illustration of the confacial bioctahedral parameters d', d", α', and β	85
Figure 7.	A molecular orbital diagram for an octahedral complex in which the ligands have no significant π interaction with the metal	91
Figure 8.	D_{3h} symmetry coordinates for a confacial bioctahedron	94
Figure 9.	A molecular orbital diagram for a confacial bioctahedron of D_{3h} symmetry	95
Figure 10.	Metal-metal molecular orbital overlap diagram for a confacial bioctahedron of D_{3h} symmetry	98
Figure 11.	C_{2v} symmetry coordinates for a confacial bioctahedron such as $Ta_2Br_6(SC_4H_8)_3$	101
Figure 12.	Bridging atom triangle parameters for $Ta_2Br_5(SC_4H_8)_3$ and relative positions of important d-orbital lobes	105
Figure 13.	Schlenk reaction vessel and gas collection cylinder for preparing $[(n\text{-}C_3H_7)_4N]_2[W_2Br_9]$	130
Figure 14.	Curie plot (χ_M vs 1/T) for $[(n\text{-}C_3H_7)_4N]_2[W_2Br_9]$	147
Figure 15.	A perspective view of the 50% probability thermal ellipsoids of the $W_2Br_9^{2-}$ anion	159

Figure 16. A perspective view of the 33% probability thermal ellipsoids of the two independent $[(n\text{-}C_3H_7)_4N]^+$ cations 160

Figure 17. Schematic diagram of the canted terminal ligand planes in $W_2Br_9^{2-}$ 171

Figure 18. Metal orbital rotation proposed to influence the energy of the metal-metal π-bonds 173

Figure 19. Schematic diagram of nonbonded distances in $W_2Br_9^{2-}$ which identify $Br_{br}(8)$ as unique 177

Figure 20. Orbital motion of a metal d-orbital upon rotation by an angle of $\Delta\theta$ 180

INTRODUCTION

Recent research activity in the field of metal-metal bonded compounds has led to the realization that this is an area ripening toward the fruition of systematic approaches to the preparation and understanding of such systems. Several excellent reviews have been published dealing with the phenomenon of metal-metal bonding (1,2,3). The term metal as used here is intended to refer only to the transition metal portion of the periodic table. The relatively recent increase in the number of discrete metal clusters isolated, where cluster connotes a molecular species containing two or more metal atoms, has transformed an inorganic curiosity into a viable chemical concept. The preparation and characterization of metal clusters, while historically limited in scope, has become extensive enough during the past two decades to warrant considerable confidence in further expansion of the area with regard to the discovery of new metal cluster species and improved synthetic routes to currently existing metal-metal bonded compounds.

Interest in the research project chosen for investigation focused on metal halide clusters, while systems involving metal-metal bonding in oxides, carboxylates, carbonyls and organometallics were not incorporated into the plans and goals. The research reported here was designed to add further information to the extant data regarding metal clusters; more specifically emphasizing dimeric units which serve as the simplest case for

study and understanding of the attractive interaction between two metal atoms.

Since the research performed relates exclusively to metal-metal bonds it would be appropriate to define a bonding criterion for such interactions. A rigorous definition is elusive, but there are several factors which are considered to be germane and these are discussed below.

The advent of widespread computer accessibility has enabled many researchers to utilize x-ray diffraction techniques to unravel the exact structural details of various metal cluster compounds. This is doubtless the most powerful yet also the most demanding tool available for amassing accurate data pertaining to the compounds of interest. Not only is the distance between metal atoms a guide to the extent and type of interaction present, but also considerable insight can be gained by examining the structural distortions resulting from either attraction or repulsion of the metal atoms for one another. Generally the distance of closest approach in the metal itself serves as an estimate of the maximum separation consistent with a metal-metal attraction. The correlation between bond length and bond order is not always unequivocal, but typically the metal-metal distance is more responsive to environmental changes when the bond order is low and varies less with chemical changes as the bond order increases. It is clear that x-ray structural determinations will play an integral part in the characterization of species purported to

contain metal-metal bonds.

Magnetic properties can furnish significant information related to the presence or absence of metal-metal interactions. As an example one could consider the case of an even electron metal cluster species which exhibits diamagnetic behavior or temperature independent paramagnetism as a result of strong metal-metal bonding. Paramagnetism in the same material, on the other hand, could be interpreted as indicative of no constructive d orbital overlap between metal atoms and hence no net attraction. Exchange interactions through bridging ligands can cause antiferromagnetic behavior and low magnetic moments are difficult to interpret since large spin-orbit coupling constants may lead to such results for monomers. Disregarding the difficulties of generalizing the interpretation of magnetic data, it remains true that magnetic studies can be very effectively applied to discerning the electronic status of particular individual cases.

Analytical data can sometimes lead to a nonstoichiometric composition and the dilemma of nonintegral units within the simple formula is most easily resolved by considering multiples of the basic unit. Such a result suggests that more than one metal atom is present in the molecular unit although no evidence is obtained relating to the forces holding the metal atoms together. In other words, bridging ligands may cause several metal atoms to reside in the same unit even though no

metal-metal attraction exists. Alternatively one could envision a cation-anion pair in which both ions contain a metal atom or atoms yet the only attractive force between them is the ionic force as a result of the overall charge. Such stoichiometric data is helpful in guiding one to an early decision as to whether a specific product should be abandoned or investigated further in hopes of isolating a species containing multiple metal atoms.

One can also list the existence and persistence of a multiple metal segment throughout substitution and oxidation-reduction reactions as another metal-metal bond criterion. All of the above criteria have been applied to clusters at one time or another by various investigators and the concepts represented in the above discussions will serve as a basis for considering the metal-metal interactions in the two new dimeric compounds isolated and described during the course of this work.

The physical description of a new compound must by necessity be preceded by the successful synthetic route chosen to prepare the desired product. The common characteristics of related systems which have been studied previously must be pondered and conditions optimizing the production of such properties should be employed in the synthetic approach selected. A brief review of traits shared by the majority of metal clusters is therefore appropriate background material.

The transition metals most prone to form metal-metal bonds are located in the lower left portion of the transition metal series; particularly noteworthy are the following elements:

Nb Mo

Ta W Re

The propensity for forming metal clusters displayed by these elements may be attributed to two basic trends leading to this corner of the periodic chart.

Sheldon (4) has noted the orbital size factor as an important component of metal-metal bonding. It is credible to cite the lack of metal-metal bonding among the elements of the first transition series as due to the small size of the 3d orbitals available for overlap. The larger atoms of the second and third series are capable of greater orbital overlap and this results in greater stability for homonuclear bonded compounds of these elements. Another factor influencing orbital size is the effective charge located on the metal nucleus and inner electron shells. As one proceeds across the periodic chart from left to right the orbitals contract slightly due to the increased charge associated with the addition of more protons at the nucleus while the added charge is not completely screened by the accompanying outer shell electrons.

Low oxidation states are prevalent among metal clusters and this provides for greater orbital expansion than high oxidation states common to many heavy metals where more polar

metal-halogen bonds contract the orbitals inward. Oxidation states of 2+ and 3+ are typical of many heavy metal clusters, but even such low formal valencies fail to form metal clusters within the 3d series with any facility. One discussion of the thermodynamics of low oxidation state metal-halides has led to the conclusion that the highly unfavorable energy of sublimation required for the metals of interest dictates that some attractive metal-metal force be retained in order that the overall reaction is thermodynamically favorable (5). A further condition favoring the left section of the series is that the metal atom involved must be electron deficient. If metal orbitals are to interact and lower the energy of the system the number of electrons available for filling the resulting bonding orbitals must be greater than the number of electrons which will be placed in antibonding orbitals. Thus the total number of electrons involved in metal-metal molecular orbitals would optimally equal the number of atomic orbitals contributing to effective overlap, as then two electrons per orbital would occupy only the bonding molecular orbitals. If both metal atoms are electron-rich the resulting molecular configuration will have filled antibonding orbitals and destabilize the metal-metal interaction. Thus it is reasonable that metal configurations of five d-electrons or less are found in metal clusters to the exclusion of higher electron configurations. Steric requirements are also eased for low oxidation state

metals of the second and third series. The larger metals to the left of the chart can support more ligands and metal-metal bonds can be more easily accommodated due to the space available. The properties and restrictions listed above do indeed guide one to that section of the periodic table which is most noted for the formation of metal clusters. It should be mentioned that many of the points essential for metal-metal bonding in halide complexes are not applicable to carbonyl clusters due to the exceptional electron accepting ability of the carbon monoxide ligand and the extremely low oxidation states accessible to such systems. In summary, one can conclude that any successful synthetic route which condenses monomeric metal moieties into clusters containing one or more metal-metal bonds will have to bring to bear conditions promoting the principles which have been reviewed.

Preparative routes to metal clusters have historically involved high temperature, sealed tube reactions. Perhaps the most common synthetic approach is to reduce a high oxidation state halide with a reducing agent such as hydrogen gas, aluminum or the metal itself. Formation of metal clusters via halogen oxidation of the metal is of limited utility due to the difficulties encountered in controlling the products under the oxidizing conditions required. Another tack which has produced metal-metal bonds has been disproportionation of intermediate oxidation state halide species. The synthetic aspect stressed in the orientation of this research centers on reac-

tions which actually convert monomeric metal species into clusters, so substitution of ligands or oxidation-reduction of existing metal-metal bonded species are not considered in depth, but these reactions are in fact responsible for the wide variety of metal clusters now known.

The purpose of the work performed was to add to the existing pool of information relating to metal clusters, hopefully utilizing relatively mild conditions to prepare interesting products. The proposed goals were achieved via the isolation of two new metal-metal bonded dimers, one containing tantalum in the novel 3+ oxidation state and the other an unusual paramagnetic tungsten dimer. The synthetic techniques employed in isolating these two compounds are quite dissimilar and the organization of this thesis has therefore dictated a two part division. The tantalum system will be treated first in its entirety followed by details of the research pertaining to the tungsten dimer. The original synthetic route and complete physical characterization, including an x-ray structural determination, will be presented in each case.

PART I. SYNTHESIS AND CHARACTERIZATION OF $Ta_2X_6(SC_4H_8)_3$, (X = Cl, Br)

REVIEW OF RELATED WORK

The descriptive chemistry of tantalum is dominated by the pentavalent complexes which make up the vast majority of compounds studied to date. The tetrahalides of tantalum are well characterized, but quadrivalent derivatives are rare and only recently have they been examined closely. Niobium is more easily reduced from the 5+ oxidation state than is tantalum as will become evident from comparison of lower oxidation state halide derivatives which have been synthesized. A review of the chemistry of tantalum(IV) succeeded by enumeration of lower halide phases will provide adequate background for placing isolation of a discrete tantalum(III) species in perspective. Although it has been stated that differences in the chemistry of tantalum and niobium are not profound (6), it would be naive to expect duplicate behavior for compounds of the two elements, and discrepancies are particularly marked for species of oxidation state 4+ or less for the metals. The following account will illuminate the contrasting behavior of tantalum and niobium in sundry cases.

Reduction of Niobium(V) in Aqueous Solution

Niobium(V) has been successfully reduced electrochemically in aqueous solution by Cozzi and Vivarelli (7) who found a reduction wave proportional to the niobium concentration in 0.1 N nitric acid when niobic acid was electrochemically reduced. The same workers concluded that Nb(III) was the

ultimate product when Nb(V) was reduced in concentrated hydrochloric acid (8). An initial reduction to Nb(IV) was postulated followed by disproportionation to Nb(III) and Nb(V). Addition of 10-20% by volume of ethylene glycol slowed the disproportionation reaction and Nb(IV) was then electrochemically reduced to Nb(II) which in turn combined with Nb(IV) to form Nb(III) species and no further reduction occurred. Thus Nb(III) was the final electrochemical product both with and without added ethylene glycol. No evidence of electrochemical reduction has been found for any aqueous tantalum(V) system.

Reduction of Nb(V) has also succeeded with various amalgams in acidic solutions (9). Zinc amalgam produced Nb(III) species in both hydrochloric and sulfuric acid solutions. Cadmium amalgam also produced Nb(III) in hydrochloric acid, but reduction ceased at Nb(IV) in sulfuric acid solutions. Oxidation state determinations on products of the amalgam reductions were performed via permanganate titrations for sulfuric acid media and ferric chloride titrations for hydrochloric acid media. Again the corresponding tantalum systems were not reduced under similar conditions.

Descriptive Chemistry of Tantalum(IV)

Tantalum dioxide, TaO_2, has been prepared by high temperature (1700°C) carbon reduction of the pentoxide. Metal-metal bonding presumably plays a role in the solid state structure as in the case of NbO_2 (10) where a distorted rutile structure

allows metal atoms to pair in distances of 2.80 and 3.20Å along the c-axis. At this point it should be noted that the metal-metal distance in both elemental niobium and tantalum is 2.85Å.

Niobium and tantalum tetrahalides are known for all the various combinations except for tantalum tetrafluoride which is conspicuous in its absence. In view of the stability of high oxidation state fluorides, the difficulty encountered in reducing NbF_5, and the comparative facility of reducing niobium compounds as compared to their tantalum analogues, the absence of TaF_4 is easily rationalized. Niobium tetrafluoride has been formed at 300-350°C by reducing NbF_5 with powdered niobium metal (11). The black solid is unique among the tetrahalides in that it is not diamagnetic. The magnetic properties of NbF_4 are consistent with the solid state structure in which the niobium-niobium separations preclude bonding interactions between metal atoms.

Tantalum pentachloride is much more difficult to reduce than is its niobium counterpart. Schäfer and Kahlenberg have described the synthesis of $TaCl_4$ (12) while McCarley and Boatman have described a convenient preparation of $TaBr_4$ involving aluminum foil as the reducing agent (13). The metal pentabromide can be formed from elemental tantalum and bromine followed by a temperature gradient reaction to form tantalum tetrabromide. Tantalum pentabromide at 250°C maintains a vapor

pressure of approximately 60 mm while aluminum foil at 500°C reduces the $TaBr_5$ vapor to form $TaBr_4$. The diamagnetic properties of all the niobium and tantalum tetrachlorides and tetrabromides are indicative of metal-metal bonding in the solid with concomitant pairwise grouping of the metal atoms. An x-ray study of niobium tetrachloride (5) confirmed the pairwise interaction in that case; the shorter niobium-niobium separation along the one-dimensional chain of edge-shared octahedra was found to be 3.06Å. The remaining chloride and bromide 4+ analogues appear to be isomorphous with $NbCl_4$ based on powder pattern x-ray data (13).

Niobium tetraiodide is easily prepared from NbI_5 by elimination of elemental iodine at 270°C in a sealed tube cooled at one end to condense the iodine (14). Although NbI_4 is not isomorphous with $NbCl_4$, it has been determined that the structure does involve pairwise metal interactions with a niobium-niobium distance of 3.31Å between alternate pairs along the chain of octahedra (15). Once more the corresponding tantalum system requires more stringent conditions if reduction is to occur. Vapor phase reduction of TaI_5 with aluminum metal in a gradient of 500°C (aluminum) to 350°C (tantalum pentaiodide) produces TaI_4 over a period of seven days (13). A preferable route to tantalum tetraiodide utilizes $TaI_4(py)_2$, (py = pyridine), which quantitatively loses pyridine when evacuated at 200°C for two days (13).

Relatively few tetrahalide adducts of tantalum have been reported. Typical preparations of chloride and bromide tetrahalide adducts proceed in excess ligand over a period of several days. Fowles, Tidmarsh and Walton isolated TaX_4L_2 and TaX_4B where B was bidentate 1,10-phenanthroline (phen) or 2,2'-bipyridyl (bipy) and L was pyridine or acetonitrile for both X = Cl and X = Br (16). Reaction times for 1,10-phenanthroline might be considered typical: ten days for $TaCl_4$ and five days for $TaBr_4$ to form the adducts. Fowles also prepared the acrylonitrile derivatives $TaCl_4(CH_2CHCN)_2$ and $TaBr_4(CH_2CHCN)_2$ via tantalum tetrahalide and excess ligand reactions (Fowles and Gadd (17)).

Reduction of Ta(V) occurs with some nitrogen donor ligands and adducts of Ta(IV) result. 4-Picoline reduced tantalum pentabromide over a period of five days at reflux to form $TaBr_4(4\text{-picoline})_2$ while the corresponding chloride adduct formed in six days at room temperature (18). Five weeks of reacting $TaCl_5$ and pyridine at 50°C did in fact lead to reduction and formation of $TaCl_4(py)_2$. Reduction also occurred with the bidentate ligands 1,10-phenanthroline and 2,2'-bipyridyl. McCarley and co-workers reported reduction of NbX_5 (X = Cl, Br) by pyridine at room temperature while tantalum formed monoadducts without reduction (19). Identification of the oxidized organic species provided hitherto unattainable insight into the mechanism of reduction. Both niobium and tantalum pentaiodide were reduced by pyridine in the same study, but the oxidation

product was the elemental iodine adduct of pyridine rather than 1-(4-pyridyl)pyridinium ion as was elucidated for NbX_5 (X = Cl, Br). It seems clear that the stability of $MI_4(py)_2$ and $py(I_2)$ shifts the dissociation of MI_5 towards $MI_4 + 1/2\ I_2$.

To further emphasize the contrasts in chemical behavior of niobium and tantalum it is interesting that niobium(IV) adducts of tetrahydrofuran, tetrahydropyran and 1,4-dioxane were cleanly isolated while tantalum(IV) invariably led to intractable oils with the same ethers (16).

The paramagnetism exhibited by adducts of both niobium(IV) and tantalum(IV) contrasts sharply with the diamagnetism associated with the parent MX_4, which is more informatively formulated as M_2X_8 due to the metal-metal bonding present. Typical magnetic moments for NbX_4L_2 are in the range of 1.0 to 1.6 Bohr magnetons, and TaX_4L_2 moments are commonly less than 1.0 BM, probably due to the increased size of the spin-orbit coupling constant.

Dialkyl sulfide ligands are of particular interest due to the stability of both the niobium(IV) adducts and the pentahalide adducts of both niobium and tantalum. The selection of tetrahydrothiophene for use in the preparation of a reduced tantalum halide dimer was based on previous studies of adducts formed with sulfur donors. Fairbrother and Nixon (20) isolated monoadducts of MX_5 (M = Nb, Ta; X = Cl, Br) with dimethyl sulfide and diethylsulfide by reaction of the neat ligand with the appropriate pentahalide. Tetrahydrothiophene was unique in

forming 2:1 complexes with these same pentahalides. Cowley, Fairbrother and Scott (21) had previously prepared 1:1 diethyl ether complexes which readily decomposed at 100°C to MOX_3 and C_2H_5X. The sulfide analogues displayed much greater thermal stability than the oxygen bound adducts and no decomposition to form MSX_3 was detected. Reactions of MX_5 with tetrahydrofuran resulted in polymerization of the ether, so no direct comparison of the oxygen versus sulfur five-membered cyclic ligand was possible. Feenan and Fowles (22) later isolated 1:1 adducts of tetrahydrothiophene (tht) with all four pentahalides (Nb, Ta; Cl, Br), by utilizing a benzene dilutent. Pentamethylene sulfide, 1,4-dioxane and 1,4-thioxan were also employed as ligands in this report by Feenan and Fowles, but pentamethylene oxide polymerized as had tetrahydrofuran in earlier studies. Nuclear magnetic resonance spectra and infrared evidence were cited supporting coordination of thioxan through the sulfur atom rather than through the oxygen atom.

The accumulated data, which includes sulfur-bound thioxan adducts, displacement of diethyl ether by diethyl sulfide, selective absorption of diethyl sulfide from a gaseous mixture of 10% $(C_2H_5)_2S$ to 90% $(C_2H_5)_2O$ by $NbCl_5$, and greater thermal stability for sulfide adducts than ether adducts, clearly indicates preferential bonding to sulfur by the pentahalides. The d^0 configuration of the pentavalent group V metals invalidates arguments of stability due to supplemental metal electron density donation into the vacant 3d-orbitals of sulfur which

are not available to first row donors such as oxygen. A review of sulfur containing ligands (23) addresses itself to the factors stabilizing metal-sulfur bonds and notes that polarizability and dipole moment considerations may favor sulfur coordination in some cases.

In addition, dialkyl sulfides are of importance with respect to the stability exhibited by niobium(IV) adducts as investigated by Hamilton and McCarley (24). Diethyl sulfide, dimethyl sulfide and tetrahydrothiophene were employed in this study of niobium tetrahalide adducts. Although bis-adducts of $(CH_3)_2S$ and SC_4H_8 and mono-adducts of $(C_2H_5)_2S$ were cleanly prepared with niobium(IV), the tantalum tetrahalides reacted with the same dialkyl sulfides to produce only intractable tars. Steric requirements for diethyl sulfide rationalized mono-adduct formation in the niobium(IV) case and the minimal requirements of CS_4H_8 due to ring constraints could be important in the 1:2 pentahalide adduct, $MX_5(SC_4H_8)_2$. On the other hand, isolation of both niobium and tantalum tetrahalide adducts with $(CH_3)_2S$ and SC_4H_8 was reported by Fowles, Tidmarsh and Walton (25). Utilizing benzene as a solvent and refluxing the tetrahalide with excess ligand for several days in a sealed tube led to products formulated as TaX_4L_2 (X = Cl, Br; L = $(CH_3)_2S$, SC_4H_8). Oils were produced initially but extensive evacuation while heating or alternatively distilling solvent on and off the oil several times eventually solidified the material. Characterization included elemental analysis, room

temperature magnetic moments, infrared and electronic absorption spectra.

Reaction of lithium dialkylamides with tantalum pentachloride produced $Ta(NR_2)_5$ (26) for a series of six different R = alkyl groups. The corresponding niobium system underwent reduction in increasing yields as the length of the alkyl chain increased and $Nb(NR_2)_4$ was formed (27). Heating the $Ta(NR_2)_5$ compounds produced $RN{=}{=}Ta(NR_2)_3$ so no reduction of tantalum(V) occurred even when a four coordinate complex was synthesized. Again it is important to notice the difference in chemistry as here tantalum(V) maintains its integrity which can be compared to the facile production of niobium(IV) under similar reaction conditions.

The above compendium serves to document the fact that niobium and tantalum differ appreciably with respect to the reduction reactions interrelating the d^0 and d^1 metal systems. The inability to reduce tantalum(V) in aqueous solutions, the facile reduction of niobium(V) by nitrogen donor ligands, the nonexistence of TaF_4, the ease of preparation of NbI_4 from NbI_5, and the difficulty experienced in isolating tantalum(IV) derivatives with dialkyl sulfide ligands and tantalum(V) derivatives with ethers all contribute to the overall depiction of the vagarious behavior of tantalum as based on predictions extracted from the chemistry of niobium under similar chemical conditions.

Niobium(III) and Tantalum(III)

No trivalent complexes of tantalum have been confirmed in the literature to date. Discrete halide dimers of niobium(III) have, however, been prepared by Broll, von Schnering and Schäfer (28) via a sealed tube reaction between Nb_3X_8 and CsX or RbBr with production of the salts $Cs_3Nb_2X_9$ (X = Cl, Br, I) and $Rb_3Nb_2Br_9$. The reactants were maintained at 640 to 690°C in the high temperature end of the quartz ampoule and the dimeric species then formed at the opposite end in a temperature range of 600 to 650°C. X-ray techniques confirmed the 3+ oxidation state and revealed a confacial bioctahedral structure for the $Nb_2Br_9^{3-}$ anion, that is, two octahedra sharing a common trigonal face, with a niobium-niobium distance of 2.77Å for the bromide salt and 2.70Å for the chloride salt. A magnetic moment of 2.68 BM as reported for $Cs_3Nb_2Br_9$ is consistent with two unpaired electrons per dimer, such as would result if the four available d-electrons go into metal-metal bonding orbitals, the first two into a low energy nondegenerate orbital and the remaining two into degenerate orbitals. No description of the analogous tantalum(III) salts has ensued.

Blight, Deutscher and Kepert reported the reaction of $TaCl_4$ and acetonitrile and characterized the resultant green product as $[TaCl_3(CH_3CN)_2]_2$ (29), which formally appears to be tantalum(III). The proposed dimeric structure, based on the unusual structure found for $[WCl_3(py)_2]_2$ (30), involved a

tantalum-tantalum double bond to account for the observed diamagnetism of the dimer. More recently McCarley and co-workers communicated the crystal structure of $([(C_6H_5)_3P]_2N)_2(Nb_2Cl_8(CH_3CN)_2C_4H_6N_2)$ after a thorough investigation of the chemistry of tantalum and niobium tetrahalides in acetonitrile led to the above salt in elucidating the reaction products (31). While simple $NbX_4(CH_3CN)_2$ adducts are formed in acetonitrile as would be predicted (32), the chemistry of tantalum digresses in a complicated reaction leaving 0-20% of the tantalum in an insoluble green precipitate and the remainder is lost in a red solution from which no products were isolated. Addition of zinc to the tantalum tetrahalide-acetonitrile solution substantiated the hypothesis that tantalum(III) resulting from disproportionation of tantalum(IV) was involved in the reaction producing the green solid as the yield increased to 20-50%. Furthermore, addition of zinc to the niobium system produced similar green insoluble products and both metal halide solids had a chlorine:metal ratio of 3:1. Substitution of one acetonitrile per metal atom was accomplished in acetonitrile with bis(triphenylphosphine)iminium chloride and recrystallization from acetonitrile-chlorobenzene solution provided crystals of $([(C_6H_5)_3P]_2N)_2(Nb_2Cl_8(CH_3CN)_2C_4H_6N_2)\cdot 2C_6H_5Cl$ suitable for x-ray diffraction studies. The culmination of the investigation was the identification of a unique bridging ligand revealed by the structure which resulted from the reductive coupling of two acetonitrile molecules and was accompanied by

oxidation of niobium to the 5+ oxidation state, where the bridging ligand is considered to be the tetraanion of

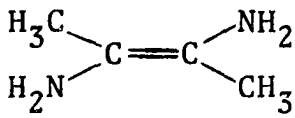

It seems probable that the species isolated from earlier acetonitrile-$TaCl_4$ work is a similar ligand-bridged tantalum(V) dimer.

Both niobium and tantalum form dark and unreactive halides of stoichiometry MX_3. Tantalum trichloride and tribromide display homogeneity ranges from $TaX_{2.9}$ to $TaX_{3.1}$ and thus resemble the niobium trichloride phase in which the halide to metal ratio varies from 2.67 to 3.13. Both the chloride and bromide TaX_3 phases can be prepared by the three temperature sealed tube method: tantalum metal at one end at 600-620°C, tantalum pentahalide at 320-365°C at the opposite end, and the central portion of the tube at 365-380°C where the trihalide is deposited (33).

Tantalum trichloride is isomorphous with niobium trichloride and the description of the tantalum trihalides is generally assumed to parallel that of the niobium trichloride phase which has been thoroughly investigated (34). Schäfer and Dohmann prepared homogeneous crystals spanning the stoichiometric range from $NbCl_{2.67}$ to $NbCl_{3.13}$ by chemical transport methods starting with niobium metal and $NbCl_5$. After reaction of all the metallic niobium the residual $NbCl_5$ vapor

and "$NbCl_3$" form $NbCl_4$ in the high temperature section of the tube (390°C) which then diffuses and disproportionates to deposit $NbCl_x$ at the low temperature end of the tube (355°C). The residual pressure of $NbCl_5$ determines the stoichiometry of the final product. The color of the product changes gradually from green to brown as the stoichiometry passes from 2.67 through 3.00 to 3.13, but x-ray powder patterns indicate retention of the basic crystal structure.

A single-crystal x-ray structure determination of the $NbCl_{2.67}$ phase (35) revealed a CdI_2-type layer lattice with 3/4 of the metal sites occupied in agreement with the Nb_3Cl_8 composition. A magnetic moment of 1.86 BM is obtained based on the trimeric formulation thus indicating one unpaired electron per trimeric unit. Considering that a total of seven metal valence electrons are available for metal-metal bonding, one could conclude that six electrons are paired by interactions among the three metal atoms. The niobium-niobium distances, 2.81Å for all three sides of the triangle, are clearly indicative of metal-metal bonding. Orderly removal of one of the metal atoms from each trimeric unit of Nb_3Cl_8 produces both the correct composition and solid state structure of Nb_2Cl_8. The homogeneity range of niobium trichloride, of which $NbCl_{3.0}$ is merely an intermediate composition, results from statistical replacement of Nb_3Cl_8 units by Nb_2Cl_8 units throughout the lattice. For chloride to niobium ratios between 3.13 and 4.00 a two phase system exists containing both

$NbCl_{3.13}$ and $NbCl_4$.

Preparation of Nb_3Br_8 via a transport method similar to that described for Nb_3Cl_8 produces α-Nb_3Br_8 which is isomorphous with the monomorphic Nb_3Cl_8 (36). Stoichiometric combination of niobium metal and bromine at temperatures above 500°C followed by recrystallization using vapor phase transport techniques produces β-Nb_3Br_8, a second polymorph (37). The metal-metal distance in β-Nb_3Br_8 is 2.88Å which is again compatible with the proposed bonding scheme.

Although the tantalum trihalide phases are of variable composition, the range of homogeneity is much smaller than in the niobium case and indeed the tantalum analogue of Nb_3X_8 has never been isolated.

Hexanuclear Tantalum Clusters

Hexanuclear metal clusters of tantalum have been recognized since Chapin correctly formulated $TaBr_2 \cdot 2H_2O$ and $TaCl_2 \cdot 2H_2O$ as $Ta_6X_{14} \cdot 7H_2O$ in 1910 (38). The chemistry of these octahedral metal clusters of niobium and tantalum has since been thoroughly investigated (39) and a detailed review would not be germane to the research topic under consideration. Nonetheless, the metal-metal bonded octahedra of tantalum atoms with halogen bridges along each edge forming $Ta_6X_{12}^{n+}$ (n = 2, 3, 4) cations provide further documentation of the propensity for homonuclear bonding interactions in low valent tantalum halides.

Anhydrous $TaCl_{2.5}$ and $TaBr_{2.5}$ have been formed from reduction of the appropriate pentahalide with tantalum metal using a three temperature method (33,40). The structure consists of $Ta_6X_{12}^{3+}$ units linked in a three dimensional array by bridging X^- ions in the terminal positions of the octahedral cluster which is perhaps more clearly formulated as $Ta_6X_{12}X_{6/2}$.

The solid structure of Ta_6Br_{14} and Ta_6I_{14} again involves hexanuclear clusters but only a two-dimensional array results from halide bridges in the plane of the metal octahedron, $M_6X_{12}^{2+}$, with the correct formulation $Ta_6X_{12}X_{4/2}$ (41). It is interesting to note that aluminum foil reduction of $TaBr_5$ and TaI_5 at elevated temperatures produces $TaX_{2.33}$ compositions while reduction of $TaCl_5$ under similar conditions ceases at $TaCl_{2.5}$ (42).

Hydrated tantalum hexanuclear clusters were first characterized structurally in 1950 from x-ray studies of concentrated ethanolic solutions (43). The metal atom separations in the regular octahedra of $Ta_6Cl_{12}^{2+}$ and $Ta_6Br_{12}^{2+}$ were estimated to be 2.88Å and 2.92Å, respectively. $Ta_6X_{14}\cdot 7H_2O$ clusters do indeed have two ionizable halides per cluster as the bridging halides are retained in solution with the $Ta_6X_{12}^{2+}$ unit surviving terminal substitution reactions as well as oxidation of the cluster to $Ta_6X_{12}^{3+}$ and $Ta_6X_{12}^{4+}$ (44).

Cotton and Haas have proposed a molecular orbital scheme (45) which is indicative of the results obtained by applying simple molecular orbital arguments to these highly symmetrical

clusters regardless of the exact assumptions involved. For a hexanuclear metal cluster with twelve doubly-bridging halides there are eight bonding molecular orbitals resulting from overlap of the available d-orbitals, and for tantalum clusters with an average oxidation state of 2.33 there are sixteen electrons in the metal valence orbitals which fit nicely to fill only these bonding orbitals. The average bond order is then 8/12 or 2/3 for $Ta_6X_{12}^{2+}$. The magnetic properties of the oxidized species are in accord with the proposed bonding scheme, i.e. $Ta_6X_{12}^{3+}$ exhibits paramagnetic behavior consistent with one unpaired electron per six metal atoms.

Organometallic Tantalum(III)

Few organometallic derivatives of tantalum have been well characterized, but two tantalum(III) compounds have been described in the organometallic literature. Refluxing a deuteriobenzene solution of $(\pi\text{-}C_5H_5)_2TaH_3$ evolves hydrogen gas and proton exchange occurs with the solvent. Addition of excess triethylphosphine to such a solution produces a red crystalline solid which has been identified as $(\pi\text{-}C_5H_5)_2Ta(H)(PEt_3)$ (46) by analysis of its proton magnetic resonance spectrum in solution. A doublet of doublets at τ = 5.68 is consistent with splitting of the cyclopentadienyl protons' resonance by the phosphorus and the hydride (J_{PH} = 1.7, J_{HH} = 0.5, all coupling constants in Hertz). A five-line resonance at τ = 8.91 results from overlapping quartets as ^{31}P splits these methylene reso-

nances into a doublet and the methyl protons cause the quartet splitting (J_{PH} = 7.0, J_{HH} = 7.5). The methyl resonance is likewise split by ^{31}P and the methylene protons (J_{PH} = 13.5, J_{HH} = 7.5) and five lines result from the overlapping triplets. The metal hydride resonance appears as a doublet at τ = 19.48 due to ^{31}P coupling (J_{PH} = 21). The integrated intensity ratios are 10:15.5:0.9 for the three basic regions of resonance in agreement with two π-bound cyclopentadienyl ligands, one triethylphosphine and one hydride per metal atom. The above chemistry is consistent with the following scheme:

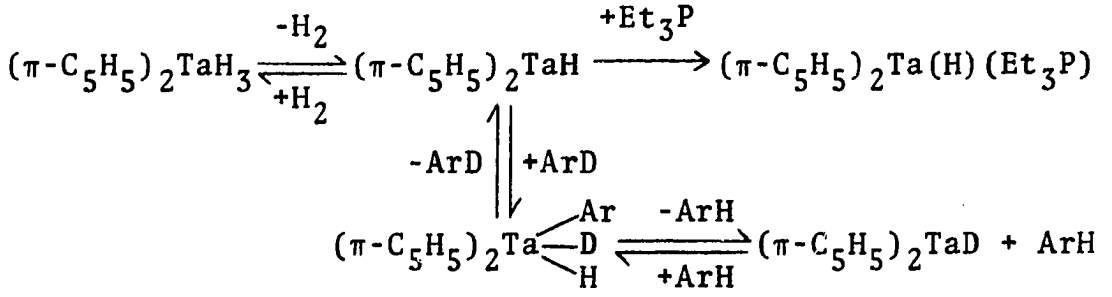

Another organometallic compound which contains tantalum (III) was briefly described in a communication reporting the crystal structure of $[(\pi\text{-}C_5H_5)Nb(CO)(Ph_2C_2)]_2$ (47). The photochemical reaction of diphenylacetylene (Ph_2C_2) with $(\pi\text{-}C_5H_5)Ta(CO)_4$ resulted in substitution of three of the carbon monoxide ligands to produce $(\pi\text{-}C_5H_5)Ta(CO)(Ph_2C_2)_2$. Thermal decomposition of this compound proceeded with dimerization and loss of one acetylene per metal atom. $[(\pi\text{-}C_5H_5)Ta(CO)(Ph_2C_2)]_2$ was isolated as a diamagnetic tantalum(III) dimer. The formal oxidation state can be derived by considering the oxidative

addition of Ta(I) across the carbon-carbon triple bond of the acetylene to form Ta(III). The structure of the corresponding niobium dimer was reported with a discrepancy factor of 13% and a niobium-niobium distance of 2.74Å which fits nicely with the postulated double bond required to satisfy the effective atomic number rule. This method of counting electrons to attain an inert gas configuration has been successfully applied to many organometallic compounds.

Derivatives of niobium(III) of the type $(\pi\text{-}C_5H_5)_2NbR$ (R = alkyl or allyl) have been characterized (48,49), but no data on such tantalum(III) compounds have been reported.

An unusual trimeric tantalum cluster was synthesized by Fischer and Röhrscheid in 1966 (50). Trimetallic cations of Ti, Zr, Nb and Ta were isolated with the composition $[(Me_6C_6)_3M_3Cl_6]^+$ (where Me_6C_6 is hexamethylbenzene) from aluminum reduction of metal halides in hexamethylbenzene in the presence of aluminum halides. The structure of $(Nb_3(Me_6C_6)_3Cl_6]Cl$ was revealed by x-ray diffraction techniques (51) to consist of trimers with a distance of 3.33Å separating adjacent metal atoms. Although there are eight total valence electrons in this organometallic trimer, the bonding description may in some ways parallel that of the Nb_3X_8 trimers where only seven electrons are available for metal-metal bonding. Recently a one-electron oxidation of the trimeric cation with Ce^{4+}, N-bromosuccinimide, I_2 or O_2 has been reported to produce diamagnetic hexanuclear cluster compounds (52).

$Nb_2X_6(SC_4H_8)_3$, (X = Cl, Br, I)

The previous work most relevant to the tantalum dimers to be described is the corresponding niobium study made by Maas and McCarley (53). A detailed comparison of spectral and magnetic properties of the two systems will be appropriate as the results of the tantalum study are presented, and only the preparative procedure for the niobium dimer will be discussed at this time. The niobium(IV) tetrahydrothiophene adduct first isolated by Hamilton and McCarley (24) was reduced with sodium amalgam in a benzene solution to prepare $Nb_2X_6(SC_4H_8)_3$ (where X = Cl, Br, I). Yields of 60-70% were reported for these neutral dimers which were soluble in nonpolar organic solvents. Physical characterizations, which included proton magnetic resonance, magnetic susceptibility, electronic absorption spectra and infrared spectra were all consistent with a confacial bioctahedral structure; a later x-ray diffraction study (54) confirmed the postulated face-shared dimer with one bridging tetrahydrothiophene and two bridging halides.

The diamagnetism exhibited over a wide range of temperatures was consistent with a formal bond of order two joining the two d^2 metal atoms. Replacement of the sulfur containing ligands could be performed in a stepwise manner to obtain $(Et_4N)_2Nb_2Cl_8(SC_4H_8)_1$ via displacement of the two terminal tetrahydrothiophene ligands while under more rigorous conditions $(Et_4N)_3Nb_2Cl_9$ was produced. Spectral properties indi-

cated that $(Et_4N)_2Nb_2Cl_8(SC_4H_8)$ was similar to the parent dimer, but major changes occurred in the electronic spectrum and magnetic susceptibility of the species upon replacement of the bridging tetrahydrothiophene when the completely chloride substituted dimer formed. Such changes are possibly due to the change in molecular symmetry accompanying the third chloride substitution, but no detailed rationalization was given.

EXPERIMENTAL

The reactants and products of interest in this study were sensitive to moisture and oxygen due to the possibility of rapid hydrolysis and/or oxidation. Manipulations of solids were therefore performed in a nitrogen-filled drybox with a circulation system designed to remove moisture and maintain a dewpoint of -72°C which corresponds to 4 ppm H_2O. Solvents were routinely dried prior to use, and standard vacuum line techniques were employed for transfer of solvents. Reactions were performed in vacuo and crystalline products were stored in screw-capped vials in the nitrogen atmosphere of a drybox.

Materials

Tantalum metal was obtained in the form of sheets from laboratory stock. The metal was utilized to generate tantalum pentahalides for use as starting materials.

Chlorine gas was purchased in lecture size cylinders from the Matheson Company. The cylinders were thoroughly outgassed at liquid nitrogen temperatures prior to use without further purification.

Bromine from J. T. Baker Chemical Company was dried over anhydrous phosphorus pentoxide and stored under vacuum. The bromine storage vessel was submerged in liquid nitrogen and extensively evacuated before distilling the elemental halogen into the reaction vessel.

Tetrahydrothiophene was purchased from Mathison, Coleman,

and Bell. It was dried either by stirring over lithium aluminum hydride or by setting over Linde 4A Molecular Sieves for several days. In either case the tetrahydrothiophene was stored over the drying agent in a round bottom flask equipped with a high vacuum Teflon needle valve.

Benzene was refluxed over sodium metal to remove moisture prior to vacuum distillation into a storage flask containing niobium pentachloride to scavenge any remaining traces of water. Fisher Scientific was the source of reagent grade benzene.

Toluene from J. T. Baker Chemical Company was utilized as a solvent. Molten sodium metal served as an effective drying agent in refluxing toluene. The solvent was then stored over sodium and distilled prior to use.

Mercury was obtained from the triply distilled laboratory stock and was used without further purification.

Sodium metal from J. T. Baker was stored in the drybox. Sodium was cut and handled under nitrogen or in evacuated vessels to avoid premature oxidation in the preparation of sodium amalgam.

Analytical Procedures

The tantalum content of compounds synthesized during the course of this work was determined gravimetrically as the oxide, Ta_2O_5. Typical samples of 100 to 200 mg were loaded in screw-capped vials in the drybox and accurately weighed by

difference into tared porcelain crucibles. The samples were wet with acetone and then hydrolyzed in aqueous ammonia. After heating to aid digestion, dilute nitric acid was added to acidify the solutions and oxidation proceeded as the crucibles were gently heated to dryness. Final conversion of the hydrous tantalum oxide to the pentoxide was effected by ignition in a muffle furnace at 600°C for several hours.

Halides were determined by potentiometric titration utilizing a silver sensitive working electrode with a saturated calomel reference electrode. Samples underwent basic hydrolysis followed by acidification to pH 1 with nitric acid prior to titration with a standard silver nitrate solution.

Mr. J. J. Richard of the Ames Laboratory Analytical Service Group, Iowa State University of Science and Technology, Ames, Iowa, performed carbon and hydrogen analyses on selected samples.

Synthesis

Large amounts of tantalum pentachloride and tantalum pentabromide were prepared by direct halogenation of the metal at elevated temperatures. Tantalum metal sheet was cut into thin strips and loaded in the center portion of an elongated reaction tube. The appropriate halogen was then vacuum distilled into one of the receptacle bulbs on either end of the tube and the vessel was sealed off under vacuum. The vapor pressure of the halogen was controlled with a cold bath while

the metal was oxidized by halogen gas in the high temperature region and sublimed to the cooler sections as metal pentahalide. The reaction tube was broken open in the drybox where the products were stored for later use as reactants.

Sodium amalgam was prepared in an evacuated vessel by dropwise addition of 241 grams of mercury per gram of sodium metal. Typically two to three grams of sodium were weighed into the glass cylinder in the drybox and a cap with two stopcocks, one connected to the cup-shaped well for addition of mercury, sealed the tube. After evacuation of the container through the unhindered stopcock the calculated amount of mercury was slowly added while the sodium remained in vacuo. The amalgamation process is very exothermic, but after an initial flash the reaction proceeds smoothly with no danger of excessive heat generation. Water baths were avoided due to the potential hazard presented by the metallic sodium. Such a preparation produced an amalgam consisting of 3.5 mole per cent sodium which was stored in the drybox until needed.

Tantalum pentahalide and tetrahydrothiophene served as reactants for a one-step synthetic procedure which led to the isolation of $Ta_2X_6(SC_4H_8)_3$ where X = Cl, Br. In a typical preparation $TaCl_5$ (3.6 g, 10 mmoles) was loaded into the 100 ml reaction flask with a Teflon coated stirbar in the drybox and sodium amalgam (100 g, 20 mmoles) corresponding to a two to one mole ratio of sodium to tantalum was funneled into the sidearm bulb. The sidearm was then carefully inserted into

the receptacle joint of the flask to avoid premature addition of the mercury solution. A vacuum line adapter equipped with a Teflon needle valve capped the round bottom flask before it was transported to the vacuum line. After thoroughly outgassing the flask, approximately fifty ml of dry aromatic solvent, either benzene or toluene, was condensed onto the pentachloride at liquid nitrogen temperatures. If allowed to warm to room temperature at this point a light yellow solution resulted as a small amount of the white starting material dissolved. Dry tetrahydrothiophene was first distilled into a graduated cylinder, suitably modified for vacuum manipulations, to assure excess ligand. The cyclic sulfide (3 ml, 35 mmoles) was then distilled into the reaction vessel where a bright orange solution resulted from dissolution of the tantalum pentachloride as the 1:1 adduct formed almost instantaneously. Addition of the reducing agent was then initiated by rotating the sidearm to elevate the bulb and drain the amalgam into the solution which was being vigorously mixed with a magnetic stirrer. All of the sodium amalgam was poured into the solution within a few minutes and a series of color changes followed. Within thirty minutes the solution stabilized as a dark, Burgundy wine-colored liquid containing the soluble dimeric tantalum product. At this point the volatile components, notably toluene or benzene and excess ligand, were removed from the heterogeneous reaction mixture by vacuum evaporation. The

solid products and liquid mercury were removed from the flask in the drybox where a mechanical separation of phases was attempted. Finely dispersed mercury tended to coalesce into droplets when ground with the dry solids in a mortar and decantation at this time separated most of the liquid metal. The remaining traces of mercury were transferred with the solids to an extractor suitable for high vacuum usage. Fresh aromatic solvent solubilized the desired product and a continuous extraction process effected a complete separation of $Ta_2Cl_6(SC_4H_8)_3$ from the mercury and insoluble by-products, which consisted of sodium chloride and a small amount of some unidentified powder. Prolonged extraction periods of several days were often required as insoluble particles tended to clog the frit. Slow solvent evaporation from the extractor left nicely crystalline tris(tetrahydrothiophene)hexachloroditantalum which was dark red violet in color. The analogous blue-violet or plum colored bromide dimer was isolated in the same manner, or alternatively both halide derivatives could be more conveniently purified by using a slightly modified reaction vessel. The union of a second 100 ml flask to the original was accomplished with an inverted, hollow U-tube and upon completion of the reaction this allowed a preliminary division of the soluble material and co-products by alternately decanting the colored solution into the vacant flask and then distilling the solvent back into the reaction products. When no further color was evident in the reaction portion of the vessel the solvent was

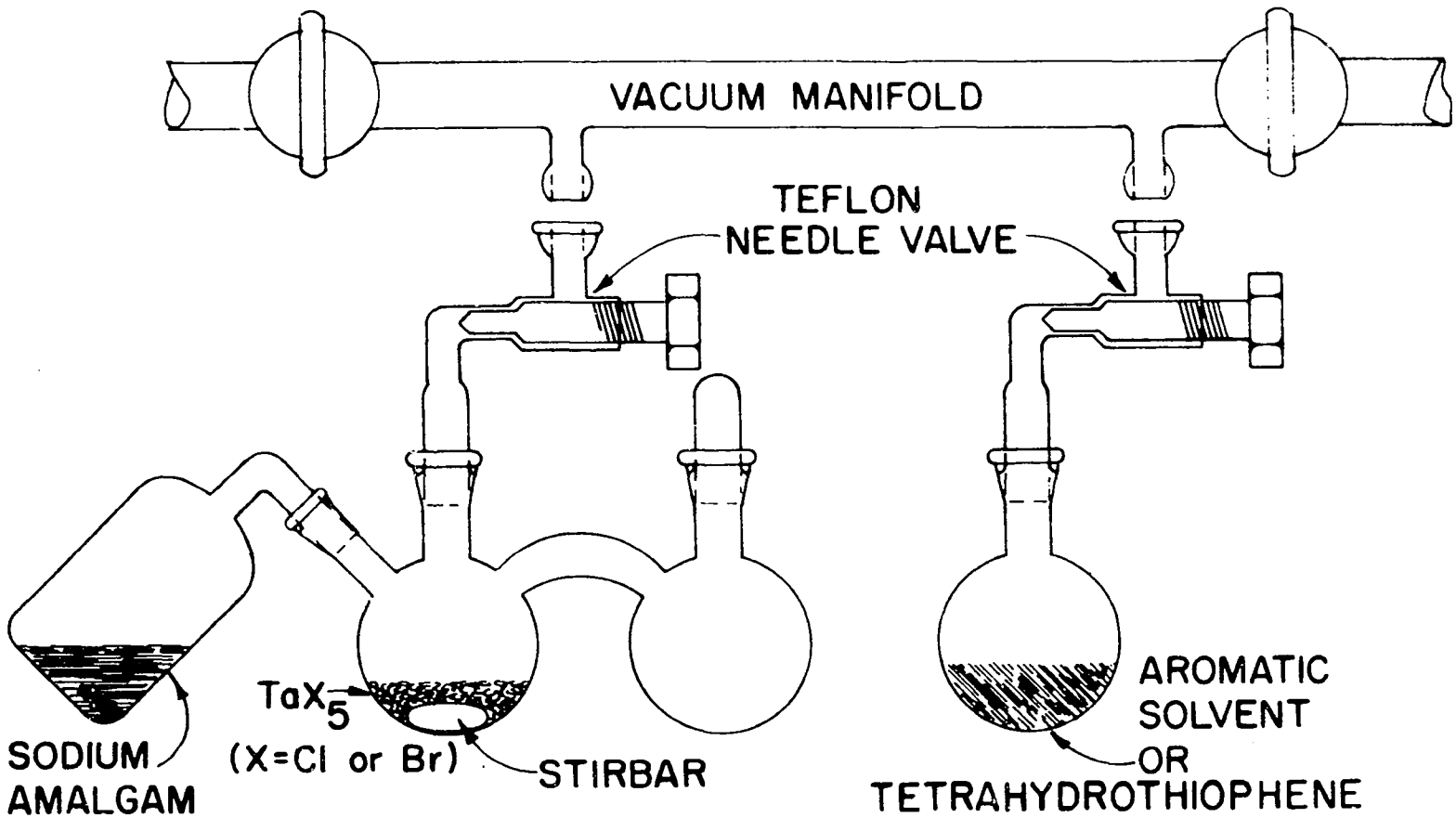

Figure 1. Modified reaction vessel for preparing $Ta_2X_6(SC_4H_8)_3$

distilled away and the products were transported to the drybox where by-products were discarded and the soluble fraction was placed in an extractor. The extraction now proceeded rapidly and the highly colored substance was completely solubilized in a few hours. Further recrystallization of the product was possible by cooling a toluene solution which had been saturated at room temperature. Anal. Calcd. for $Ta_2Cl_6(SC_4H_8)_3$: Ta, 43.13; Cl, 25.34; C, 17.18, H, 2.88. Found: Ta, 42.49; Cl, 24.80; C, 17.04; H, 3.16. Calcd. for $Ta_2Br_6(SC_4H_8)_3$: Ta, 32.73; Br, 43.35; C, 13.03; H, 2.19. Found: Ta, 33.21; Br, 42.33; C, 13.15; H, 2.44.

Physical Measurements

Proton magnetic resonance spectra were obtained with either a Varian A-60 or a Hitachi Perkin-Elmer R-20B spectrometer. The crystalline material to be investigated was loaded in the drybox into a specially designed cell equipped with a sintered glass frit and adapted for vacuum line use. Several milliliters of an appropriate solvent and a trace of tetramethylsilane were then distilled into the cell and the solution was saturated at room temperature prior to filtration into the sample tube. The solvent was then distilled back through the frit and the procedure was repeated to assure a saturated solution in the probe at ambient temperature. The tube was sealed under vacuum while the solution remained frozen in liquid nitrogen. Chemical shifts were measured in ppm relative to

TMS at $\delta = 0$.

Solution electronic spectra were obtained using a Cary Model 14 Recording Spectrophotometer and an evacuable cell similar to that utilized for the preparation of nuclear magnetic resonance samples. By carefully weighing the apparatus before and after the solid was added in the drybox and weighing a third time after addition of the solvent via distillation the concentration of the solution could be calculated when all of the solid was dissolved. The extinction coefficients of low intensity bands could then be determined and successive dilutions allowed the remaining extinction coefficients to be computed by intensity comparisons with the previously characterized bands utilizing a Beer's Law assumption.

The Faraday balance used to measure room temperature susceptibilities has been adequately described by Converse (55). An Ainsworth analytical balance reading to 0.01 mg measured the force at each of five field strengths monitored during each run. Calibration of the apparatus was carried out with nickel ammonium sulfate hexahydrate as a standard after recrystallization from aqueous solution and analyses for nickel content and cobalt impurities verified the composition of the crystals. The samples of interest were placed in screw-capped Teflon buckets under an inert atmosphere and no decomposition was detected when the contents of the container were examined upon completion of the magnetic measurements. Corrections to the raw data were made on the basis of the previously deter-

mined bucket susceptibility so that only the force resulting from the sample was considered in later computations.

Infrared spectra of the solids were obtained as Nujol mulls. A Beckman IR-11 spectrophotometer was employed with thin polyethylene sheets as transparent sample holders for the region from 700 cm^{-1} to 100 cm^{-1}. Absorptions from 600 cm^{-1} to 4000 cm^{-1} were monitored with either a Beckman IR-7 or Beckman IR-12 instrument and CsI or NaCl windows. Nujol was stored over sodium in the drybox where the mull was prepared as a thick paste and applied to the salt plates, which were consequently sealed in an O-ring fitted sample holder. The sample was transported to the instrument in a nitrogen filled jar and spectra were obtained quickly with no evidence of decomposition.

Nuclear quadrupole resonance spectra were obtained with a Wilks NQR-1A superregenerative spectrometer as described in detail by Edwards (56). More accurate frequency measurements for resonances in the region of 5 to 50 MHz were possible with the wide line induction spectrometer designed by Torgeson (57). Frequencies from 5 to 350 MHz were accessible with the oscillator circuits and associated sample coils of the Wilks instrument. Samples were sealed <u>in vacuo</u> in 15 mm outside diameter tubes after being loaded in the drybox; several grams of material were required to fill the tube to a sufficient depth such as to fully occupy the space inside the sample coil. A systematic scanning procedure was initially employed in searching for resonances, i.e. 5 to 20 MHz for chlorine and 40 to 100 MHz

for bromine. Resonance locations were estimated and checked before a slow scan was employed to allow accurate frequency values to be measured via superposition of a generated signal onto the oscilloscope display of the oscillator signal.

Single crystal x-ray diffraction data was collected after selection and mounting were completed in the crystal mounting drybox kindly made available by Professor John Corbett. Promising crystals were loaded in 0.2 mm thin-walled Lindemann capillaries and sealed with a hot nichrome wire in the drybox. Preliminary Buerger precession exposures and Weissenberg photographs were made with nickel-filtered Cu K_α radiation. Unit cell parameters were calculated from accurate diffractometer settings of three independent reflections whose centers were located by left-right, top-bottom beam splitting on a previously aligned four-circle diffractometer designed and built for the Ames Laboratory under the direction of Professor R. A. Jacobson. This same diffractometer was used to measure the integrated intensities of all data within a 2θ sphere of $45°$ with a graphite monochromator passing only Mo K_α radiation of wavelength 0.71069Å. Computer controlled data collection operated a θ-2θ scan mode at a counting rate of 0.2048 seconds per step of $0.01°$ in θ with a variable scan range of 50 steps plus 2 steps per degree θ. Stationary-crystal, stationary-counter background measurements were made at the beginning and end of each scan for half the total scan time. The intensities of three standard reflections were measured every fifty reflec-

tions during the data collection as a general check on electronic and crystal stability. Data reduction and analysis of the structure factors were completed with the aid of computer programs generously maintained and made available by the x-ray crystallography group at the Ames Laboratory under the guidance of Professor R. A. Jacobson.

RESULTS AND DISCUSSION

Synthesis

Previous work had shown that preparation and isolation of $NbX_4(SC_4H_8)_2$ (where X = Cl, Br or I) furnished suitable niobium(IV) species for a one-electron reduction with a sodium reducing agent in the form of an amalgam. The solubility of these niobium(IV) adducts in benzene made possible the heterogeneous reduction across the amalgam-solution interface with the resultant production of the dimeric niobium(III) species, $Nb_2X_6(SC_4H_8)_3$ (53). The highly unusual oxidation state exhibited by niobium in these compounds produced informative chemical investigations. The complete absence of any discrete tantalum(III) species made the analogous tantalum system perhaps of even greater interest. Unfortunately the intractable products resulting from interaction of tantalum(IV) halides with tetrahydrothiophene precluded isolation and characterization of $TaX_4(SC_4H_8)_2$ and thus a one-electron reduction route to tantalum(III) was not available. In addition, it was known that the anhydrous trihalides of tantalum were unreactive and unsuitable for starting materials in the preparation of discrete molecular tantalum(III) compounds.

The greater tendency towards disproportionation displayed by tantalum(IV) as compared to niobium(IV) could explain some of the difficulties encountered with tantalum(IV) systems, yet in no way would this allow one to conclude that Ta(III) would

be inaccessible or intractable. On the contrary, one might consider the disproportionation of Ta(IV) to be a harbinger of Ta(III) stability; rigorously the data can only be interpreted as indicating that the combined stability of Ta(III) and Ta(V) is greater than that of Ta(IV) and in some instances reaction pathways exist for just such a conversion to occur.

The synthetic approach employed in the preparation of tantalum(III) was simple and direct rather than sophisticated or intricate. The reactants selected were soluble tantalum(V) halide mono-tetrahydrothiophene adducts to which two moles of sodium were added per mole of tantalum. In anticipation of a tetrahydrothiophene to metal ratio of 1.5 to 1.0 in the final product, excess ligand was present in the solution to assure that adequate sulfide was available for coordination during the reaction. A series of color changes following addition of the sodium amalgam was evidence that a reaction was proceeding through several intermediate species. Precipitation of sodium halide occurred as a consequence of elemental sodium oxidation and halide ion extraction and these observations in conjunction with the intensely colored aromatic solution pointed to the existence of a soluble reduced tantalum compound. The solubility of the reduced species made it amenable to chemical purification via extraction techniques, and analytical data on the purified solid was consistent with the formulation $[TaX_3(SC_4H_8)_{1.5}]_n$. The relative rate of the reaction was slightly surprising in view of the heterogeneous system involved.

Yields of 75% were typical for the production of reduced chlorides and bromides best described as $Ta_2X_6(SC_4H_8)_3$.

Another trivalent tantalum compound of interest would be a salt containing the $Ta_2X_9^{3-}$ anion which has not been prepared by any route to date. The corresponding dimeric niobium anion, $Nb_2Cl_9^{3-}$, was prepared via a high temperature sealed tube reaction (28) or by chloride ion substitution of the neutral sulfur donor ligands present in $Nb_2Cl_6(SC_4H_8)_3$ (53). While an excess of $(C_2H_5)_4NCl$ reacted with $Nb_2Cl_6(SC_4H_8)_3$ in CH_2Cl_2 to form an insoluble gray crystalline product characterized as $[(C_2H_5)_4N]_3Nb_2Cl_9$ (53), the tantalum dimer failed to undergo metathesis in the same manner. Excess tetraethylammonium chloride (12:1 = chloride:dimer) reacted with $Ta_2Cl_6(SC_4H_8)_3$ in CH_2Cl_2 to form a mixture of several insoluble powders as well as a soluble orange-pink product. It seemed likely that dichloromethane was not acting as an inert solvent but was perhaps involved in oxidation of the reduced tantalum species in this reaction. In order to employ a less reactive solvent, such as toluene, it was necessary to use tetrabutylammonium chloride as a reactant for solubility purposes. Attempted metathesis reactions with this cation produced only oils upon solvent removal by vacuum evaporation. More stringent reaction conditions were also employed unsuccessfully. Molten tetrabutylammonium chloride (100°C) was used as a reaction medium with $Ta_2Cl_6(SC_4H_8)_3$ for several days and cesium chloride was reacted with the tantalum dimer in liquid hydrochloric acid, both to no avail.

A cursory examination of the probable molecular orbitals present in the face-shared octahedra dimer, as confirmed by x-ray investigations, suggested reduction of the dimer should be possible. Analysis of confacial bioctahedral structures of D_{3h} symmetry confirms that species can exist, such as $W_2Cl_9^{3-}$, with a triple bond between the two d^3 metal atoms. If one were to imagine $Ta_2Cl_9^{3-}$ as a compound with molecular orbitals similar to those in $W_2Cl_9^{3-}$, one could then perform the Gedanken process of tetrahydrothiophene substitution for three of the chloride ions to obtain the neutral dimer with the accompanying transformation from D_{3h} symmetry to C_{2v}. The method of descending symmetry allows one to follow the degenerate molecular orbitals as they are transformed into nondegenerate orbitals in the lower symmetry and a qualitative ordering of the energy levels in the lower symmetry can be based on the more definitive high symmetry case.

A thorough discussion of bonding in metal-metal bonded dimers will be presented when the detailed structural results are examined, but at this time a brief rationale for the synthetic reduction attempts is appropriate. The point to be made in comparing $W_2Cl_9^{3-}$ and $Ta_2Cl_6(SC_4H_8)_3$ is that the tungsten d^3 case puts six electrons into bonding orbitals and hence the resulting metal-metal triple bond. In $W_2Cl_9^{3-}$ these orbitals consist of one σ and two π bonds while in the tantalum d^2 case only four electrons are available for metal-metal bonding orbitals. Although the C_{2v} symmetry applicable to the tantalum

dimer no longer constrains the two π orbitals to be energetically equivalent, it would seem most probable that in fact both of these molecular orbitals remain as bonding orbitals. Based on this logic the lowest unoccupied orbital in the tantalum dimer should be a bonding molecular orbital between the two metal atoms. It would then seem plausible to add one or two more electrons to the dimer and increase the tantalum-tantalum bond strength, but sodium amalgam proved to be incapable of effecting further reduction of the isolated dimer.

Proton Magnetic Resonance

The proton magnetic resonance of neat tetrahydrothiophene exhibits two areas of resonance corresponding to the methylene protons adjacent to the heteroatom in the five-membered ring and protons on the methylene groups further removed from the sulfur atom. For purposes of discussion these protons will be labeled type b and type a, respectively, as illustrated in Figure 2. The type a resonance is in the form of an inexact quintet at δ 1.87 (relative to TMS at δ 0) and the type b proton resonance appears as a skewed triplet at lower field (δ 2.74) due to electron density withdrawal from the carbon atoms adjacent to the more electronegative sulfur atom. The five-membered cyclic thioether is nonplanar and thus second order couplings dominate the spectrum and lead to the observed triplet and quintet structures.

Although the chemical shifts are influenced by dilution

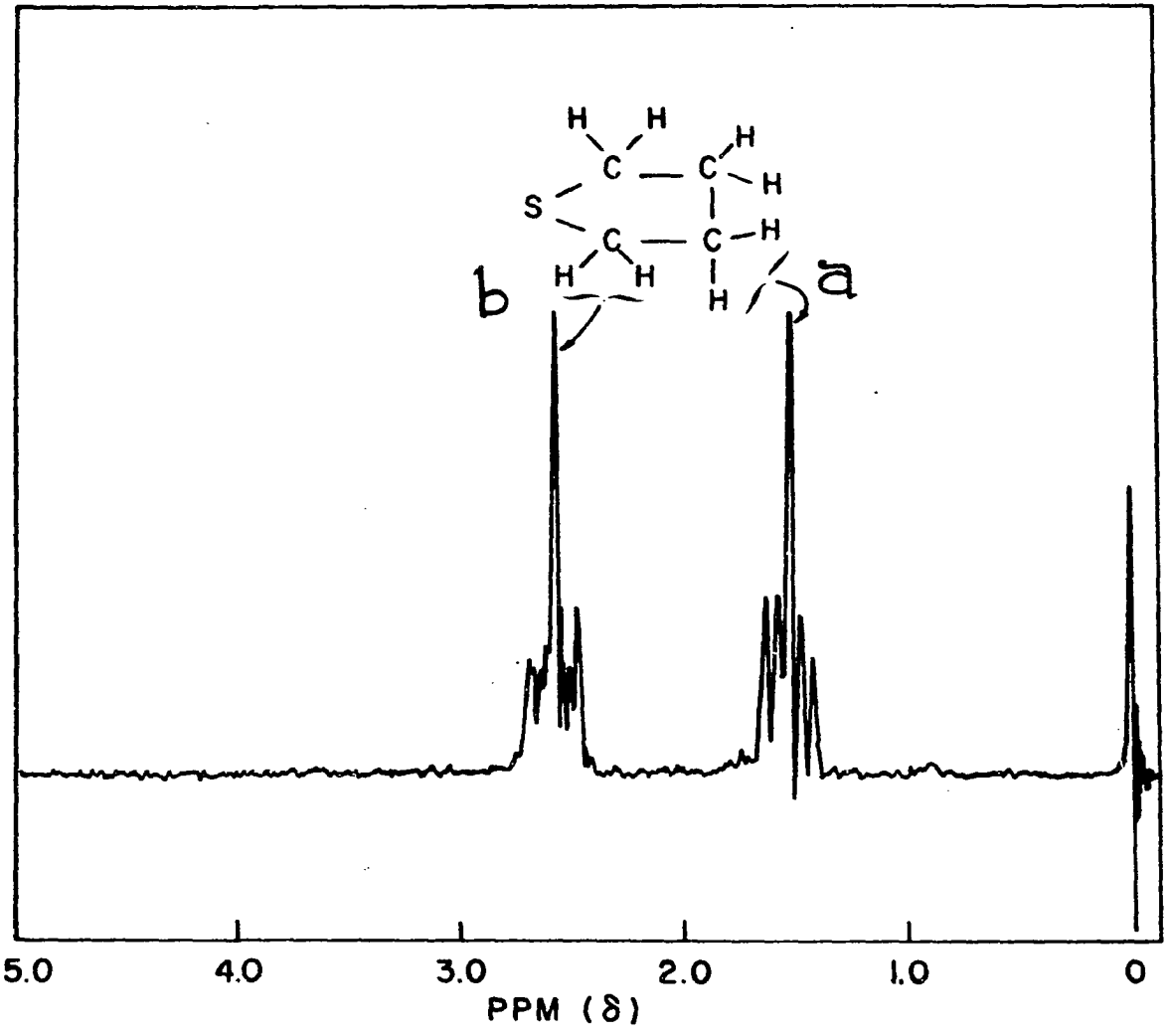

Figure 2. ^{1}H nmr spectrum of SC_4H_8 in benzene solution

with organic solvents (58), the splitting pattern remains unchanged. Benzene solutions of tetrahydrothiophene shift the quintet upfield to δ 1.47 and the triplet also moves upfield (δ 2.54). Slight downfield shifts are observed with carbon tetrachloride as a solvent; type a protons are centered at δ 1.92 and type b protons are centered at δ 2.76.

The nmr spectrum of $Ta_2Cl_6(SC_4H_8)_3$ was obtained from a saturated benzene solution with TMS as an internal standard. The spectrum revealed four multiplets due to tetrahydrothiophene in the complex of interest as shown in Figure 3. Two triplets were present at low fields with an integrated intensity ratio of one to two and two quintets were present at higher field with the same intensity ratio. None of the observed resonances were attributable to free tetrahydrothiophene and the conclusion reached was that tetrahydrothiophene was present in the molecular species in two different environments in a ratio of two to one. The above nmr data was combined with the analytical results, which indicated a multiple of the composition $TaCl_3(SC_4H_8)_{1.5}$, to postulate a dimeric species, $Ta_2Cl_6(SC_4H_8)_3$, analogous to the niobium dimers characterized by Maas (59). In the postulated confacial bioctahedron one tetrahydrothiophene serves as a bridging ligand while two are terminally coordinated to opposite metal atoms and six halogen atoms complete the coordination spheres by occupying the remaining four terminal positions and two bridging positions.

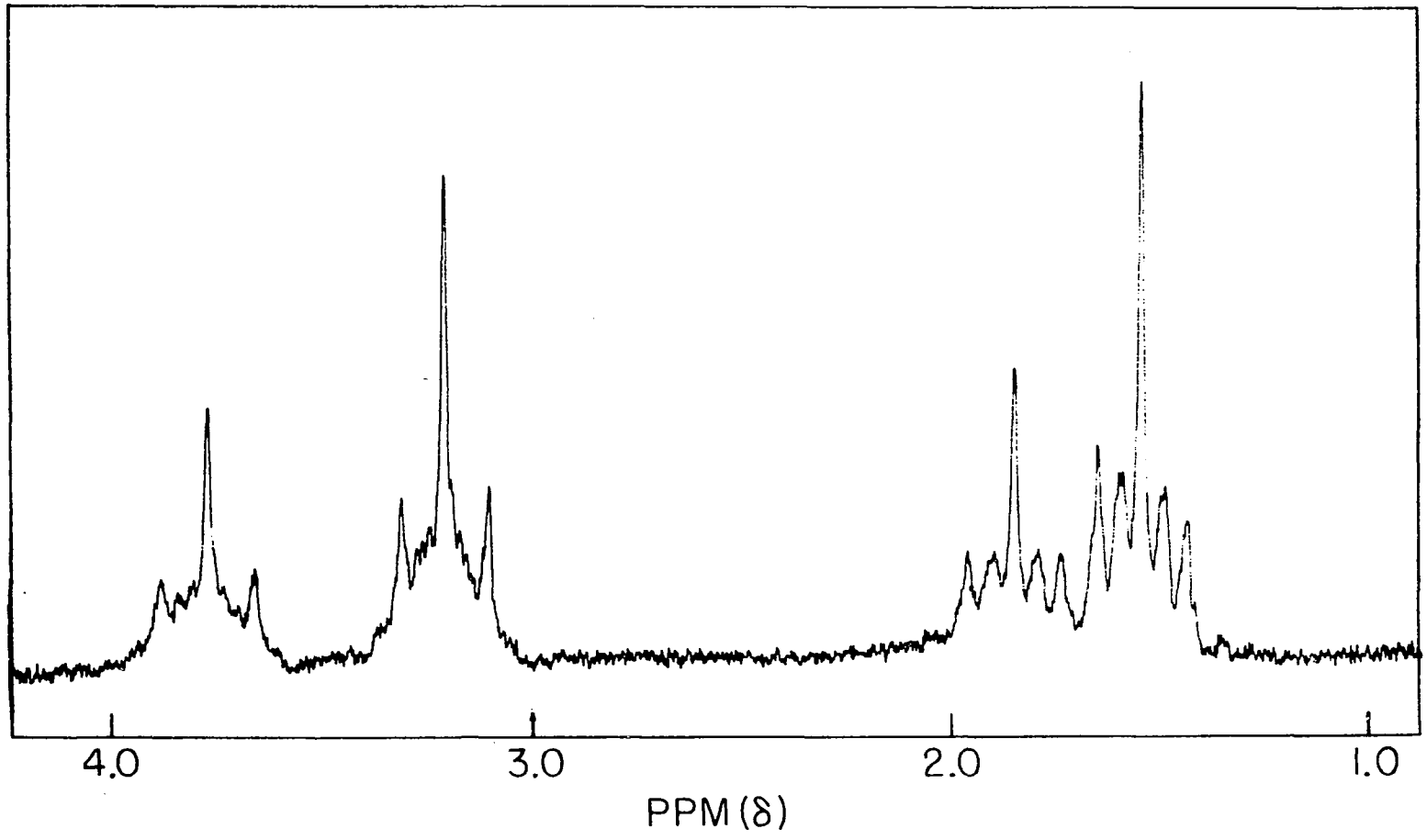

Figure 3. ^{1}H nmr spectrum of a saturated solution of $Ta_2Cl_6(SC_4H_8)_3$ in benzene

A similar distribution of three dialkyl sulfide ligands was proposed for $Rh_2(CH_3)_4I_2(S(CH_3)_2)_3$ as early as 1966 on the basis of nmr data (60). A later x-ray structure confirmed the dimeric nature of the rhodium species with the ligands located as predicted (61). In the rhodium dimer the terminal dimethyl sulfide ligands exhibited proton resonances as a doublet at δ 2.45 due to ^{103}Rh (I = 1/2) coupling. The bridging dimethyl sulfide resonance was only one half as intense as the terminal resonance and existed as a triplet due to coupling to two equivalent metal atoms. Thus the nuclear spin of one half for the one hundred per cent naturally abundant ^{103}Rh isotope considerably simplified interpretation of the nmr spectrum where doublet and triplet splitting patterns resulted from coupling to one and two rhodium atoms, respectively. The location of the bridging dimethyl sulfide resonance was indeed lower than the terminal resonance, δ 2.53 compared to the aforementioned δ 2.45, but the difference of only 0.08 ppm was considered a small shift. The methyl protons of dimethyl sulfide produce one sharp singlet in deuteriochloroform at δ 2.14 (62), so one can gauge the impact of coordination of the sulfur atom on the methyl proton chemical shift to range from 0.3 to 0.4 ppm in the rhodium dimer case. It should be noted that Rh(III) has a d^6 configuration which is incompatible with metal-metal bond formation, and indeed the separation reported in the structure communication was a long 3.38Å between rhodium atoms in the dimer.

In analyzing the nmr spectrum of the tantalum complex it was possible to extend the rhodium dimer interpretation in order to account for the observed multiplicities and intensities even though no metal-proton coupling was observed. The intensity ratio of one to two for both the two low field triplets and the two upfield quintets was entirely consistent with a tantalum dimer analogous to the rhodium dimer, where all the uninegative ligands present in the rhodium case are replaced by halide ions and tetrahydrothiophene ligands replace dimethyl sulfide. The observed downfield shift of the bridging tetrahydrothiophene resonances is consistent with an inductive effect removing electron density from the methylene protons as the sulfur lone pair electrons are donated into metal-ligand bonds. The formation of two dative bonds from the bridging ligand would remove more electron density than the single bond formed by the terminal sulfides. Thus the difference of 0.56 ppm between bridging type b and terminal type b chemical shifts can be satisfactorily explained. Such a rationalization tends to overlook the similarity of chemical shifts found for bridging and terminal dimethyl sulfide ligands in the rhodium dimer, where a difference of 0.08 ppm was observed. It is tempting to speculate that vacant d-orbitals on the sulfur atom are available for backbonding in both dimers, but only in the electron rich rhodium species is there a significant electron density shift back to the donor atom from the metals. In the d^2 case of the tantalum dimer the metal valence electrons are

stabilized by the bonding interactions between the metals, thus decreasing further any chance of back donation. The rhodium d^6 system could, on the other hand, neutralize the inductive effect of the σ-bond electron donation from sulfur by back-bonding to the dimethyl sulfide ligand through a π-interaction. The observation that the chemical shift of dimethyl sulfide methyl protons changes less upon coordination to rhodium for both bridging and terminal ligands than the type b methylene proton resonance of tetrahydrothiophene changes upon coordination in either a bridging or terminal position of the tantalum dimer is consistent with the hypothesis that the total electron withdrawal from the sulfide ligand is less in the rhodium dimer.

The clear separation of the upfield quintets in $Ta_2Cl_6(SC_4H_8)_3$ is somewhat unexpected in view of the distal location of the type a methylene protons relative to the metal-sulfur interaction. The resolution of these two quintets in the tantalum dimer contrasts the overlapping multiplet present in the niobium spectrum as seen in Figure 4. Thus the nmr data leads one to conclude that the type a methylene protons of the bridging tetrahydrothiophene communicate more intimately with the sulfur-metal dative bonds in the tantalum case than in the niobium case. Although it is possible that dissimilarities in the metal atomic orbitals are responsible for the difference in behavior no highly plausible explanation has been uncovered. The relevant proton magnetic resonance data is summarized in

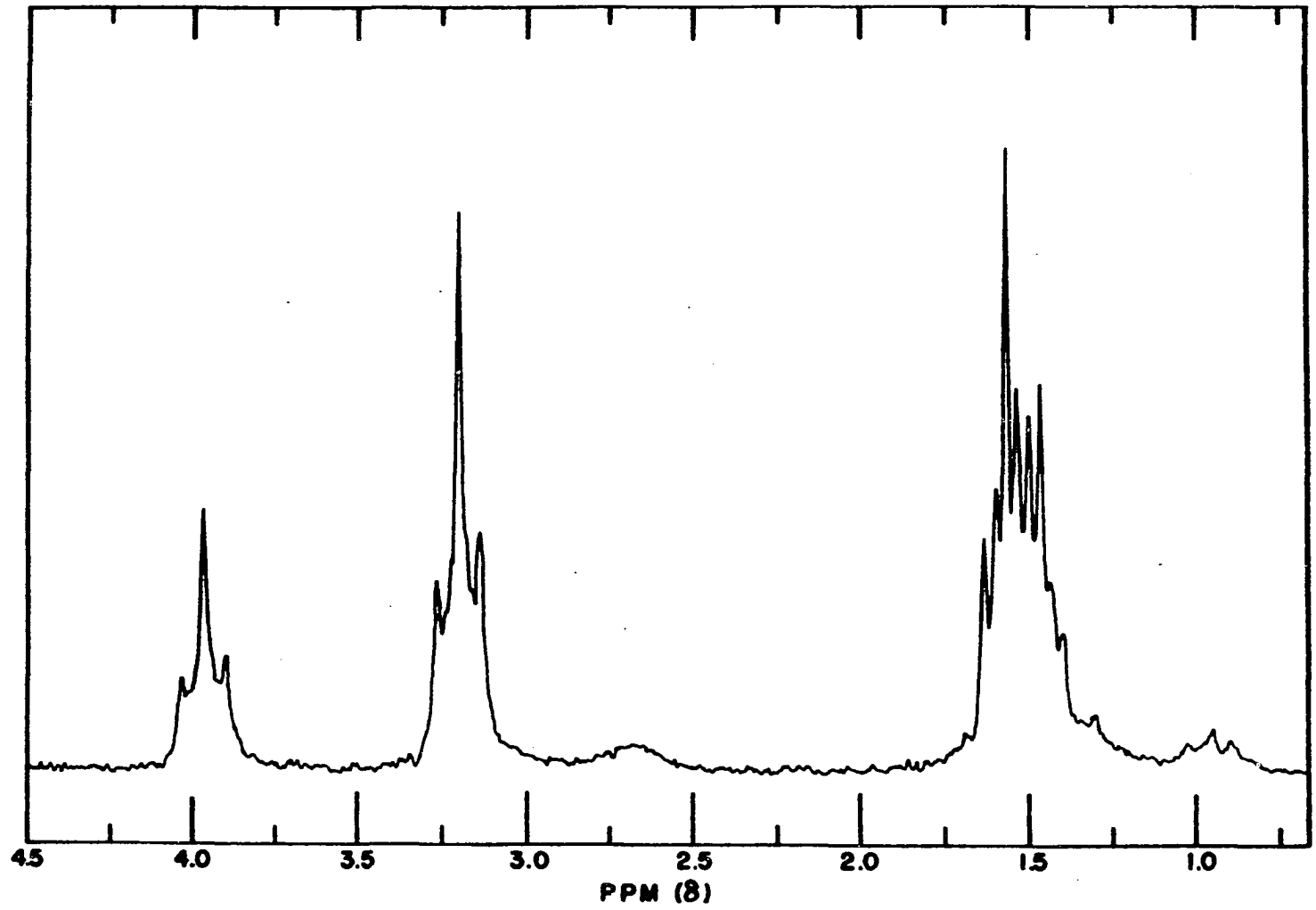

Figure 4. ^{1}H nmr spectrum of a saturated solution of $Nb_2Cl_6(SC_4H_8)_3$ in benzene

Table 1 for both $Ta_2Cl_6(SC_4H_8)_3$ and $Ta_2Br_6(SC_4H_8)_3$.

Magnetic Susceptibility

The Faraday method was utilized to determine the room temperature susceptibilities of the two tantalum dimers in the solid state. The results are listed in Table 2 where the magnetic susceptibility of $Nb_2Cl_6(SC_4H_8)_3$ is listed for comparative purposes. The observation of well resolved nuclear magnetic resonance spectra indicated the absence of paramagnetic species and indeed the bulk susceptibility of the dimers was found to be diamagnetic overall. A diamagnetic correction factor based on Pascal's constants was applied to the observed susceptibility (63) and the resultant was a small paramagnetic contribution. Such a small positive susceptibility was similar to that of $Nb_2Cl_6(SC_4H_8)_3$ as established by a temperature dependent study. By analogy with the niobium case this value of the corrected susceptibility was attributed to temperature independent paramagnetism. This interpretation is consistent with a diamagnetic ground state in which all of the electrons are paired while an admixture of excited states via quantum mechanical perturbation theory introduces a small amount of paramagnetism. This paramagnetism is distinguished from unpaired electrons by the lack of temperature dependence. Although the corrected susceptibility values are small in magnitude and therefore have fairly large relative errors associated with them the expected trends are nonetheless observed. An

Table 1. Proton magnetic resonance data for $Ta_2X_6(SC_4H_8)_3$[a]

	X = Cl	X = Br	
Assignment	δ[b]	δ[b]	Relative intensity
	1.39	1.39	
	1.45	1.45	
type "a", terminal	1.51	1.50	2
	1.54	1.55	
	1.60	1.60	
	1.69	1.86	
	1.75	1.91	
type "a", bridging	1.80	1.98	1
	1.85	2.03	
	1.91	2.09	
	3.09	3.19	
type "b", terminal	3.21	3.30	2
	3.30	3.41	
	3.65	4.02	
type "b", bridging	3.77	4.11	1
	3.88	4.23	

[a]Spectra obtained from saturated benzene solution at ambient temperatures.

[b]Chemical shifts are relative to TMS in ppm.

Table 2. Magnetic susceptibility data[a]

Compound	$10^6\chi_{app}$	$10^6\chi_M$	$10^6\chi_D$	$10^6\chi_{cor}$
	emu/g	emu/mole	emu/mole	emu/mole
$Ta_2Cl_6(SC_4H_8)_3$	-.33	-276	-371	+95
$Ta_2Br_6(SC_4H_8)_3$	-.24	-254	-431	+177
$Nb_2Cl_6(SC_4H_8)_3$[b]	-.28	-187	-380	+193

[a]Solid samples were used for susceptibility measurements. Abbreviations: χ_{app} = apparent susceptibility per gram; χ_M = molar susceptibility = molecular weight times apparent susceptibility; χ_D = calculated diamagnetic susceptibility per mole; χ_{cor} = corrected susceptibility = χ_M-χ_D.

[b]Data taken from reference 53.

inverse energy separation dependence is predicted by perturbation theory, because the excited paramagnetic state contribution to the ground state is inversely proportional to the energy difference between the two states. Chloride ion typically exhibits greater ligand field strength than bromide and the third row transition metals are known to undergo larger energy splittings than first or second row metals, so the qualitative energy predictions are consistent with the measured magnitudes of the temperature independent paramagnetism: $Ta_2Cl_6(SC_4H_8)_3$ has a smaller value than $Ta_2Br_6(SC_4H_8)_3$ and $Ta_2Cl_6(SC_4H_8)_3$ has a smaller value than $Nb_2Cl_6(SC_4H_8)_3$. The diamagnetic behavior of the tantalum dimers could be interpreted as a direct consequence of metal-metal bonding in which the four metal valence electrons are paired; other consistent interpretations are possible, but the nmr data discussed previously in conjunction with later characterizations confirm the metal-metal double bond hypothesis.

Electronic Spectra

Electronic spectra of $Ta_2Cl_6(SC_4H_8)_3$ and $Ta_2Br_6(SC_4H_8)_3$ were obtained in benzene solutions. Band maxima and extinction coefficients are listed in Table 3 as well as the corresponding data for $Nb_2Cl_6(SC_4H_8)_3$ and $Nb_2Br_6(SC_4H_8)_3$ for comparative purposes. Although it would be satisfying to draw a molecular orbital diagram and assign the experimentally observed transitions, in truth there is sufficient data such that only a few

Table 3. Electronic absorption band parameters[a]

$Ta_2Cl_6(SC_4H_8)_3$		$Ta_2Br_6(SC_4H_8)_3$		$Nb_2Cl_6(SC_4H_8)_3$[b]		$Nb_2Br_6(SC_4H_8)_3$[b]	
ν,kK[c]	ε[d]	ν,kK[c]	ε[d]	ν,kK[c]	ε[d]	ν,kK[c]	ε[d]
9.5	17	8.5	22	9.1	3	8.0	3
11.0	29	9.6	28	11.5	5	10.5	8
14.8	300	13.6	320	13.1	8	11.9	11
20.5	4000	19.4	5300	18.4	430	17.4	600

[a]Spectra obtained in benzene solutions.

[b]Data taken from reference 53.

[c]1kK = 1000 cm^{-1}.

[d]Molar extinction coefficients are in units of $\ell mole^{-1}cm^{-1}$.

generalizations can be safely expounded.

The similarity among the four spectra is quite striking, and it therefore seems highly probable that the gross electronic structure of all four is the same. The spectrochemical relationship between chloride and bromide mentioned in regard to temperature independent paramagnetism is again evident in the electronic spectra. The energy level separations show a clear trend in both the tantalum and niobium compounds to increase from bromide to chloride, as well as exhibiting the expected tendency towards larger energy spacings for tantalum than for niobium.

The extinction coefficients show similar trends for corresponding bands in both metal species, that is, they vary in tandem, but one quickly notes that the absolute values differ greatly. The tantalum compounds regularly exhibit extinction coefficients almost an order of magnitude larger for comparable wavelength absorptions than the niobium analogs. While no quantitative explanation has been forthcoming, it seems likely that the increased value of the spin-orbit coupling constant for tantalum, a third row transition metal, as compared to niobium, a member of the second row, must play an important role in determining the oscillator strength of electronic transitions.

A few further comments concerning the magnitude of the extinction coefficients and the likely origins of the observed transitions are in order. For an isolated octahedral complex

electronic transitions within the d-orbital manifold are Laporte forbidden due to the inversion symmetry inherent in the d-orbitals themselves. Such Laporte forbidden bands are typically found to have extinction coefficients on the order of 10 $\ell mole^{-1}cm^{-1}$, largely due to intensity resulting from vibronic coupling. Bands that are also spin forbidden ($\Delta S \neq 0$) in such monomeric octahedral complexes are found to be perhaps 100 times less intense than the spin allowed transitions, so that extinction coefficients might be on the order of 0.1 $\ell mole^{-1}cm^{-1}$. In spectra recorded for the dimeric tantalum species the smallest extinction coefficient is 17 $\ell mole^{-1}cm^{-1}$ and the values range upward to 5300 $\ell mole^{-1}cm^{-1}$ for the 19.4 kK band in $Ta_2Br_6(SC_4H_8)_3$. This range of intense absorptions is consistent with a metal-metal interaction which destroys the applicability of simple monomeric selection rules. Indeed metal clusters are commonly highly colored, and the reason cited most frequently is the effective overlap of the metal d-orbitals to form molecular orbitals which by their parentage encompass the highest occupied molecular orbital and the lowest unoccupied molecular orbital. It then follows that electronic transitions will ordinarily be limited to this arena of metal-metal interactions. The incorporation of atomic orbitals from both metal atoms into molecular orbitals eliminates the Laporte restrictions which determine the oscillator strength in monomeric complexes, and the result is more intense absorption bands. One could speculate that the two lowest energy bands

with extinction coefficients near 20 $\ell mole^{-1}cm^{-1}$ are spin-forbidden and gain intensity via spin-orbit coupling, although there is no firm basis for such a conclusion. The two transitions at higher energy could then be interpreted as spin-allowed with the observed 10 to 100-fold increase in intensity in agreement with theoretical predictions.

Nuclear Quadrupole Resonance

Nuclear quadrupole resonance spectra of the halogen nuclei were successfully obtained for both tantalum(III) dimers under investigation. Although no attempt will be made to present the theory of nuclear quadrupole resonance (nqr) spectroscopy, it will be necessary to introduce several terms and equations in order to discuss the results at hand. Excellent books concerning the theory and instrumentation of nqr have been written by Lucken (64) and Das and Hahn (65).

The interaction between a non-spherical nucleus with an electric quadrupole moment (eQ) and an inhomogeneous electric field gradient due to the asymmetry of surrounding electrons (eq) establishes nondegenerate nuclear spin states. A Boltzmann distribution accurately describes the unperturbed ground state, and these nuclear spin states differ only slightly in energy so radiofrequency radiation is appropriate for absorption spectroscopy. The field gradient is a traceless tensor and it is therefore adequately described by only two parameters after diagonalization. The two quantities q and η,

as defined in Equations 1 and 2, completely define the electric field gradient since Equation 3 imposes a third constraint on the three variables. The asymmetry parameter η varies between

$$q \equiv \frac{\partial^2 V}{\partial z^2} \tag{1}$$

$$\eta \equiv \left(\frac{\partial^2 V}{\partial x^2} - \frac{\partial^2 V}{\partial y^2}\right) / \frac{\partial^2 V}{\partial z^2} \tag{2}$$

$$\frac{\partial^2 V}{\partial x^2} + \frac{\partial^2 V}{\partial y^2} + \frac{\partial^2 V}{\partial z^2} = 0 \tag{3}$$

limits of 0 and 1 and serves as a gauge to the extent of distortion of the electric field gradient from axial symmetry.

Both ^{35}Cl and ^{37}Cl have a nuclear spin of 3/2, as do ^{79}Br and ^{81}Br, all accompanied by a nonzero nuclear quadrupole moment. A single transition from the degenerate $\pm$ 1/2 energy levels to the degenerate $\pm$ 3/2 levels can therefore theoretically be observed for any chlorine or bromine atom with a nonzero electric field gradient in a crystalline solid. The energy levels for a nuclear spin of 3/2 (I = 3/2) can be written in closed form for the most general case (64) as listed in Equations 4 and 5.

$$E_{\pm 3/2} = \frac{3e^2Qq}{4I(2I-1)}\left(1+\frac{\eta^2}{3}\right)^{1/2} = \frac{e^2Qq}{4}\left(1+\frac{\eta^2}{3}\right)^{1/2} \tag{4}$$

$$E_{\pm 1/2} = \frac{-3e^2Qq}{4I(2I-1)}\left(1+\frac{\eta^2}{3}\right)^{1/2} = \frac{-e^2Qq}{4}\left(1+\frac{\eta^2}{3}\right)^{1/2} \tag{5}$$

The frequency of energy absorbed in a transition from m = $\pm$ 1/2 to m = $\pm$ 3/2 will then be determined by the difference in the above energy levels and Planck's well-known relationship, $\Delta E = h\nu$. In the axially symmetric case $\eta = 0$ and the transition

$$\Delta E = \frac{e^2Qq}{2}(1+\frac{\eta^2}{3})^{1/2} \tag{6}$$

$$\nu = \frac{e^2Qq}{2h}(1+\frac{\eta^2}{3})^{1/2} \tag{7}$$

frequency equation reduces to $\nu = e^2Qq/2h$. It should be noted that Q is a constant for a given nucleus so the only variables in any particular case will be q and η. Since only one experimental value is obtained for nuclei with 3/2 spin the magnitudes of q and η cannot be determined in the general case, but if η is zero due to symmetry imposed axial equivalence then q is easily calculated from the observed transition frequency.

Table 4 lists the resonance frequencies found for chlorine nuclei in $Ta_2Cl_6(SC_4H_8)_3$ and bromine nuclei in $Ta_2Br_6(SC_4H_8)_3$. Identification of all the reported resonances was confirmed by location of the mated resonance, either ^{37}Cl or ^{79}Br, at the frequency calculated on the basis of the ratio of the nuclear quadrupole moments, $Q_{^{79}Br}/Q_{^{81}Br} = 1.1971$ and $Q_{^{35}Cl}/Q_{^{37}Cl} = 1.2688$ (66).

A survey of the six resonances in the $Ta_2Br_6(SC_4H_8)_3$ case divides the absorptions into two types based on the frequency differences. The four lowest frequency values span a range of 1.92 MHz and the two high energy absorptions differ by 2.47

Table 4. Nuclear quadrupole resonance data for $Ta_2Cl_6(SC_4H_8)_3$ and $Ta_2Br_6(SC_4H_8)_3$

Compound	Isotope	Frequency (MHz)	Assignment
$Ta_2Cl_6(SC_4H_8)_3$	^{35}Cl	9.230	terminal
		9.286	terminal
		9.356	terminal
		10.321	bridging
		10.623	bridging
$Ta_2Br_6(SC_4H_8)_3$	^{81}Br	62.78	terminal
		63.22	terminal
		63.83	terminal
		64.70	terminal
		71.47	bridging
		73.94	bridging

MHz while a much larger gap, 6.77 MHz, separates the two types. Such a distribution of energies can be clarified by examining not only nonequivalent atoms on the molecular level, but also the nonequivalency of atoms based only on their positions in the solid state lattice. The lattice contribution to the electric field gradient is expected to be small relative to the effects of molecular nonequivalences, and the multiplicity and spacing of the lines observed in $Ta_2Br_6(SC_4H_8)_3$ lends itself to interpretation on this basis. For early transition metal halides containing both terminal and bridging halogens the bridging halogens typically absorb energy at a higher frequency than the terminal halogens. One can thus visualize a confacial bioctahedral structure for $Ta_2Br_6(SC_4H_8)_3$, such as was described in analyzing the pmr spectrum, and the four terminal bromides and the two bridging bromides correspond in an enticing 1:1 fashion with the observed nqr spectrum. The magnitude of the frequency variations between the groups of four and two clearly distinguish between the terminal and bridging halogen ligands, and this furnishes a key piece of evidence in unraveling structural possibilities. The hope of profitable extension of this type of nqr analysis to other solid metal halide compounds that are often difficult to characterize by classical techniques is promoted by these results.

The x-ray structure of $Ta_2Br_6(SC_4H_8)_3$ later confirmed the nqr interpretation as only one independent dimer was found in the unit cell and hence the multiplicities were correct for

both chemically nonequivalent atoms and chemically equivalent atoms in nonequivalent lattice positions.

The analysis of the nqr spectrum of $Ta_2Cl_6(SC_4H_8)_3$ is similar although the multiplicities are not quite so neatly related to the molecular confacial bioctahedral structure. The frequency distribution is again clearly indicative of both terminal and bridging atoms with the three lower resonances separated by 0.13 MHz, then a gap of 0.94 MHz, and finally two resonances within 0.30 MHz. The two observed bridging resonances are consistent with one independent molecule per unit cell, but only three terminal resonances are observed while four would be predicted; certainly this is not a serious discrepancy.

The relative positions of bridging and terminal halogen resonances have been discussed by various authors in terms of the importance of back π-bonding from terminal halogen lone pair electrons into the vacant d-orbitals of the metal atom. An important consideration in any rationalization must be the reversal of positions for group III metal halide bridged dimers where the electric field gradient is larger for the terminal halogen atoms than for the bridging atoms (64). Without indulging in the rigors of a mathematical treatment it should be evident that the aluminum atoms in Al_2Br_6, for example, are incapable of accepting electron density from the unshared electron pairs present on the terminal bromines since the four available valence orbitals of Al are all fully

involved in σ-bonding to the ligands. The early transition metal dimers, on the other hand, have vacant valence d-orbitals which are appropriately located to participate in π-interactions with terminal halogens.

The existence of π-interactions has been documented for a series of hexahalometallates (67) and indeed the resonant frequencies of halogens are very responsive to the extent of electron donation from the unshared halogen electron pairs to the metal. A simple qualitative description of the origins of the electric field gradient clarifies the balance between σ and π contributions. The molecular coupling constant, $|e^2Qq|_{mol}$, can be related to the atomic coupling constant, $|e^2Qq|_{atom}$, by an "unbalanced p" factor designated as U_p. For the axially symmetric case the major contribution to the halogen electric field gradient comes from the p-orbitals electron occupancy and U_p is given by Equation 8, where N is the electron density of the orbital in question.

$$U_p = \frac{1}{2}(N_{px}+N_{py}) - N_{pz} \qquad (8)$$

The role of U_p can be illustrated by examining Cl^-, where all three p-orbitals are fully occupied and therefore $U_p = 0$, and Cl_2, where the occupancy of p_z is decreased to one as a result of the symmetrical σ-bond and hence $U_p = 1$. The experimental resonance frequency will thus vary from a theoretical value of zero for the spherically symmetric case to a value of 54.9 MHz for ^{35}Cl in the limiting case of a single nonpolar

σ-bond. If only σ-bonding were important in all cases the observed frequency would correlate directly with the bond polarity, but this is not the case. Since $|e^2Qq|_{mol}$ determines the nuclear quadrupole resonance frequency it is the difference in p_π and p_σ as reflected in N_{pz}, N_{px} and N_{py} which is crucial rather than the absolute magnitude of these components. Increased covalency in the metal-halogen σ-bond causes an increase in the nqr frequency, but increased π-bonding decreases the frequency. In the dimeric species studied here the lower frequencies observed for terminal halogens are probably attributable to increased π-donation from these ligands while the bridging ligands are dominated by σ-interactions only.

An interesting interplay between σ and π electron donation by halide ions is demonstrated nicely by a comparison of the nqr results for tantalum(V) halide dimers (68) with the tantalum(III) dimer results of this study. As the oxidation state of the metal increases greater covalency is expected in the metal-halogen bonds, or more crudely one can visualize a shift from chloride ion behavior towards chlorine-like bonding behavior. If only σ-bonding is important, as is the case for bridging halides, the higher oxidation state should promote higher frequency absorptions than the lower oxidation state due to the increased covalency of the σ-bond which effectively decreases N_{pz} and thereby increases U_p. A comparison of the bridging halogen resonance locations in Table 5 shows that such a variation occurs between Ta(V) and Ta(III). One also notices that

Table 5. Comparison of halogen nqr frequencies in Ta(III) and Ta(V) compounds[a]

Compound	$Ta_2Cl_6(SC_4H_8)_3$	Ta_2Cl_{10}	$Ta_2Br_6(SC_4H_8)_3$	Ta_2Br_{10}
Bridging ν(MHz)	10.321	13.334	71.47	90.13
	10.623	13.356	73.94	90.32
		13.377		90.43
Terminal ν(MHz)	9.230	7.598	62.78	55.02
	9.286	7.641	63.22	55.15
	9.356	7.663	63.83	55.28
		8.141	64.70	56.19
		8.231		56.69
		8.261		56.96

[a]Data for Ta_2Cl_{10} and Ta_2Br_{10} taken from reference 68; ^{81}Br frequencies were calculated from ^{79}Br frequencies by the division factor 1.1971, $\nu_{^{81}Br} = \nu_{^{79}Br}/1.1971$.

the terminal resonances display exactly the opposite behavior; they tend to decrease as the oxidation state of the metal is increased. The introduction of a significant π-contribution allows one to consistently explain this apparent paradox. Indeed N_{pz} will decrease for both terminal and bridging halogens as the metal is oxidized, but only for the terminal halogens will N_{px} and N_{py} also decrease as electron density is shared via the π-interaction. If the total change in π-donation exceeds the σ-donation change upon oxidation then U_p will actually decrease, and this is evidently the case for the terminal halogens in $Ta_2X_6(SC_4H_8)_3$ and Ta_2X_{10} (X = Cl, Br).

Infrared Spectra

Infrared spectra were obtained in the region of 700-1400 cm^{-1} utilizing salt plates and a Beckman IR-7 instrument suited for optimal operation over that range of energies while polyethylene sheets and a low energy Beckman IR-11 were employed for absorption spectra spanning energies from 100-700 cm^{-1}. It will be convenient to extend these arbitrary divisions into the discussion of the infrared data since metal-ligand vibrations will be limited to energies well below 700 cm^{-1} and most of the intraligand vibrations will be in the fingerprint region from 700 to 1400 cm^{-1}.

Table 6 lists the absorptions evident from 700 to 1400 cm^{-1} for the two tantalum dimers as well as data for other tetrahydrothiophene containing complexes of interest. It

Table 6. Tetrahydrothiophene infrared frequencies (700-1400 cm^{-1})[a]

SC_4H_8 (in CS_2)[b]	$Ta_2Cl_6(SC_4H_8)_3$	$Ta_2Br_6(SC_4H_8)_3$	$Nb_2Cl_6(SC_4H_8)_3$[c]	$Nb_2Br_6(SC_4H_8)_3$[c]	$NbCl_4(SC_4H_8)_2$[b]
		800 s(sh)			801 m
816 m	809 s	810 s	810 s	806 m-s	
					872 m
882 s	883 s	881 s	886 s	882 s	881 m
	956 s	958 s	959 s	958 m-s	960 m
	967 m	968 s	964 s		
996 s		999 vw			
		1023 w	1027 w-m(sh)	1021 w	1025 w
1035 w-m	1039 m	1038 m	1041 m	1037 w-m	1038 w
1060 w-m		1060 vw			
	1075 m	1073 m		1072 w-m	1075 w-m
	1082 w	1082 w	1083 m	1082 w	
1129 w-m	1126 s	1127 s	1129 s	1125 m-s	1128 w-m
	1128 s	1132 s(sh)			
		1189 w(sh)	1194 w-m(sh)		
1197 m	1200 m	1199 m	1203 m	1200 w	1193 w
1215 w(sh)	1214 w	1211 m	1214 m	1211 w-m	1214 w-m
			1248 m(sh)		
1256 s	1257 s	1255 s	1256 s	1252 m	1254 m
	1268 s	1268 s	1270 m-s	1267 m	1267 w-m
1308 w-m	1307 s	1306 s	1308 s	1306 s	1308 w-m
	1322 w	1320 w	1326 w		
		1329 w		1330 vw	

[a]Spectra obtained from Nujol mulls unless otherwise noted. Abbreviations: s, strong; m, moderate; w, weak; sh, shoulder.

[b]Reference 69.

[c]Reference 59.

should be noted that the only absorptions above 1400 cm^{-1} were those near 3000 cm^{-1} due to carbon-hydrogen stretching modes. The major conclusion to be drawn from these data is that, at least to the extent detectable via infrared measurements, tetrahydrothiophene is coordinated in a normal manner in these dimers. The term normal here is only meant to imply that the ligand retains its integrity while datively bonding through the sulfur atom.

A second and slightly more subtle observation involves the splitting of several infrared bands in the dimers, and particularly noteworthy is a comparison of data for $Ta_2Br_6(SC_4H_8)_3$ and $Nb_2Br_6(SC_4H_8)_3$. Four single bands in the niobium spectrum are split in the tantalum case, and it may be that whatever factors were operative in displacing the two quintets from one another in the nmr spectrum of the tantalum dimer also play a role in splitting the vibrational bands in the bridging and terminal ligands more clearly for tantalum than for niobium. Thus both the infrared and nmr data are consistent with the premise that the properties of bridging versus terminal tetrahydrothiophene vary more within the tantalum dimer than in the niobium analog.

Spectral data in the low frequency region offers the possibility of more information with regard to metal-ligand bond strengths, but positive identification of vibrational bands is inherently difficult and interpretation of the low frequency infrared data should be undertaken with considerable caution.

Table 7. Low frequency infrared data for $Ta_2Cl_6(SC_4H_8)_3$ and $Ta_2Br_6(SC_4H_8)_3$ (100-700 cm^{-1})[a]

$Ta_2Cl_6(SC_4H_8)_3$	$Ta_2Br_6(SC_4H_8)_3$
106 vw, v broad	124 m
120 s	172 m
130 m, broad	207 vs, sh
158 m	214 vvs
187 m, sharp	227 vs
204 w	238 s, sharp
213 w	331 m
226 m	477 w, broad
242 vw, broad	506 s, sharp
271 m	518 m
320 vvs	622 w
432 w, broad	642 vw
476 w	663 m, sh
510 s, sharp	670 s
517 m, sh	
627 w, sh	
646 w, sh	
664 s, sh	
669 s	

[a]Spectra obtained from Nujol mulls unless otherwise noted. Abbreviations: s, strong, m, moderate; w, weak; v, very; sh, shoulder.

The most definitive band assignment in this region is the C-S ring stretch which occurs at 683 cm^{-1} in the free tetrahydrothiophene molecule (70). Upon coordination this band shifts to somewhat lower frequencies, typically 660-670 cm^{-1} (69). A strong doublet is seen in both $Ta_2Cl_6(SC_4H_8)_3$ and $Ta_2Br_6(SC_4H_8)_3$ between 660 and 670 cm^{-1}; this splitting is probably due to slightly different C-S stretching frequencies for the bridging and terminal tetrahydrothiophene ligands. It was noted previously that several single bands in the 700-1400 cm^{-1} region in the niobium dimer were split in the tantalum case and the C-S stretch is another example of such behavior, further confirming the strong bonding present in the tantalum dimer tetrahydrothiophene bridge.

The identification of metal-halogen stretching bands can be made confidently in the region of 320 cm^{-1} for $Ta_2Cl_6(SC_4H_8)_3$ and 214 cm^{-1} for $Ta_2Br_6(SC_4H_8)_3$. The large dipole associated with these bonds is expected to absorb infrared radiation very effectively and hence the most intense bands in the low energy portion of the spectrum were assigned to metal-halogen vibrations. The tantalum(III) bromide containing dimer actually exhibits three strong bands in this region, 207, 214 and 227 cm^{-1}, which could all be attributed to metal-bromide stretching modes since the molecular C_{2v} symmetry is sufficiently low that more than three of the metal-halogen normal vibrations are infrared active. In the chloride dimer the band at 320 cm^{-1} is extremely broad and intense, but no struc-

ture is evident. The frequency ratio between 320 cm^{-1} and 214 cm^{-1} is appropriate for a change in mass from chloride to bromide with retention of similar force constants. The energy of a vibration theoretically changes as the square root of the mass ratio, and in this case $\sqrt{m_{Cl}/m_{Br}} = 1.5$ and 320 $cm^{-1}/214\ cm^{-1} = 1.5$.

Prudence dictates that no further bands be assigned in this region even though it would be quite informative to locate metal-sulfur vibrations for both bridging and terminal tetrahydrothiophene ligands as well as distinguish between bridging and terminal metal-halogen vibrations. Such definitive vibrational analyses seem inappropriate until further data is available. Particularly for the metal-sulfur stretching vibrations the amount of literature data is not sufficient to provide adequate data for interpretations based on comparable systems.

X-ray Structural Determination of $Ta_2Br_6(SC_4H_8)_3$

The x-ray structure determination of a single crystal of $Ta_2Br_6(SC_4H_8)_3$ successfully revealed the molecular configuration of the dimer. Crystals examined by precession and Weissenberg film techniques exhibited $\bar{1}$ Laue symmetry indicative of a triclinic space group. No systematic absences were observed. The unit cell parameters at ambient temperature were a = 12.08Å, b = 12.74Å, c = 8.98Å, $\alpha = 83.98°$, $\beta = 112.45°$, and $\gamma = 105.40°$.

A single crystal suitable for data collection was selected after recrystallization from toluene. Approximate dimensions of the crystal were 0.06x0.08x0.40 mm along the a, b, and c axes, respectively. Drybox techniques were used to mount the crystal in a Lindemann glass capillary with the needle (c) axis of the crystal parallel to the spindle axis. All data within a 2θ sphere of 45° were collected in each of four unique octants. A total of 3216 possible reflections were monitored.

The intensities of three standards were measured every fifty reflections during the data collection period. The intensities of these three standards uniformly decreased to twenty per cent of their original intensity before data collection was terminated. A linear least squares fit of intensities of the standard reflections versus the number of data points monitored was made using a weighting factor of $1/C_t$ for the intensities (C_t = total counts). The correlation coefficient was greater than 0.99 for each of the three plots indicating the validity of the fit. The average slope of I/I_o versus n (where I = intensity, I_o = initial intensity and n is the number of data points monitored) was $-2.47\text{x}10^{-4}$. Thus the data fit linear Equation 9 which can be rearranged to scale the data to the original intensity as expressed in Equation 10.

$$I/I_o = 1 - 2.47\text{x}10^{-4} \cdot n \qquad (9)$$

$$I_o = I/(1-2.47\text{x}10^{-4} \cdot n) \qquad (10)$$

The intensities were scaled by the factor $K(n) = (1-2.47x10^{-4}\cdot n)^{-1}$ before further data reduction. The error introduced by this scaling procedure can be incorporated into the expression for $[\sigma(I)]^2$ as follows:

$$[\sigma(I)]^2 = K^2C_t+K^2C_b+(C_t-C_b)^2\sigma_K^2+(0.3KC_t)^2+(0.3KC_b)^2$$

where K is the scale factor, σ_K is the absolute error in the scale factor, and C_b is the background count. The intensity data were also corrected for Lorentz-polarization effects. The estimated standard deviation in each structure factor, $\sigma(F_o)$, was calculated by the finite difference method (71). These standard deviations were used during the least-squares refinement to weight the observed structure factors where w, the weighting factor, was defined as $1/[\sigma(F_o)]^2$. Transmission factors ranged from 0.20 to 0.30 perpendicular to the needle axis based on a linear absorption coefficient of 198.9 cm^{-1}. The extensive data manipulation required to correct for crystal decay seemed more likely to limit the quality of the data than did absorption problems, and refinement was initiated without absorption corrections. Successful location and refinement of all nonhydrogen atoms confirmed the minor contribution of intensity variations due to absorption and no corrections were ever applied. A total of 1930 data points were used for refinement with corrected intensity $\geq 3\sigma(F)$.

Examination of the Patterson function, which was calculated from sharpened data, led to ready location of the two

asymmetric tantalum atoms present in each unit cell. The succeeding structure factor and electron density map based on the tantalum phasing allowed locations to be determined for the bromine and sulfur atoms and successive cycles led to location of the carbon atoms.

These positions were refined by full-matrix least-squares techniques (72). Anisotropic refinement of the non-carbon atoms led to a conventional discrepancy factor $R = \Sigma||F_o| - |F_c||/\Sigma|F_o| = 0.069$ and a weighted R factor of $R_w = [\Sigma w(|F_o| - |F_c|)^2/\Sigma w(F_o)^2]^{1/2} = 0.070$. The scattering factors were those of Hanson et al. (73), with tantalum, bromine, and sulfur modified for the real and imaginary parts of anomalous dispersion (74). The final positional and thermal parameters are listed in the Appendix along with their standard deviations as derived from the inverse matrix of the final least-squares cycle (75). The final values of F_o and F_c are also tabulated in the Appendix.

The molecular structure is depicted in Figure 5. Parameters of interest including bond distances, nonbonded intramolecular distances, and angles are listed in Tables 8, 9 and 10, respectively. The structure shown in the figures confirms the oxidation state of 3+ for each of the tantalum atoms in this complex. The earlier review of lower oxidation state tantalum compounds clearly established the significance of the first structural confirmation of a discrete tantalum(III) halide compound. The structure is best described as a con-

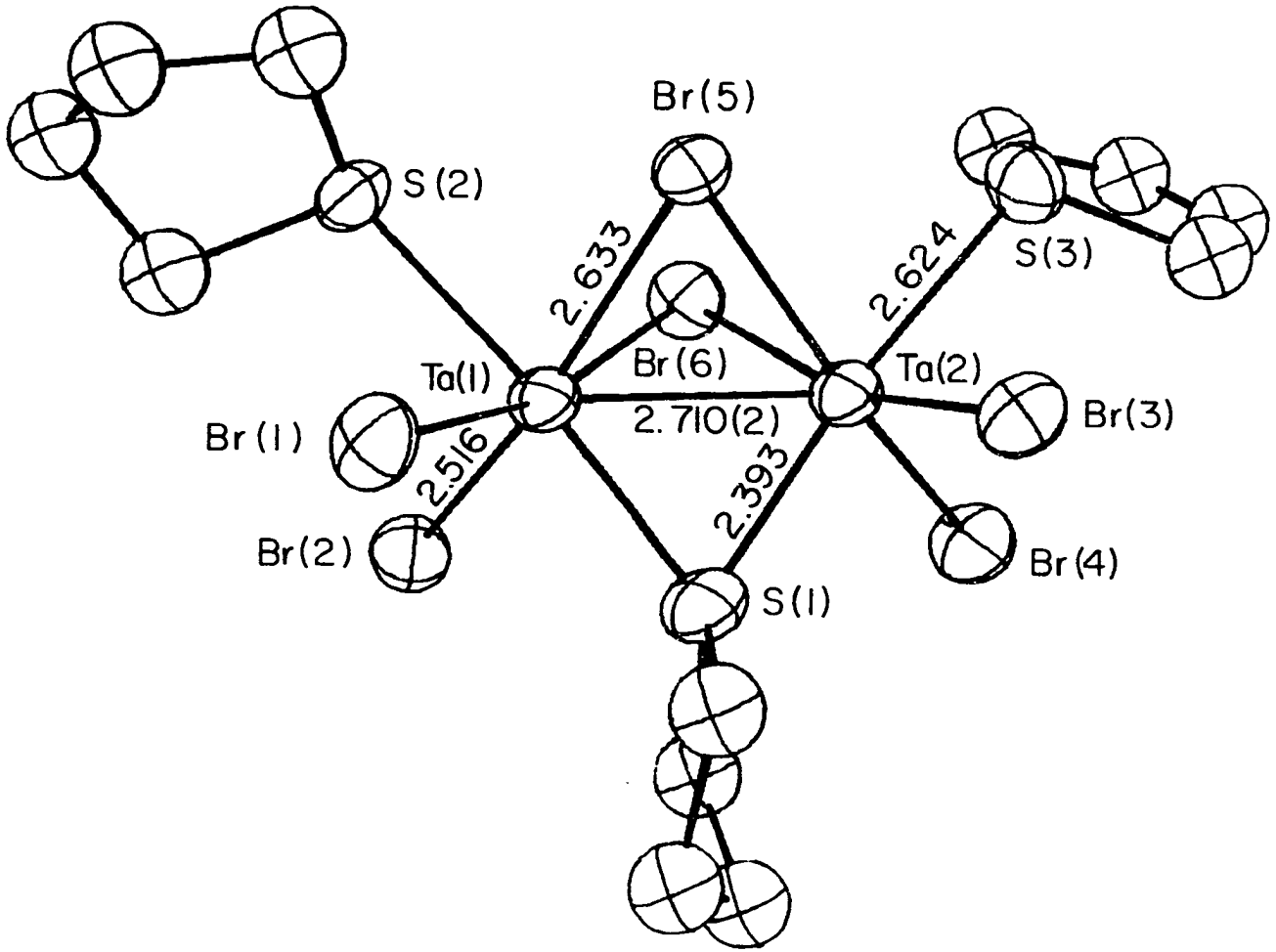

Figure 5. A perspective view of the 50% probability thermal ellipsoids of the $Ta_2Br_6(SC_4H_8)_3$ molecular unit

Table 8. Bond distances in $Ta_2Br_6(SC_4H_8)_3$, Å

Ta-Ta	2.710(2)
Ta(1)-Br(5)	2.611(3)
Ta(1)-Br(6)	2.647(4)
Ta(2)-Br(5)	2.630(3)
Ta(2)-Br(6)	2.643(5)
Average Ta-Br_{bridge}	2.633
Ta(1)-Br(1)	2.519(4)
Ta(1)-Br(2)	2.519(4)
Ta(2)-Br(3)	2.519(5)
Ta(2)-Br(4)	2.507(3)
Average Ta-$Br_{terminal}$	2.516
Ta(1)-S(1)	2.396(10)
Ta(2)-S(1)	2.390(10)
Average Ta-S_{bridge}	2.393
Ta(1)-S(2)	2.620(9)
Ta(2)-S(3)	2.627(10)
Average Ta-$S_{terminal}$	2.624
S(1)-C(1)	1.869(43)
S(1)-C(4)	1.901(35)
S(2)-C(5)	1.900(39)
S(2)-C(8)	1.840(37)
S(3)-C(9)	1.849(41)
S(3)-C(12)	1.825(59)
Average S-C	1.864
C(1)-C(2)	1.61(6)
C(2)-C(3)	1.37(7)
C(3)-C(4)	1.57(7)
C(5)-C(6)	1.53(5)
C(6)-C(7)	1.45(5)
C(7)-C(8)	1.60(5)
C(9)-C(10)	1.50(7)
C(10)-C(11)	1.31(9)
C(11)-C(12)	1.52(8)
Average C-C	1.50

Table 9. Nonbonded distances in $Ta_2Br_6(SC_4H_8)_3$, Å

Br(1)-Br(2)	3.848(6)
Br(3)-Br(4)	3.904(6)
Average $Br\text{-}Br_{terminal\text{-}terminal}$	3.876
Br(1)-Br(5)	3.686(5)
Br(3)-Br(5)	3.611(6)
Br(2)-Br(6)	3.626(6)
Br(4)-Br(6)	3.643(6)
Average $Br\text{-}Br_{terminal\text{-}bridging}$	3.642
$Br(5)\text{-}Br(6)_{bridging\text{-}bridging}$	3.298(5)
S(1)-Br(1)	3.438(9)
S(1)-Br(2)	3.507(12)
S(1)-Br(3)	3.455(11)
S(1)-Br(4)	3.458(11)
Average $S_{bridging}\text{-}Br_{terminal}$	3.465
S(1)-Br(5)	3.862(9)
S(1)-Br(6)	3.902(13)
Average $S_{bridging}\text{-}Br_{bridging}$	3.882
S(2)-Br(1)	3.539(12)
S(2)-Br(2)	3.509(9)
S(3)-Br(3)	3.366(13)
S(3)-Br(4)	3.622(10)
Average $S_{terminal}\text{-}Br_{terminal}$	3.509
S(2)-Br(5)	3.464(11)
S(2)-Br(6)	3.506(9)
S(3)-Br(5)	3.445(10)
S(3)-Br(6)	3.649(11)
Average $S_{terminal}\text{-}Br_{bridging}$	3.516

Table 10. Angles (degrees) within $Ta_2Br_6(SC_4H_8)_3$

Ta-bridge-Ta angles	
Ta(1)-Br(5)-Ta(2)	62.3(1)
Ta(1)-Br(6)-Ta(2)	61.6(1)
Ta(1)-S(1)-Ta(2)	69.0(3)
bridge-Ta-bridge angles	
Br(5)-Ta(1)-Br(6)	77.7(1)
Br(5)-Ta(2)-Br(6)	77.4(1)
Br(5)-Ta(1)-S(1)	100.8(3)
Br(5)-Ta(2)-S(1)	100.4(2)
Br(6)-Ta(1)-S(1)	101.3(3)
Br(6)-Ta(2)-S(1)	101.5(3)
Br-Ta-Br angles	
Br(1)-Ta(1)-Br(2)	99.6(2)
Br(3)-Ta(2)-Br(4)	102.0(2)
Br(1)-Ta(1)-Br(5)	91.9(1)
Br(2)-Ta(1)-Br(6)	89.1(1)
Br(3)-Ta(2)-Br(5)	89.0(1)
Br(4)-Ta(2)-Br(6)	90.0(2)
S-Ta-Br angles	
S(1)-Ta(1)-Br(1)	88.7(3)
S(1)-Ta(1)-Br(2)	91.0(3)
S(2)-Ta(1)-Br(5)	82.9(2)
S(2)-Ta(1)-Br(6)	83.5(3)
S(2)-Ta(1)-Br(1)	87.0(3)
S(2)-Ta(1)-Br(2)	86.1(2)
S(1)-Ta(2)-Br(3)	89.4(3)
S(1)-Ta(2)-Br(4)	89.8(2)
S(3)-Ta(2)-Br(5)	81.9(2)
S(3)-Ta(2)-Br(6)	87.6(3)
S(3)-Ta(2)-Br(3)	81.7(3)
S(3)-Ta(2)-Br(4)	89.7(2)
trans angles	
S(1)-Ta(1)-S(2)	174.4(3)
S(1)-Ta(2)-S(3)	170.8(4)
Br(5)-Ta(1)-Br(2)	163.7(2)
Br(5)-Ta(2)-Br(4)	165.1(2)
Br(6)-Ta(1)-Br(1)	166.6(1)
Br(6)-Ta(2)-Br(3)	163.9(1)

facial bioctahedron where the dimer can be visualized as two octahedra joined across a common trigonal face with the three bridging ligands equally shared. A distinctive feature of this particular confacial bioctahedron is the participation of one tetrahydrothiophene ligand in the bridge bonding; the other two sulfur ligands are trans to the unique sulfide on separate metal atoms. The confacial bioctahedral formulation is distorted from D_{3h} symmetry due to the presence of dissimilar ligands, notably three tetrahydrothiophene rings and six bromines. Disregarding the ring carbon atoms an effective symmetry of C_{2v} pertains to the dimer and this symmetry group will be appropriate for later molecular orbital considerations.

The tantalum-tantalum distance of 2.710(2)Å is consistent with the presence of a strong metal-metal bond, formally of bond order two since a total of four electrons are involved in the metal-metal interaction. The internuclear separation of 2.85Å in elemental tantalum metal serves as a point of reference, as do tantalum-tantalum distances of 2.88Å in $(Ta_6Cl_{12})^{2+}$, (43), 2.92Å in $(Ta_6Br_{12})^{2+}$ (43), and 2.96Å in $(Ta_6Cl_{12})^{4+}$ (76) where the average formal bond orders are 2/3, 2/3 and 7/12, respectively. The length of the metal-metal distance is the most commonly used criterion for bonding, but, as was noted in the introduction, other parameters may be equally informative in accurately depicting the strength of the interaction. Cotton and Ucko (77) have published a survey of metal-metal interactions in confacial bioctahedra of D_{3h} symmetry and the

moduli they present can be slightly modified and applied to the C_{2v} symmetry of the tantalum dimer.

Three moduli of general applicability described by Cotton and Ucko are derived from an idealized geometry involving two congruent octahedra joined to form a confacial bioctahedron; the bridging and terminal bonds are equal in length, the metal atoms lie in the center of their respective octahedra, all cis-ligands are 90.0° apart, and the symmetry is D_{3h} as a consequence of this construction. The moduli are then defined in terms of deviations from this idealized structure based on axial contraction or elongation due to metal-metal attraction or repulsion.

The displacement of metal atoms along the C_3-axis can be conveniently described by the ratio of d' to d" where d' is the distance from the plane of the three bridging atoms to the metal and d" is the distance from the plane of the three terminal atoms to the bonded metal atom. Structural parameters such as d' and d" are defined in Figure 6 for the case of a general confacial bioctahedron. In the idealized model d'/d" = 1.0, but there is no special chemical significance to this value of unity. In fact, the underlying repulsive forces that are inevitably present between two metal atoms require that a d' to d" ratio of one be associated with attractive metal-metal forces. For the tantalum dimer the three planes defined by ligands encircling the metal-metal axis are not parallel due to long bonds to the terminal tetrahydrothiophenes. The three

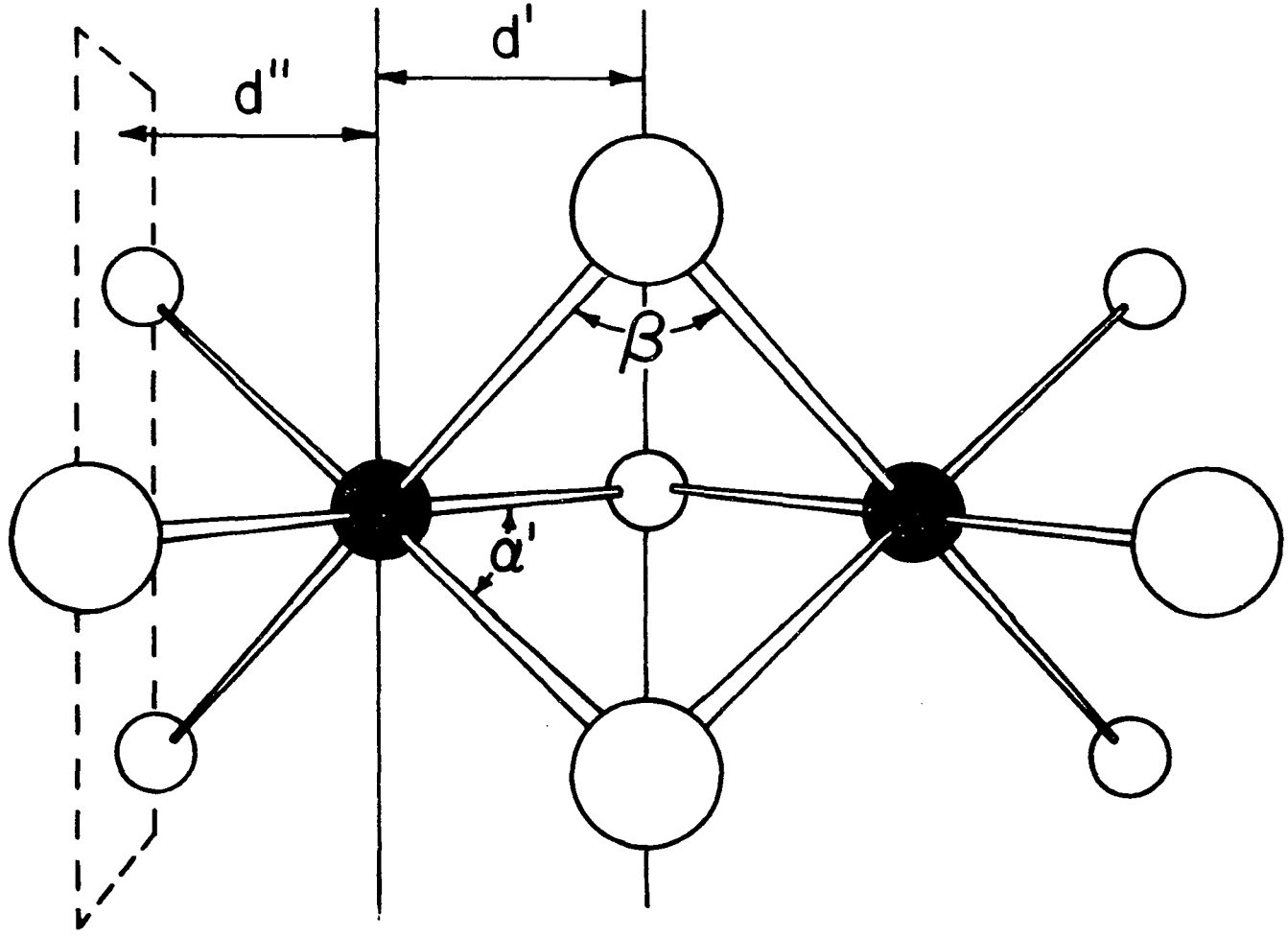

Figure 6. A general illustration of the confacial bioctahedral parameters d', d'', α', and β

bridging ligands do, however, define a plane perpendicular to and bisecting the metal-metal bond, and this reference plane allows one to calculate a d'/d" value based on the terminal bromide ligands. One can define a plane passing through the two terminal bromine atoms parallel to the central plane and the distances from the metal atom to these two planes are similar to the d" and d' defined by Cotton and Ucko. The central plane is 1.36Å from the tantalum atom and the terminal bromine plane is 1.32Å from the tantalum atom where the values listed are averages for the two ends of the dimer. The d'/d" value is 1.03 as calculated from the above figures, a result quite comparable to the value of 0.98 found in $Cs_3Mo_2Cl_9$ (78) where the formal metal-metal bond order is three.

The second and third parameters invoked are angular deviations resulting from axial distortions. The bridging ligand-metal-bridging ligand angle (α') is of course an undistorted 90.0° in the idealized bioctahedron, but as the dimeric species is axially distorted this angle will increase if the metal atoms approach more closely and decrease if elongation occurs. The quantity 90.0°-α' defines a parameter which should parallel the value of d'/d"; it should increase when d'/d" increases and decrease when d'/d" decreases. Another angular moduli can be based on the metal-bridging ligand-metal angle, β, which is 70.5° in the idealized case. The quantity β-70.5° should increase as d'/d" increases and thus one expects the same type of algebraic dependency on the metal-metal interaction for this

parameter as for d'/d" and 90.0°-α'. It should be stressed that the tantalum dimer is not a D_{3h} symmetry species and hence the above moduli are not rigorously applicable, but an examination of the various parameters as modified for C_{2v} symmetry is a valid and worthwhile exercise.

The β-70.5° criterion clearly indicates metal-metal attractive forces are present as all three values are negative: Ta(1)-Br(5)-Ta(2), -8.2°; Ta(1)-Br(6)-Ta(2), -8.9°; Ta(1)-S(1)-Ta(2), -1.5°. Although the presence of one bridging tetrahydrothiophene with metal-sulfur bonds 0.24Å shorter than the metal-bridging bromine bonds is a very large perturbation from D_{3h} symmetry and should not be overlooked, the magnitudes of the β-70.5° moduli presented still offer cogent insight into the force existing between the two metal atoms in $Ta_2Br_6(SC_4H_8)_3$. The average value of β-70.5° is -6.2°, again similar to the corresponding value for $Cs_3Mo_2Cl_9$ (78) of -6.0°.

The variance in 90.0°-α' is surprisingly large as a result of the tetrahydrothiophene occupying a unique position among the three bridging ligands. The four Br_{br}-Ta-S_{br} angles average 101.0° while the average of the two Br_{br}-Ta-Br_{br} angles is only 77.6° - a difference of 23.4° among angles which are equal in the D_{3h} case regardless of axial distortions. Accordingly, 90.0°-β is -11.0° for the four angles involving the bridging sulfur atom and +12.4° for the two angles involving only bridging bromine atoms. Such a wide variance prohibits interpretation based on axial contraction or elongation alone, although

the average of -3.2° for 90.0°-β is again indicative of metal-metal bonding and even compares favorably with the $Cs_3Mo_2Cl_9$ value of -4.2°.

The metal-bromine bond lengths vary as expected in that the average tantalum-bromine bridging distance is 0.12Å longer than the bonds to terminal bromines. This result is typical for species containing both bridging and terminal halogen atoms, as for example in Nb_2Cl_{10} where $Nb\text{-}Cl_{br}$ = 2.56Å and $NbCl_t$ = 2.25Å or 2.30Å depending on whether the terminal chlorine is <u>cis</u> or <u>trans</u> to a bridging chlorine (79).

The covalent radius of bromine has been reported to be 1.14Å (80), so assuming this value to be applicable to the tantalum-terminal bromine distance the covalent radius of tantalum in the dimer is 1.38Å by difference. A covalent radius of 1.02Å for sulfur then leads to a sum of 2.40Å for the metal-sulfur covalent radii. This value is 0.22Å less than the observed $Ta\text{-}S_t$ distance of 2.62Å, but agrees to within 0.01Å with the $Ta\text{-}S_{br}$ bond distance. This situation contrasts markedly with the halogen behavior where bridging bonds were considerably lengthened relative to terminal bonds.

Steric factors may be employed to account for the large discrepancy between $Ta\text{-}S_t$ and $Ta\text{-}S_{br}$ bond lengths. The four bromine atoms bound to each tantalum form a least-squares plane to within 0.01Å, but the metal-metal attraction pulls the tantalum atoms toward one another and out of their respective planes by 0.22Å and 0.21Å for Ta(1) and Ta(2), respec-

tively. The fact that nonbonded interactions are important in determining the tantalum-terminal sulfur distance is substantiated by noticing that the terminal sulfur atoms are hindered from closer approach to the tantalum atoms by repulsion of the four cis-bromine atoms in the plane which is 2.40Å (average) away from the sulfur atom. The average nonbonded contact distance between the terminal sulfur and the four bromine atoms is 3.51Å, which is already less than the sum of the van der Waals radii, 3.68Å. The van der Waals radius of bromine has been reported in the range of 1.8-2.0Å (80), but for our purpose the value of 1.85Å will be used for bromine and 1.83Å for sulfur (81) with the understanding that these numbers do not set absolute limits but rather guide one in surveying nonbonded distances. Some deviations from van der Waals radii constraints are expected in view of the dative bonding of unshared electron pairs of these ligands to the same metal atom, but it remains clear that steric repulsion makes it impossible for the terminal sulfur atoms to maintain a normal covalent bond distance to the displaced tantalum atom. Perhaps it is only coincidental that the terminal sulfur atoms are 2.40Å from the bromine plane and the tantalum-bridging sulfur distance is an almost identical 2.39Å.

The nonbonded distances within the molecular unit are generally in agreement with accepted values of van der Waals radii with one outstanding exception: the two bromines in bridging positions are within 3.30Å of each other. The

successful application of steric arguments in rationalizing the sulfur-metal bond lengths leads one to ponder the possibility of the bridging tetrahydrothiophene ligand repulsing the bridging halogens and thus causing the abnormally short bromine-bromine distance. The average distance of 3.88Å separating the bridging sulfur from the bridging bromines completely invalidates this hypothesis. All of the remaining eight cis-bromine-sulfur distances range from 3.37Å to 3.62Å so the bridging bromine-bridging sulfur separations are in fact 0.39Å longer than the 3.49Å average of the other comparable sulfur-bromine distances.

To satisfactorily explain this structural anomaly one must delve into the molecular orbital description of the dimer. The following analysis will involve a qualitative progression from an octahedral monomer to a D_{3h} confacial bioctahedral dimer and finally a descent to the effective C_{2v} symmetry of $Ta_2Br_6(SC_4H_8)_3$.

The molecular orbital scheme involving only σ-bonding to six equivalent ligands in an octahedral complex is frequently presented in inorganic texts. The diagram reproduced in Figure 7 is taken from Cotton's "Chemical Applications of Group Theory" (82). The basic points to be noted are listed below. The formation of six σ-bonding orbitals which will be filled by twelve electrons donated from the ligands results from the interaction of metal orbitals of symmetry a_{1g}, t_{1u} and e_g with linear combinations of ligand σ-orbitals of the same symmetry

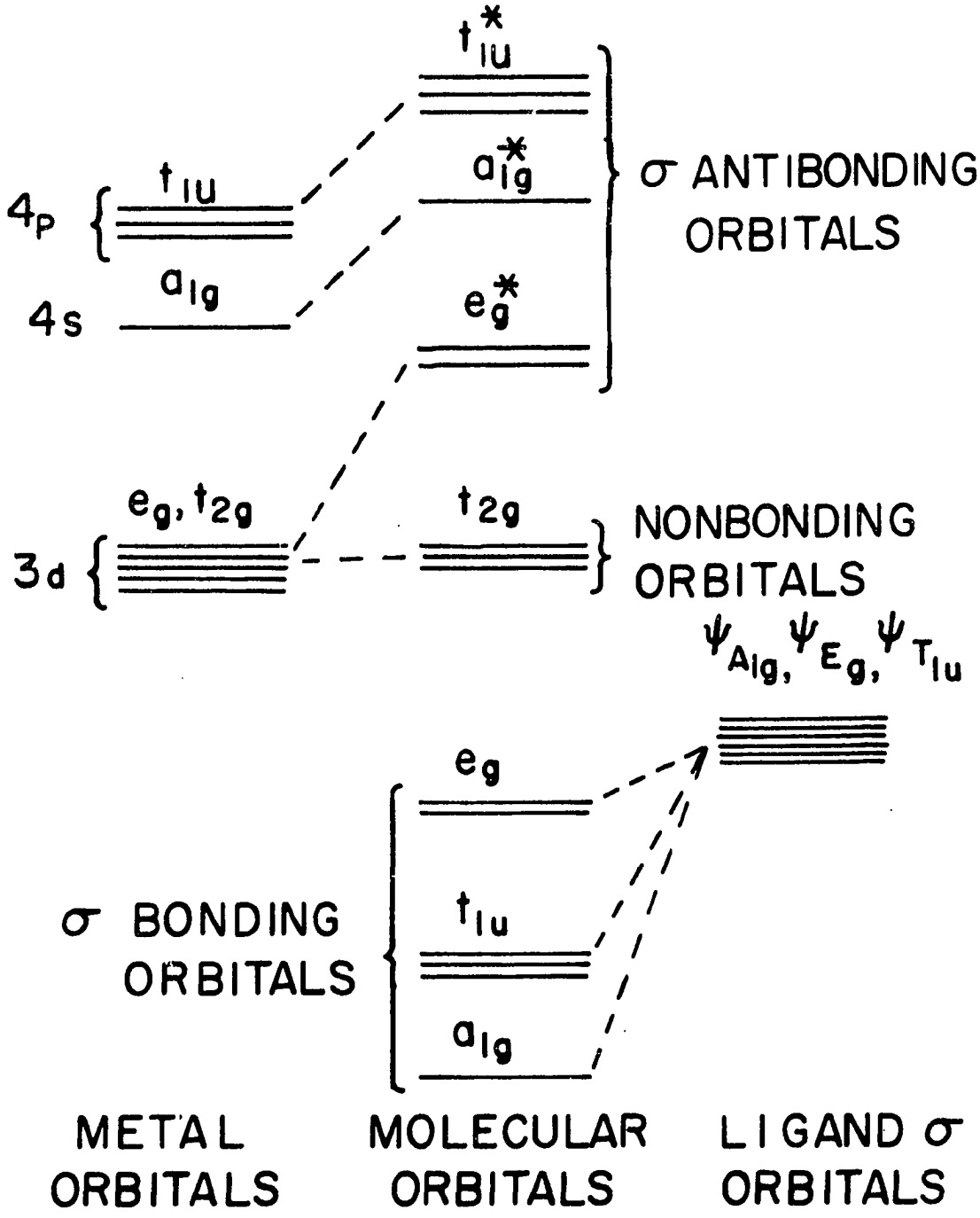

Figure 7. A molecular orbital diagram for an octahedral complex in which the ligands have no significant π interaction with the metal

representations. The two sets of molecular orbitals consisting largely of metal d-orbitals are split in energy since the t_{2g} metal orbitals are effectively nonbonding due to the absence of a t_{2g} representation among the ligand sigma symmetry combinations while the e_g representation, consisting largely of d_{z^2} and $d_{x^2-y^2}$, is raised in energy as a σ-antibonding orbital set. The number of electrons present in these orbitals is determined by the electronic configuration of the oxidized metal in the complex. For transition metals these orbitals will be partially filled and therefore these energy levels are the sites of chemical interest: the highest occupied molecular orbital and the lowest unoccupied molecular orbital. A hybrid orbital description involving sp^3d^2 orbital hybridization is similar to the molecular orbital scheme in that s, p_x, p_y, p_z, d_{z^2} and $d_{x^2-y^2}$ metal orbitals are utilized in σ-bonding to the ligands. The hybridization approach leaves the d_{xy}, d_{yz} and d_{xz} orbitals vacant except for nonbonding electrons remaining on the metal atom; the molecular orbital treatment produced similar results by forming high energy σ-antibonding orbitals which were energetically inaccessible with all of the metal valence orbitals except for these same three d-orbitals. The possible π-interaction between ligands with unshared electron pairs and the metal t_{2g} orbitals is symmetry allowed, but one can neglect such backbonding as at most a small perturbation of the σ-bonding structure.

Having established the σ-bonding scheme in an octahedral

complex one can progress to a molecular orbital description of the bonding in a confacial bioctahedron produced when two octahedral complexes merge along a trigonal face. The D_{3h} symmetry axes are defined in Figure 8 by X, Y, and Z, while x_i, y_i, and z_i refer to the axis of quantization for the metal orbitals on metal atom M_i. Although the reduction in symmetry from O_h to D_{3h} eliminates many of the restrictions which guide one in an analysis of bonding interactions, it seems logical that the σ-bonding structure will basically remain intact. The availability of two electron pairs for dative bonding from the bridging ligand to the two separate metal atoms allows the complex to retain a total of twelve σ-bonding orbitals during the imaginary convergence of six terminal ligands into three bridging ligands. These orbitals will be filled exclusively with ligand donated electrons just as in the octahedral monomer case. The symmetry representations of the twelve ligand sigma orbitals are $2a_1'+2a_2''+2e'+2e''$ and this corresponds in a one-to-one fashion with the representations of the s, p_x, p_y, p_z, d_{z^2} and $d_{x^2-y^2}$ orbitals on the two metal centers. Hence the formation of twelve σ-bonding orbitals and twelve σ-antibonding orbitals is symmetry allowed. Based on overlap considerations apparent in the octahedral instance the σ-bonding is formulated without inclusion of the d_{xy}, d_{xz}, and d_{yz} metal orbitals even though symmetry requirements no longer rigorously exclude these orbitals from entering into ligand σ-interactions. Figure 9 illustrates the D_{3h} symmetry representations appro-

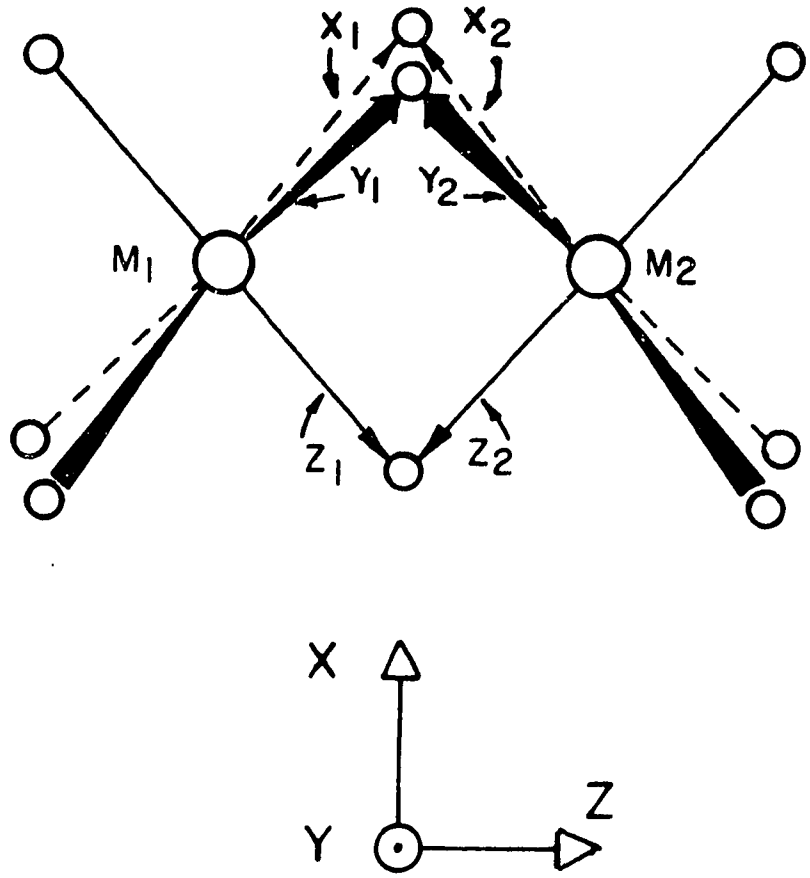

D_{3h} axes

D_{3h} Character Table

D_{3h}	E	$2C_3$	$3C_2$	σ_h	$2S_3$	$3\sigma_v$		
A_1'	1	1	1	1	1	1		x^2+y^2, z^2
A_2'	1	1	-1	1	1	-1	R_z	
E'	2	-1	0	2	-1	0	(x,y)	(x^2-y^2, xy)
A_1''	1	1	1	-1	-1	-1		
A_2''	1	1	-1	-1	-1	1	z	
E''	2	-1	0	-2	1	0	(R_x, R_y)	(xz, yz)

Figure 8. D_{3h} symmetry coordinates for a confacial bioctahedron

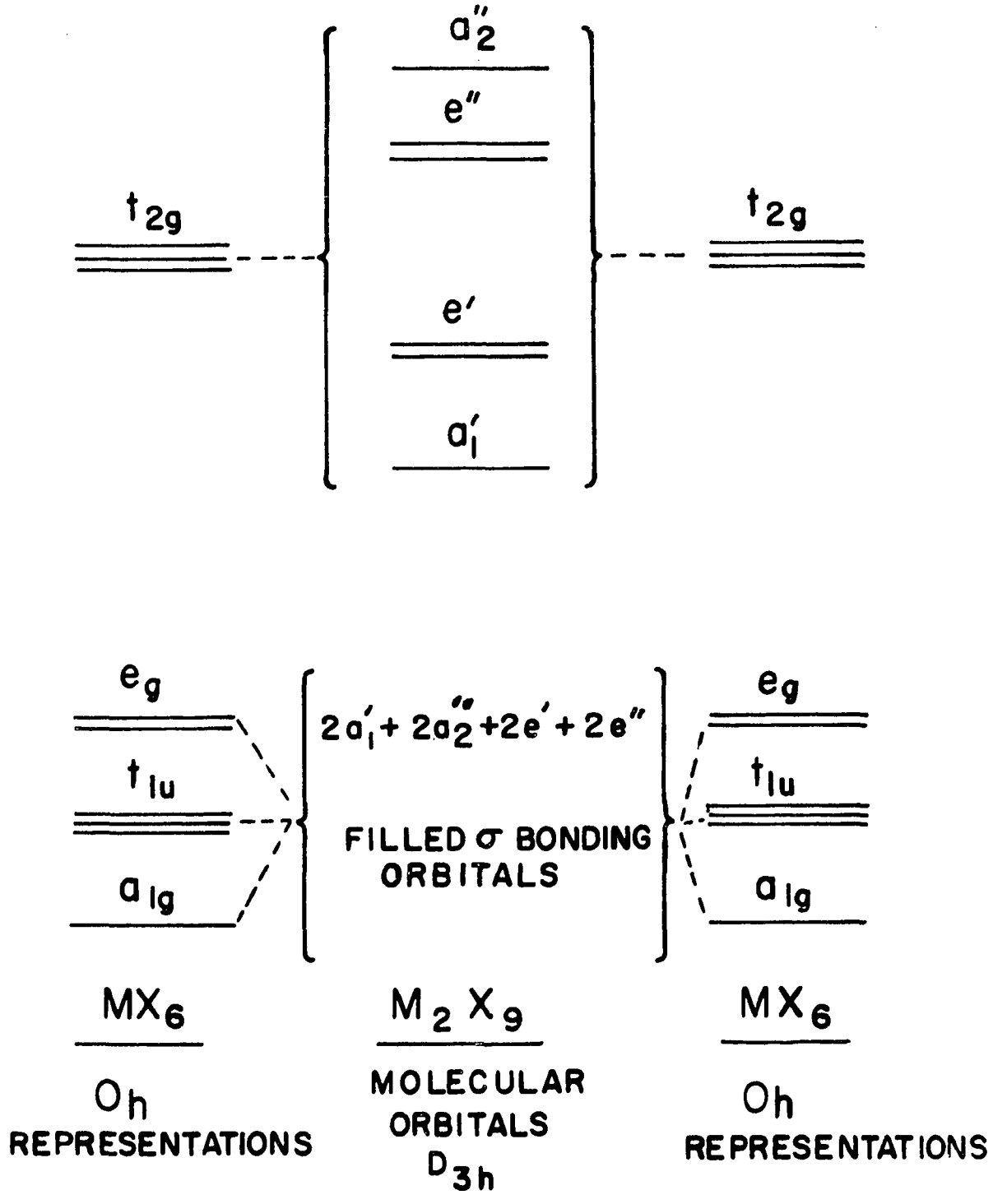

Figure 9. A molecular orbital diagram for a confacial bioctahedron of D_{3h} symmetry

priate for combining the electron-containing orbitals of two octahedral monomers along a trigonal face. As in the octahedral case the σ-bonding orbitals are low in energy and filled with electrons and the corresponding antibonding levels are quite high in energy; these high energy orbitals are vacant and they have been omitted from the diagram for purposes of clarity. This leaves the partially filled metal t_{2g} orbitals (in O_h symmetry) to interact in the center of the diagram to form a total of six molecular orbitals. The overlap between these metal d-orbitals will produce a sigma bonding molecular orbital of a_1' symmetry with an a_2'' antibonding mate and a degenerate set of e' π-bonding orbitals accompanied by an e'' antibonding set. The linear combinations of metal d-orbitals corresponding to these representations are listed below.

$$a_1'\{\frac{1}{\sqrt{6}}(d_{xy}(1)+d_{xz}(1)+d_{yz}(1)+d_{xy}(2)+d_{xz}(2)+d_{yz}(2))\} \quad (11)$$

$$a_2''^{*}\{\frac{1}{\sqrt{6}}(d_{xy}(1)+d_{xz}(1)+d_{yz}(1)-d_{xy}(2)-d_{xz}(2)-d_{yz}(2))\} \quad (12)$$

$$e'\begin{cases}\frac{1}{\sqrt{12}}(2d_{xy}(1)-d_{xz}(1)-d_{yz}(1)+2d_{xy}(2)-d_{xz}(2)-d_{yz}(2)) & (13)\\ \frac{1}{\sqrt{4}}(d_{xz}(1)-d_{yz}(1)+d_{xz}(2)-d_{yz}(2)) & (14)\end{cases}$$

$$e''^{*}\begin{cases}\frac{1}{\sqrt{12}}(2d_{xy}(1)-d_{xz}(1)-d_{yz}(1)-2d_{xy}(2)+d_{xz}(2)+d_{yz}(2)) & (15)\\ \frac{1}{\sqrt{4}}(d_{xz}(1)-d_{yz}(1)-d_{xz}(2)+d_{yz}(2)) & (16)\end{cases}$$

For our purposes the only orbital lobes of importance will be those capable of overlapping with similar orbitals on the partner metal atom and this immediately limits us to the d_{xy}, d_{xz}, and d_{yz} lobes directed between the bridging ligands towards companion lobes on the adjacent metal atom. The remaining three lobes of each of these d-orbitals are oriented away from the adjacent metal octahedron and no significant overlap is possible. Only the orbital lobes of importance in overlap considerations are shown in Figure 10 which illustrates the resultant metal-metal molecular orbitals. The energy levels can be ordered in a qualitative manner by examining overlap and nodal characteristics of the molecular orbitals. The a_1' representation has no nodes and maximum constructive overlap and it is doubtless the lowest energy orbital among these six. One node is present in each of the e' orbitals but the overlap is constructive and these will be lowered in energy relative to the initial uncombined orbital energies to form π-bonding molecular orbitals. Similar reasoning involving destructive overlap places the $a_2''^*$ representation highest in energy and the e''^* is clearly antibonding but lower than the $a_2''^*$ energy level.

In species isoelectronic with $K_3W_2Cl_9$ there are six metal valence electrons which fill the σ and two π bonding orbitals to forge a metal-metal bond of order three. The strength of the interaction varies widely from cases such as $K_3W_2Cl_9$ (83) where the bonding is quite robust (d(W-W)=2.41Å) to cases where

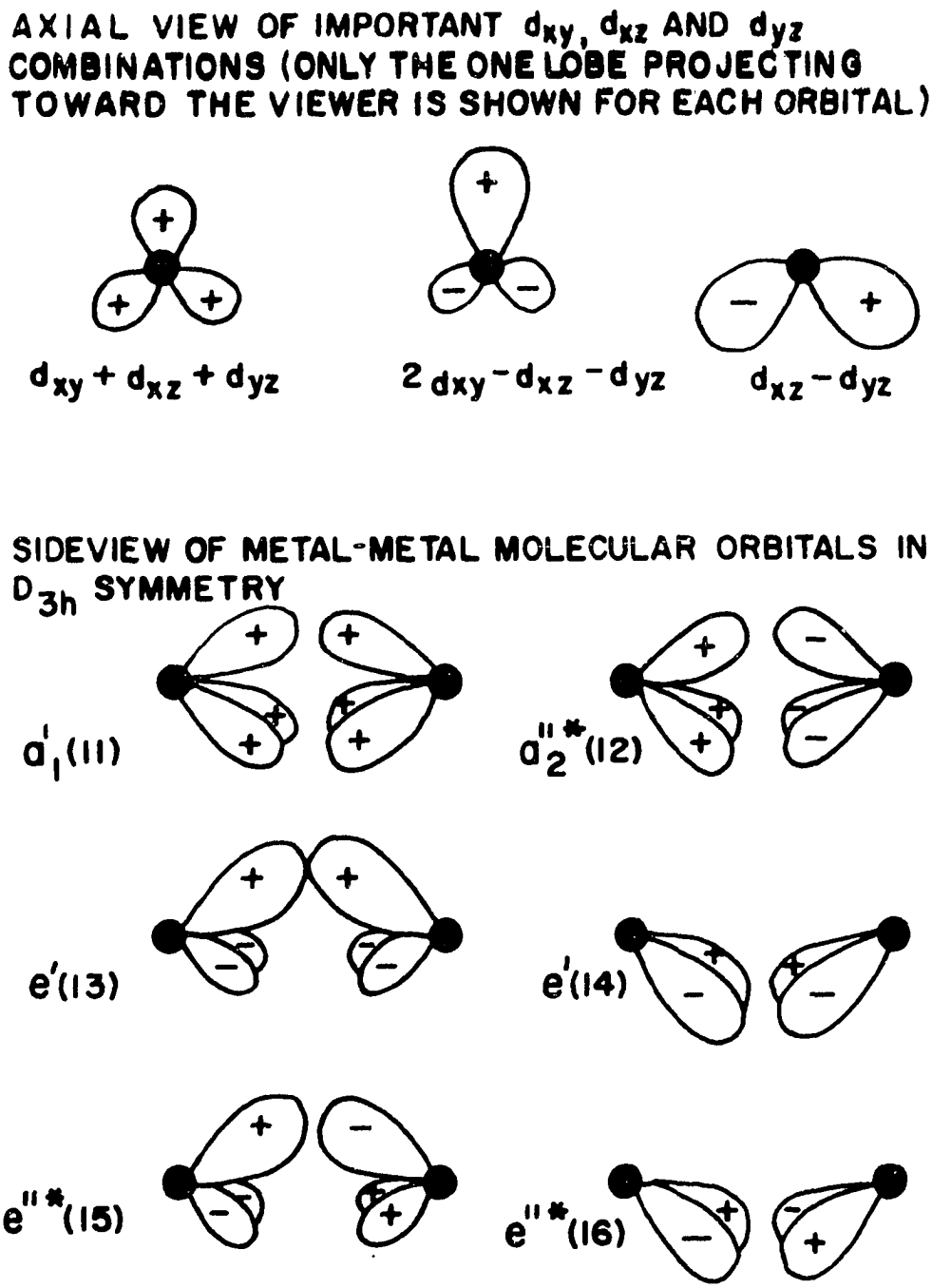

Figure 10. Metal-metal molecular orbital overlap diagram for a confacial bioctahedron of D_{3h} symmetry

there is no evidence of constructive overlap such as in $Cs_3Cr_2Cl_9$ which also has six available electrons but behaves magnetically like two independent d^3 chromium atoms. The Cr-Cr distance of 3.12Å (84) and other bonding criteria such as d'/d" = 1.23 are all consistent with the absence of an attractive metal-metal force in this dimer.

The remaining step in deriving a suitable molecular orbital description of $Ta_2Br_6(SC_4H_8)_3$ is to descend to C_{2v} symmetry and place four metal valence electrons in the appropriate orbitals. Again we will assume that the σ-bonding framework remains basically intact as the three tetrahydrothiophene ligands alter the symmetry of the molecule to C_{2v}. The region of interest consists of the σ and π metal-metal molecular orbitals where D_{3h} symmetry constrained the two π-orbitals to be energetically equivalent due to the axial three-fold symmetry. The demise of the C_3 axis upon substitution of three equivalent ligands with three dissimilar ligands as compared to the remaining six removed the degeneracy restriction which applied to the π-orbitals of a D_{3h} dimer. If one had placed four electrons in the D_{3h} molecular orbitals two electrons would have been paired in the a_1' σ-orbital and the next two electrons would have occupied the degenerate π-orbitals with parallel spins in accord with Hund's rules. The diamagnetic behavior of $Ta_2Br_6(SC_4H_8)_3$ must be a consequence of splitting the e' energy levels substantially in the lower symmetry so that spin-pairing occurs in the lower energy π-orbital while

the remaining π-orbital formally remains as a bonding molecular orbital but is devoid of electrons. The crux of this entire procedure is to establish which π-orbital is lowered in energy, and therefore occupied, and which is unoccupied. It is here that the initial question pertaining to the disposition of the bridging atoms comes into focus.

Figure 11 illustrates the C_{2v} coordinate system appropriate for $Ta_2Br_6(SC_4H_8)_3$, but it is important to note that the individual metal axes remain unchanged from those utilized in the D_{3h} analysis. At this stage the d_{xy}, d_{xz}, and d_{yz} orbitals of both metal atoms will be considered exclusively based on the premise that these orbitals are sufficiently well isolated from other orbitals by energy differences to justify such an insular treatment. The linear combinations listed in Equations 11 to 16 for D_{3h} symmetry are still valid molecular orbitals, but the descent in symmetry converts them to the following representations in the C_{2v} group:

$$a_1'(11) \rightarrow a_1$$

$$a_2''^*(12) \rightarrow b_2^*$$

$$e'(13) \rightarrow a_1$$

$$e'(14) \rightarrow b_1$$

$$e''^*(15) \rightarrow b_2^*$$

$$e''^*(16) \rightarrow a_2^*$$

Qualitative overlap considerations certainly suggest that

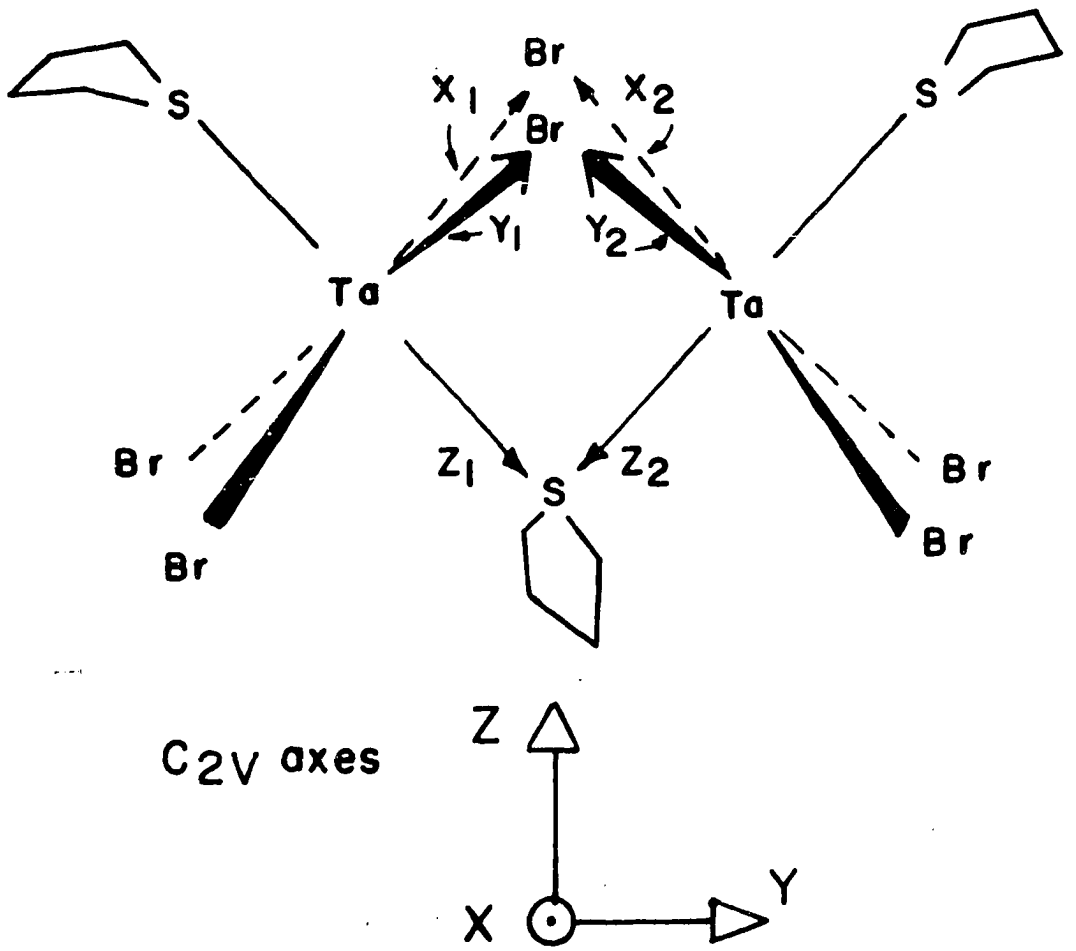

C_{2v} Character Table

C_{2v}	E	C_2	$\sigma_v(xz)$	$\sigma_v'(yz)$		
A_1	1	1	1	1	z	x^2, y^2, z^2
A_2	1	1	-1	-1	R_z	xy
B_1	1	-1	1	-1	x, R_y	xz
B_2	1	-1	-1	1	y, R_x	yz

Figure 11. C_{2v} symmetry coordinates for a confacial biocta-hedron such as $Ta_2Br_6(SC_4H_8)_3$

the a_1 molecular orbital derived from the a_1' orbital of the D_{3h} case will remain as the lowest energy metal-metal bonding orbital and two electrons are therefore assigned to this σ-bond. The correct energy ordering for the a_1 and b_1 π-orbitals descended from the e' degenerate representation is not subject to such a simple a priori analysis. Recalling that the a_1 and b_1 π-orbitals were degenerate in the D_{3h} case one can only examine the experimentally determined structure in search of distortions which are consistent with lower energy for one of the two π-orbitals and suggests electron occupancy of that level. An inspection of the a_1 π-orbital reveals that the region of greatest overlap for this molecular orbital lies between the two bridging bromine atoms with minor overlap present in the two spaces between the bridging sulfur and bridging bromine atoms. A similar investigation of the b_1 symmetry orbital shows no contribution from the two d_{xy}-orbitals between the bridging bromines, but rather the entire strength of this π-bond results from overlap of d_{xz} and d_{yz} orbitals from the two metal atoms in the vacancies between the sulfur atom and the two bromines. Considering the large S_{br}-Ta-Br_{br} angles which average 101.0° compared to the Br_{br}-Ta-Br_{br} angle average of 77.6° it seems that the b_1 π-orbital effectively fills the voids between the sulfur and the bromines with electron density which repels the bridging ligands. Although these two electrons are in a π-bonding orbital, it is an orbital which lies entirely outside the confines of the two

Br_{br}-Ta-Br_{br} triangle boundaries. These electrons are stereochemically active in the same sense that the unshared pair of electrons in ammonia forces an equilibrium pyramidal structure at the expense of a possible planar configuration.

A view of the bridging atom triangle along the metal-metal axis reinforces the π-bonding hypothesis. Even though the van der Waals radius of sulfur is less than that of bromine the sulfur-bromine distances are 0.60Å and 0.56Å longer than the bromine-bromine separation of 3.30Å. The lower limit reported for bromine's nonbonded contact radius is 1.8Å (80) which infers that any two nonbonded bromines separated by less than 3.6Å would strongly repulse one another. The 3.30Å distance here is therefore energetically unfavorable even allowing for some electron density alterations in the bridging bromide ions due to the dative bonding of two electron pairs. An explanation of the abnormal proximity of these two atoms must embrace some postulate that will dictate closure of the two bromines. There is no reason to suspect metal-ligand σ-bonding factors favor this angular distortion and the metal-metal σ-bond is axially symmetric and therefore only able to distort the dimer by contraction or elongation along the axis. The only electronic factor remaining, having earlier justified neglecting π-bonding from the ligands and steric hindrance arguments, is the metal-metal π-interaction. If one imagines an equilateral triangle formed by the three bridging atoms, two possible angular distortions immediately come to mind

which are compatible with retention of C_{2v} symmetry.

1. The two bromine atoms swing outward towards the sulfur atom. This allows more space for the d_{xy} metal orbitals of the a_1 π-bonding orbital, but at the same time the domains of the d_{xz} and d_{yz} orbitals are infringed upon and these contributions, although less than those from d_{xy} overlap, are important in influencing the energy of the resultant molecular orbital. One concludes that this distortion would not substantially lower the a_1 energy level because of opposite effects on different lobes of this molecular orbital.

2. The two bromine atoms swing inward away from the sulfur atom and towards one another. The b_1 π-orbital has no density located between the two bromine atoms and hence no increase in the b_1 energy level should occur with this distortion. In fact the energy of the b_1 π-orbital should decrease as a result of the increased space available between the sulfur and bridging bromines which corresponds to the locations of maximum overlap for the d_{xz} and d_{yz} metal orbitals which constitute the molecular orbital in question.

This second distortion accords well with the observed structure as exemplified by the bridging atom triangle in Figure 12. Whether the structure distorts to lower the energy of the b_1 π-orbital or whether the presence of two electrons in this molecular orbital causes the distortion due to electronic repulsion is a mute question. The point to be stressed

BRIDGING ATOM TRIANGLE ILLUSTRATING DISTANCES AND ANGLES

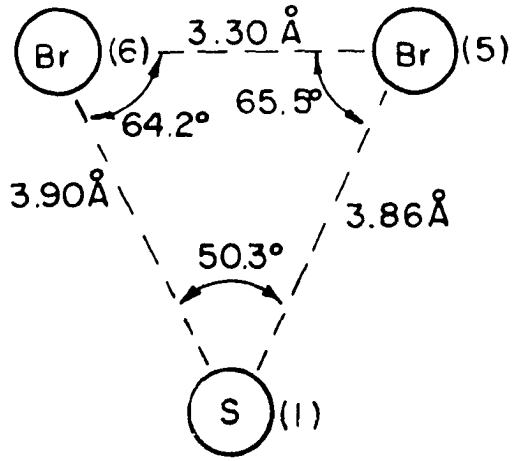

BRIDGING ATOM TRIANGLE ILLUSTRATING RELATIVE POSITIONS OF d_{xy}, d_{xz} and d_{yz} ORBITALS

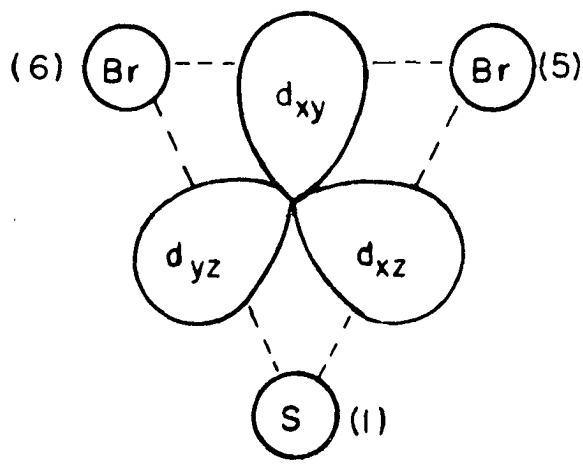

Figure 12. Bridging atom triangle parameters for $Ta_2Br_6(SC_4H_8)_3$ and relative positions of important d-orbital lobes

is that the bonding description presented successfully accounts for the anomalous bridging bromine locations under examination and this hopefully justifies the preceding excursion which developed these concepts in detail.

PART II. SYNTHESIS AND CHARACTERIZATION OF $[(CH_3CH_2CH_2)_4N]_2[W_2Br_9]$

REVIEW OF RELATED WORK

The descriptive chemistry of tungsten is extremely complex. The selection of background material from the literature must be adequate for the reader to place the synthetic route and resulting product in perspective, and yet a comprehensive review is both impractical and unnecessary. The intended bases for the three divisions which follow are to document the propensity with which tungsten forms homonuclear metal bonds via a cursory overview of tungsten chemistry, then to examine the group VI nonahalodimetallates in greater detail from both the preparative and structural viewpoints, and finally to discuss the role of carbonyl containing reactants of group VI in syntheses of metal-metal bonded compounds.

A Brief Overview of the Descriptive Chemistry of Tungsten

The descriptive chemistry of tungsten is characterized by a wide variety of oxidation states spanning the range from 2- to 6+, and the chemistry is further complicated by multiple stereochemical possibilities for coordination numbers between four and eight, inclusive. The chemistries of tungsten and molybdenum display similar trends, and analogies can be profitable in some instances. The remaining group VI metal, chromium, is only similar to tungsten in low oxidation state organometallic compounds with π-ligands. As an example of the contrasting chemistries, Cr(III) is a particularly stable oxidation state in aqueous solutions and numerous studies have been made of

cationic complexes of Cr(III), but tungsten 3+ or 4+ can be obtained in aqueous systems only as air sensitive species which are not cationic. The higher oxidation states of tungsten are much more stable to reduction than the corresponding oxidation states of chromium, and both terminal and bridging oxides of tungsten(V) or (VI) are very stable, while CrO_4^{2-} is a powerful oxidant. Molybdenum and tungsten generally favor the 4+, 5+, and 6+ oxidation states except for polynuclear or organometallic species. The anhydrous tungsten chlorides exemplify the trend towards condensation to form clusters which accompanies lower oxidation states; WCl_6 (85), WCl_5 (86), WCl_4 (87), WCl_3 (88) and WCl_2 (87) have all been isolated, but both WCl_3 and WCl_2 contain a hexanuclear cluster unit consisting of an octahedron of six metal-metal bonded tungsten atoms.

The $W_6X_8^{4+}$ hexanuclear cluster unit has not been as extensively characterized as the analogous molybdenum system, but it definitely illustrates the metal-metal bonding capability of low valent tungsten halides. All three tungsten dihalides (Cl, Br, and I) are best formulated as $[W_6X_8]X_2X_{4/2}$ (87). The cluster has eight halogens above the eight faces of the metal octahedron which are triply bridging since they are each bound to three metal atoms. The six terminal positions are occupied by halide ions in the anhydrous halide, some of which bridge to other clusters, and the terminal positions can be easily substituted by various donors, neutral or anionic. The bonding among the metal atoms in $M_6X_8^{4+}$ octahedra involves

twenty-four metal valence electrons which are not utilized in metal-ligand σ-bonds. Twelve metal-metal bonding molecular orbitals have been derived from the d-orbitals available on the six metal atoms and hence the bonding orbitals are nicely filled by the twenty-four electrons (45). A bond order of one results for each of the twelve adjacent metal-metal interactions. An x-ray structure of W_6Br_{16} revealed the presence of bridging Br_4^{2-} groups such that the formulation $(W_6Br_8)Br_4(Br_4)_{2/2}$ best represented the central $W_6Br_8^{6+}$ unit (89). The W-W distance of 2.64Å was consistent with a strong bond based on a comparison with tungsten metal where the distance of closest approach is 2.74Å.

At this time one of the inexplicable differences in the chemistry of tungsten and molybdenum will be mentioned. While $Mo_2(O_2CCH_3)_4$ (90) and many derivatives have been thoroughly investigated and shown to contain a metal-metal quadruple bond, the corresponding tungsten series remains an enigma (91). Even though a wide variety of reaction conditions has been employed ranging from those similar to the $Mo_2(O_2CCH_3)_4$ preparative routes to far different synthetic approaches, no successful isolation of quadruply bonded tungsten dimers has been reported.

Group VI $M_2X_9^{n-}$ Anions

Tungsten-tungsten metal bonds are found in the dimeric anions $W_2Cl_9^{3-}$ and $W_2Br_9^{3-}$ in addition to the hexanuclear metal halides discussed above. Olsson reported the preparation of

$K_3W_2Cl_9$ in 1914 by the reduction of tungstic acid in concentrated hydrochloric acid with elemental tin (92). In 1932 Young prepared the corresponding nonabromoditungstate anion as $K_3W_2Br_9$ (93) by a procedure similar to that of Olsson. Tungstic acid was reduced with tin in concentrated hydrobromic acid to produce analytically pure $K_3W_2Br_9$ in the form of brown hexagonal plate-like crystals.

Extreme sensitivity to the exact reduction conditions caused large fluctuations in the yield of $K_3W_2Cl_9$ when Olsson's synthetic procedure was employed, and hence several modifications of his general scheme have been published as improvements in the synthesis of the dimeric anion. Laudise and Young (94) formed complex chlorides of tungsten by dissolving tungstic acid in a boiling solution of potassium carbonate, and then added the tungstate solution to concentrated HCl while HCl gas was continuously passed through the mixture. A series of temperature controlled steps followed as the solution was reduced with mossy tin to form either $K_3W_2Cl_9$ or $K_5W_3Cl_{14}$ depending on the amount of KCl added during the reduction. Yields of 50% were reported by the authors, but later investigators reported yields of only 5% via this route (95). It should also be noted that a thorough investigation of $K_5W_3Cl_{14}$ revealed a mixture of $K_2WCl_5(OH)$ and $K_3W_2Cl_9$ which accounted for the observed properties (96), so the existence of a trimeric tungsten halide seems highly unlikely.

Heintz published an aqueous preparation of $K_3W_2Cl_9$ as a

necessary intermediate for the synthesis of cyanotungstates (97), and he noted that the difficulties in preparing cyanotungstates centered around the nonachloroditungstate anion. Wentworth and co-workers modified Heintz' procedure by lowering the reaction temperature, increasing the acidity, and employing tin powder rather than tin foil to obtain yields of 70% prior to recrystallization (95). All of the above preparative routes utilize tin reduction of tungsten(VI) chloro species in aqueous solution to synthesize $W_2Cl_9^{3-}$ salts, and only technical details differ among the various procedures.

Following the initial report of $K_3W_2Br_9$ in 1932 (93) there was no mention of this compound until 1968 when Hayden and Wentworth prepared $W_2Br_9^{3-}$ via halide exchange (98). Attempts to duplicate Young's procedure resulted in insignificant yields of the desired tungsten dimer, and results of a previous radiochloride exchange study of $W_2Cl_9^{3-}$ in acid solution (99) suggested that all nine chloride ligands were kinetically equivalent and sufficiently labile to undergo substitution. Indeed the dark green $K_3W_2Cl_9$ dissolved in concentrated HBr and complete exchange occurred within twenty-four hours if a moderate flow of HBr gas was maintained during the reaction period. Addition of rubidium bromide precipitated $Rb_3W_2Br_9$. Lower yields of the potassium salt were obtained due to the higher solubility of $K_3W_2Br_9$. The brown hexagonal plates of $K_3W_2Br_9$ dissolved in deoxygenated water to produce brown solutions when concentrated which appeared orange to pink upon

dilution. The aqueous solutions quickly decomposed in the presence of air. A mechanism which could account for both intramolecular halide kinetic equivalence and free halide exchange was presented based on the known reaction of $W_2Cl_9^{3-}$ with pyridine to form the dimeric $W_2Cl_6(py)_4$ with a total of ten ligands present (95). Addition of a halide ion could possibly proceed with the rupture of one of the bridge bonds to reversibly form $W_2Cl_{10}^{4-}$ as an intermediate which adopts the edge-shared bioctahedral structure. In this manner radiochloride or bromide could be introduced into both terminal and bridging positions of the confacial bioctahedron. No further preparations or characterizations of $W_2Br_9^{3-}$ have been published to date.

The x-ray structure of potassium nonachloroditungstate (3-) disclosed a surprisingly short tungsten-tungsten distance of 2.41Å (83). The metal-metal separation was particularly interesting when contrasted with $Cs_3Cr_2Cl_9$ where the two chromium atoms were 3.12Å apart (84). Both anions were similar in that they both conformed to the confacial bioctahedral structure, but drastic differences in the axial distortions due to metal-metal forces were evident. The chromium atoms were displaced away from each other along the three-fold axis while the tungsten atoms showed the opposite behavior and were strongly attracted towards one another.

Crystal structures of $Cs_3Cr_2Cl_9$, $Cs_3Mo_2Cl_9$ and $Cs_3Mo_2Br_9$ added detailed structural information to the data bank of

group VI nonahalodimetallates (78). Both $Cs_3Cr_2Cl_9$ and $Cs_3Cr_2Br_9$ display a complete lack of any attractive metal-metal interaction. The criteria discussed in the introduction discount any possible metal-metal bonding in $Cr_2Cl_9^{3-}$ and $Cr_2Br_9^{3-}$. The metal-metal separations of 3.12Å and 3.32Å in the chloro and bromo anions, respectively, are quite long relative to the elemental metal distance of 2.50Å. It then follows that the nonahalodichromate distortions are consistent with the presence of metal-metal repulsion, notably d'/d" = 1.23 and 1.28, 90.0°-α' = 4.2° and 7.0°, and β-70.5° = 5.9° and 9.5° for $Cs_3Cr_2Cl_9$ and $Cs_3Cr_2Br_9$, respectively. Furthermore, the magnetic and spectroscopic properties of these dimers are those of two independent d^3 chromium atoms (100): μ_{eff} is near 3.8 BM at 300° for each of the chromium atoms in the dimer, and the electronic transitions observed experimentally can be assigned independently to each chromium chromophore without invoking metal-metal overlap. The reaction of pyridine with $Cr_2Cl_9^{3-}$ cleaves the halide bridges to form monomeric $CrCl_3(py)_3$ in a manner consistent with the absence of metal-metal bonding.

Nonachloroditungstate (3-) lies at the opposite extreme in the realm of dimeric metal interactions as evidenced by application of the same criteria. The metal-metal separation of 2.41Å is quite short, and d'/d" = 0.90, 90.0°-α' = -8° and β-70.5° = -12.5° are all consistent with metal-metal bonding causing the two metal atoms to contract along the three-fold

axis. The tungsten dimer has only a small temperature independent paramagnetic contribution which confirms spin-pairing of the two d^3 configurations such as would occur due to the formation of metal-metal bonding molecular orbitals. The reaction of aromatic amines, including pyridine, with $W_2Cl_9^{3-}$ produces dimeric $W_2Cl_6(py)_4$ compounds (95) which retain metal-metal bonding as exemplified by the tungsten-tungsten distance of 2.74Å in $W_2Cl_6(py)_4$ (101). The edge-shared dimeric structure of $W_2Cl_6(py)_4$ is unusual in that two chlorine atoms occupy the bridging positions as one would expect, but the two tungsten atoms are different in that one has pyridine ligands trans to both bridging chlorines and chlorine atoms occupy the two remaining octahedral sites of this tungsten while the other metal has chlorine atoms trans to the bridges with pyridine in the remaining positions. Regardless of the exact disposition of the ligands, the observed retention of the dinuclear unit during substitution is characteristic of metal-metal bonded species and the contrast between chromium and tungsten confacial bioctahedral anions is reaffirmed.

The above comparison of chromium and tungsten dimers is a classic example of the fruitful application of metal-metal bonding distortional moduli to well characterized compounds. Based on the above data one might suppose that $Mo_2X_9^{3-}$ anions would exhibit properties characteristic of metal-metal bonds of intermediate strength. Indeed the dimeric molybdenum anions clearly display structural and magnetic properties indicative

of metal-metal bonding, but the extent of the bonding is less than in the tungsten case as judged by the magnitudes of various moduli. The Mo-Mo distance in $Cs_3Mo_2Cl_9$ is 2.66Å which is 0.25Å longer than the corresponding metal-metal distance in $K_3W_2Cl_9$ and an even longer 2.82Å separates molybdenum atoms in $Cs_3Mo_2Br_9$ (78). The confacial bioctahedral moduli introduced previously indicate the presence of metal-metal bonding: $d'/d'' = 0.98$ and 0.97, $90.0°-\alpha' = -4.2°$ and $-3.9°$, and $\beta-70.5° = -6.0°$ and $-5.6°$ for $Cs_3Mo_2Cl_9$ and $Cs_3Mo_2Br_9$, respectively. This pair of chloro and bromo anions are an excellent example of how parameters other than metal-metal distance alone are required to correctly assess the extent of the metal-metal interaction. Although the $Mo_2Br_9^{3-}$ anion has the molybdenum atoms 0.16Å further apart than the chloride analog, the values of the generalized moduli (d'/d'', $90.0°-\alpha'$, and $\beta-70.5°$) are all nearly the same for the two species which suggests that the deviation in metal-metal bond length results from constraints due to the presence of different halide ligands and not from a drastic change in the nature of the metal-metal interaction. No structural data has been published for the $W_2Br_9^{3-}$ anion but similar results would be predicted, i.e. one would anticipate the generalized moduli to be nearly equivalent to those of $K_3W_2Cl_9$ with the metal-metal distance increased by perhaps 0.16Å or so. The magnetic properties of $Cs_3Mo_2X_9$ (X = Cl or Br) are consistent with the bonding description presented thus far. The chloride exhibits only temperature independent

paramagnetism consistent with electron spin-pairing in the ground state with no paramagnetic excited states accessible at room temperature. The bromide displays weak paramagnetism which is temperature dependent and the data suggests a spin-paired ground state with some low-lying paramagnetic excited states thermally populated at room temperature (102).

Another molybdenum dimer of importance which has been characterized by x-ray diffraction is $Rb_3Mo_2Cl_8$ (103). Although the $Mo_2Cl_8^{3-}$ dimer is formed from $Mo_2(O_2CCH_3)_4$ treated with hydrochloric acid at 60°C followed by addition of rubidium chloride, the product is not structurally similar to the parent compound but rather adopts a structure based on the confacial bioctahedral conformation of $Cs_3Mo_2Cl_9$. Several aspects of the structure of this unique dimer are relevant to this review. Formation of the $Mo_2Cl_8^{3-}$ entity can be visualized by removal of a bridging chlorine atom from $Mo_2Cl_9^{3-}$ and the molecular structure corresponds exactly to the resultant dibridged species. The octachlorodimolybdate (3-) retains the D_{3h} symmetry characteristic of confacial bioctahedral structures in the solid state due to the statistical absence of 1/3 of the bridging chlorine ligands. The average oxidation state of the molybdenum atoms in this dimer is 2.5, midway between the 3+ valence of $Mo_2X_9^{3-}$ dimers and the 2+ valence of quadruply bonded dimolybdenum tetracarboxylate derivatives. The Mo-Mo distance of 2.38Å is also between the values of 2.66Å for $Mo_2Cl_9^{3-}$ and 2.09Å for $Mo_2(OCCH_3)_4$ (104). The structural

importance of removal of one of the bridging chlorine atoms from $Mo_2Cl_9^{3-}$ should not be underestimated since a considerable amount of steric repulsion and angular deformation energy accompanies the bridging ligand. The conclusions derived from applying confacial bioctahedral moduli to $Mo_2Cl_8^{3-}$ must be considered cautiously in order to avoid invalid comparisons. Nonetheless, the values of such moduli make it clear that the octachlorodimolybdate (3-) is more distorted due to metal-metal contraction than any of the true $M_2X_9^{n-}$ dimers which have been structurally characterized to date: $d'/d'' = 0.89$, $90.0° - \alpha' = -9.2°$, and $\beta - 70.5° = -13.7°$. The greater distortions present are presumably due to decreased opposition to contraction as a result of the absence of one bridging chlorine per dimer.

One-electron oxidation of $W_2Cl_9^{3-}$ has been accomplished with elemental halogen oxidants in dichloromethane (105). The green solution of nonachloroditungstate (3-) underwent electron transfer with X_2 (X = Cl, Br, or I) to form the violet $W_2Cl_9^{2-}$ without incorporation of the halogen oxidant into the molecular unit. The tetrabutylammonium salt which was isolated was characterized by a conductivity measurement in acetonitrile, electronic spectrum, far-infrared spectrum and a magnetic susceptibility consistent with one unpaired electron per dimer (μ_{eff} = 1.87 BM). Although the authors were certain of the dimeric nature of the product, retention of the confacial bioctahedral structure was not confirmed and other possible structures were mentioned.

Group VI Metal Carbonyl Halide Reactants

Wentworth and co-workers have prepared $Mo_2Cl_9^{3-,2-}$ from the redox reaction of $MoCl_6^{2-,1-}$ with $Mo(CO)_4Cl_3^-$ in dichloromethane (106). The synthetic approach employed was based on the concept of oxidative displacement of carbon monoxide from $Mo(CO)_4Cl_3^-$ with concomitant bridge formation with the oxidant, either $MoCl_6^{2-}$ or $MoCl_6^-$. Loss of the fourth carbon monoxide ligand was expected to proceed easily due to the known lability of CO bound to metals in slightly higher oxidation states, and hence the proposed $Cl_3MoCl_3MoCl_3(CO)^{3-,2-}$ intermediate would form the desired nonachlorodimolybdate. Although no attempt was made to confirm any mechanistic possibilities, the authors did successfully isolate the triply-bridged chloride anions according to the stoichiometry shown in Equations 17 and 18. Reaction 17 occurs over a thirty hour time period to pro-

$$MoCl_6^{2-} + Mo(CO)_4Cl_3^- \rightarrow Mo_2Cl_9^{3-} + 4CO \qquad (17)$$

$$MoCl_6^- + Mo(CO)_4Cl_3^- \rightarrow Mo_2Cl_9^{2-} + 4CO \qquad (18)$$

duce a 50% yield while reaction 18 produced almost quantitative yields in twenty-four hours. The anions were isolated as quaternary ammonium salts. The temperature dependence of the magnetic moment of $[(CH_3CH_2CH_2)_4N]_3Mo_2Cl_9$ was consistent with the thermal population of states with S = 1 and S = 0 at room temperature with diamagnetic behavior observed below 100°K. The magnetic susceptibility of $[(n\text{-}C_4H_9)_4N]_2Mo_2Cl_9$ below 100°K indicated a ground state with one unpaired electron per dimer

with a magnetic moment near 1.6 BM. Thermal population of states with S = 1/2 and S = 3/2 occurs as the temperature increases toward 300°K. The $Mo_2Cl_9^{2-}$ anion was easily reduced to the 3- dimer by acetonitrile or tin metal.

Further success in rational preparative routes to metal-metal bonded molybdenum dimers based on the concept of oxidative displacement of carbon monoxide was reported in 1974. Starting with $Mo(CO)_5X^-$ and an appropriate metal halide, salts of $Mo_2Cl_9^{3-}$ and $Mo_2Br_9^{3-}$ were prepared in high yields according to Equations 19 and 20.

$$6MoCl_5 + 4Mo(CO)_5Cl^- + 11Cl^- \rightarrow 5Mo_2Cl_9^{3-} + 20\ CO \quad (19)$$

$$3MoBr_4 + Mo(CO)_5Br^- + 5Br^- \rightarrow 2Mo_2Br_9^{3-} + 5CO \quad (20)$$

A brief survey of the group VI halocarbonyl anions is appropriate at this time. Particularly for the chloro species it will become evident that it is much easier to prepare $Mo(CO)_5Cl^-$ salts than $Mo(CO)_4Cl_3^-$ salts, and this fact makes reaction 19 preferable to reaction 17 for the convenient preparation of $Mo_2Cl_9^{3-}$.

In the first report of the reaction of a halide salt with molybdenum hexacarbonyl the product was incorrectly formulated as a π-complex with the N-methylpyridinium cation attached to a molybdenum tricarbonyl fragment (107). In fact the result of refluxing $Mo(CO)_6$ with N-methylpyridinium iodide in tetrahydrofuran was soon identified as $[C_5H_5NCH_3][Mo(CO)_5I]$ (108). A general preparative route to the halopentacarbonylmetallates

$M(CO)_5X^-$ (M = Cr, Mo or W and X = Cl or Br) was published in 1963 to complete the possible metal-halide combinations in this ion (109). Three carbonyl bands were observed in the infrared spectra between 1840 cm^{-1} and 2065 cm^{-1} in agreement with the number of bands expected for the predicted C_{4v} symmetry of $M(CO)_5X^-$ anions. The metal carbonyls and halide salts reacted rapidly in diethylene glycol dimethyl ether at 120°C until carbon monoxide evolution ceased. Yellow crystals were isolated in each case.

The reaction of $M(CO)_5X^-$ (M = Mo or W and X = Br or I) with X_2 at room temperature oxidizes the metal to the 2+ oxidation state with loss of one carbon monoxide ligand and addition of the two halogen atoms to form the $M(CO)_4X_3^-$ anion. Elemental iodine was first employed to prepare the $M(CO)_4I_3^-$ anions (M = Mo or W) (110) and later use of elemental bromine produced the analogous bromide anions (111), but the chloro analogs were not reported. Oxidation of $M(CO)_5X^-$ is a convenient route to the bromo and iodo trihalotetracarbonyl metallates but it was necessary to employ a different scheme to isolate $Mo(CO)_4Cl_3^-$. The previously characterized neutral metal (2+) dichlorotetracarbonyl compounds, $M(CO)_4Cl_2$ (M = Mo or W), served as starting materials for the addition of quaternary ammonium chlorides in dichloromethane under oxygen-free and moisture-free conditions to form the trichloro anion derivatives (112). The neutral parent compounds were prepared under anhydrous conditions by oxidizing either molybdenum or

tungsten hexacarbonyl with elemental chlorine at -78°C.

The systematic displacement of carbonyl ligands to form halide bridged polynuclear compounds was extended beyond $Mo_2Cl_9^{3-}$ and $Mo_2Cl_9^{2-}$ to the reaction of $Mo_2Cl_9^{2-}$ with $Mo(CO)_4Cl_3^-$ to produce a trimeric species (113). The product isolated from the reaction shown in Equation 21 was postulated

$$Mo_2Cl_9^{2-} + Mo(CO)_4Cl_3^- \rightarrow Mo_3Cl_{12}^{3-} + 4CO \qquad (21)$$

to be a linear array of three molybdenum atoms all octahedrally coordinated with trigonal faces shared between adjacent metal atoms. This article reported conductivity measurements, infrared data, electronic spectra and magnetic susceptibility data for $[(CH_3CH_2CH_2)_4N]_3Mo_2Cl_9$, $[(n\text{-}C_4H_9)_4N]_2Mo_2Cl_9$ and $[(n\text{-}C_4H_9)_4N]_3Mo_3Cl_{12}$.

The rational syntheses of polynuclear molybdenum halides via "conproportionation" reactions such as those described above are not paralleled by the corresponding tungsten systems. Tungsten hexachloride and chloropentacarbonyltungstate react in dichloromethane in the presence of added chloride to form a mixture of monomeric products which include WCl_6^- and WCl_6^{2-} (114). In the absence of added chloride salts polynuclear tungstates could be isolated from these same reactants, but the nature of the products depended on the cation present as well as the solvent employed and the stoichiometry of the reactants. Violet-colored $[(CH_3CH_2CH_2)_4N]_2W_2Cl_9$ was isolated from the one to one reaction of WCl_6 and $W(CO)_5Cl^-$ in dichloro-

methane. Tetrabutylammonium cations under similar conditions formed no detectable amounts of $W_2Cl_9^{2-}$, but rather the unusual $W_4Cl_{17}^{2-}$ anion was inferred from spectroscopic data to be present in these solutions. The difference in products depending on the cation present was attributed to the virtual insolubility of $[(CH_3CH_2CH_2)_4N]_2W_2Cl_9$ in dichloromethane while $[(n\text{-}C_4H_9)_4N]_2W_2Cl_9$ is quite soluble and thereby promotes further reaction. The $W_4Cl_{17}^{2-}$ species referred to above was not isolated from the dichloromethane solvent, but the use of tetrahydrofuran as a reaction solvent precipitated the $[(n\text{-}C_4H_9)_4N]_2W_4Cl_{17}$ solid which exhibited an effective magnetic moment of 1.95 BM at 298°K consistent with a single unpaired electron as required by the stoichiometry.

Several examples of dinuclear compounds which contain carbon monoxide ligands and bridging halide ions provide a basis for the concept of generating potential metal-metal attractions through the use of metal carbonyl reactants. One might hope that establishing a bridged dimeric compound would promote metal-metal bonding by synthetic manipulations of the ligands and metal oxidation states since the two metal atoms would be held in close proximity by the halide bridges. A review of halide-bridged polynuclear compounds of group VI which have been characterized provides hope for intermediates of a similar nature, perhaps in route to metal-metal bonded compounds.

In a study concerned with π-allyl complexes of molybdenum

and tungsten Murdoch prepared halide-bridged dimers of the formulation $[M_2Y_3(C_3H_5)_2(CO)_4]^-$ (where M = Mo or W and Y = Cl or Br) via the reaction shown in Equation 22 (115). All the halide present in the resulting dimeric anion was derived from

$$2M(CO)_5X^- + 3C_3H_5Y \rightarrow [M_2Y_3(C_3H_5)_2(CO)_4]^- + C_3H_5X + X^- + 6CO \quad (22)$$

the allyl halide; either C_3H_5Cl or C_3H_5Br effected reaction while allyl iodide failed to react with the pentacarbonylhalometallate. The presence of three carbonyl stretching bands in the infrared spectra above 1840 cm^{-1} was consistent with the absence of bridging carbon monoxide ligands. Reaction of the dinuclear product with pyridine produced monomeric $(\pi\text{-}C_3H_5)Mo(CO)_2Cl(py)_2$ and tetraethylammonium chloride. Cleavage of the halide bridges was not unexpected in this reaction since no metal-metal bond is necessary in the dimeric anion for each of the metals to attain the noble gas configuration.

The anionic dimers $[M_2(CO)_6X_3]^{3-}$ (M = Cr, Mo, W and X = Cl, Br, I) have been prepared either from arenemetal tricarbonyls reacting with tetraalkylammonium halides or directly from the metal hexacarbonyls and halide salts (116). These triply-bridged dimers with all the halides present in bridging positions satisfy the effective atomic number rule without invoking metal-metal bonds. The compounds were generally unstable in the presence of oxygen, particularly when in solution. It is perhaps surprising that aqueous solutions were

stable under oxygen-free conditions and in fact conductivity studies were performed in water. Two carbonyl bands were typically observed in the infrared at 1880 cm^{-1} and 1740 cm^{-1} which is consistent with the presence of three terminal cis-carbonyls on each metal atom trans to ligands which are not π-acceptors. Monomeric $Mo(py)_3(CO)_3$, for example, absorbs at 1888 cm^{-1} and 1746 cm^{-1}.

Neutral dimeric carbonyl iodides of molybdenum and tungsten were prepared photochemically from the reaction of various iodination reagents with the metal hexacarbonyls (117). The $[M(CO)_4I]_2$ compounds were best prepared from silicon tetraiodide for the molybdenum case and from elemental iodine in the tungsten case. Infrared data and analytical data complemented the observed diamagnetism of the solid to suggest a conlateral bioctahedron bridged by two iodides with a formal single bond uniting the d^5 metal atoms to cause spin-pairing. An x-ray structural determination of $Mo_2(CO)_8I_2$ confirmed the hypothetical structure and a molybdenum-molybdenum distance of 3.16Å compared favorably with other single bond distances in organometallic molybdenum dimers.

EXPERIMENTAL

The reactants and products in this study displayed varying degrees of sensitivity to moisture and oxygen. Schlenk techniques proved to be the most efficient procedures for manipulating these materials since routine operations could be performed conveniently and quickly, and yet careful work under a nitrogen atmosphere protected air sensitive solids and solutions from decomposition. Pre-purified nitrogen gas was passed directly from the cylinder to a T-joint leading to a mercury bubbler which maintained an excess nitrogen pressure of approximately five centimeters of mercury in the system. Solvent transfers were commonly performed with a syringe after extensively flushing the syringe with nitrogen gas. Solid products were stored in Schlenk tubes either under vacuum or under a nitrogen atmosphere and solid samples for physical measurements were prepared in a drybox as described in Part I. Further details of the Schlenk techniques employed will be presented as necessary in the section dealing with synthetic methods.

Materials

Tungsten hexacarbonyl was purchased from Pressure Chemical Company and used as received.

Tetrapropylammonium bromide was obtained from Eastman. Discoloration of the solid in the bottle was commonly observed and recrystallization from an ethanol solution was promoted by

dilution with ether followed by cooling the resultant solution. Crystals of the colorless salt were rinsed with anhydrous ether and dried under dynamic vacuum.

Chlorobenzene was stored over 4-A molecular sieves in the Fisher Scientific Company commercial bottle in which it was received. Nitrogen gas was vigorously bubbled through the solvent for five to ten minutes prior to use to expel dissolved molecular oxygen.

1,2-Dibromoethane was obtained from J. T. Baker Chemical Company and handled in the same manner as chlorobenzene to minimize water and oxygen contamination.

Acetonitrile from Fisher Scientific Company was dried over phosphorus pentoxide and distilled under nitrogen into a Schlenk storage flask for later use.

Analytical Procedures

Gravimetric analysis for tungsten was performed by direct ignition to the oxide, WO_3. Analytical samples of between one and two hundred milligrams were quickly transferred into tared porcelain crucibles and weighed directly to avoid cumulative errors due to the extra handling and measurements necessary for weighing by difference. Addition of a few ml of dilute nitric acid and gentle heating initiated hydrolysis. Addition of concentrated nitric acid promoted complete oxidation and the solutions were cautiously evaporated to dryness to avoid spattering. At this point a steady increase in tem-

perature caused the fine yellow powder to darken until a grey solid remained after applying maximal heat to the crucibles while on the hotplate. The sample crucibles were then transferred to the muffle furnace and ignited at 550°C for several hours. The lemon yellow of tungsten trioxide was the only color evident when the samples were removed from the muffle furnace and cooled in a desiccator prior to weighing.

Bromide samples were weighed directly into 250 ml beakers and fifty ml of concentrated sodium hydroxide solution of known molarity were immediately added to each beaker. The dropwise addition of hydrogen peroxide decomposed the resultant brown solid to rapidly produce a clear solution which was subsequently boiled to remove any remaining peroxides. Two equivalents of acetic acid per equivalent of base initially present were added to the cooled solutions to form an acetic acid-sodium acetate buffer of pH 4.8 and thus avoid the precipitation of insoluble polytungstates which accompanies acidification to pH values near one. The solutions were then titrated potentiometrically with a standardized silver nitrate solution using a silver sensitive working electrode and a saturated calomel reference electrode.

Carbon and hydrogen were determined by Mr. J. J. Richard of the Ames Laboratory Service Group.

Synthesis

The preparative route to $[(n\text{-}C_3H_7)_4N]_2W_2Br_9$ was conveniently carried out in a single reaction vessel in two steps, as

isolation of the tetrapropylammonium bromopentacarbonyltungstate intermediate was unnecessary. A schematic diagram of the Schlenk reaction vessel equipped with a water-cooled condenser and connected to an inverted graduated cylinder to monitor gas evolution is shown in Figure 13. The one-piece construction of the 200 ml flask and condenser was convenient to handle, and the location of the stopcock above the condenser proved to be especially effective in protecting the solution below and also minimized the loss of hot solvent vapors when the vessel was opened under a vigorous nitrogen gas flow.

In a typical reaction the solid reactants, $W(CO)_6$ (3.52 g, 10 mmole), $(n\text{-}C_3H_7)_4NBr$ (2.66 g, 10 mmole), were loaded along with a magnetic stirbar into the reaction flask without precautions. The vessel was then left under dynamic vacuum for approximately thirty minutes to remove moisture and oxygen before purging with nitrogen gas and syringing in about forty ml of chlorobenzene. The colorless reactants appeared insoluble at room temperature. The reaction flask was lowered into an oil bath heated to near 150°C with a magnetic stirrer positioned to thoroughly mix the solution as it was heated. A rapid reaction ensued; the carbon monoxide gas evolved was collected for volume measurement. The cessation of continuous evolution of carbon monoxide signaled completion of the reaction within fifteen minutes and the oil bath was lowered to allow the golden solution of $[(C_3H_7)_4N]W(CO)_5Br$ to cool to

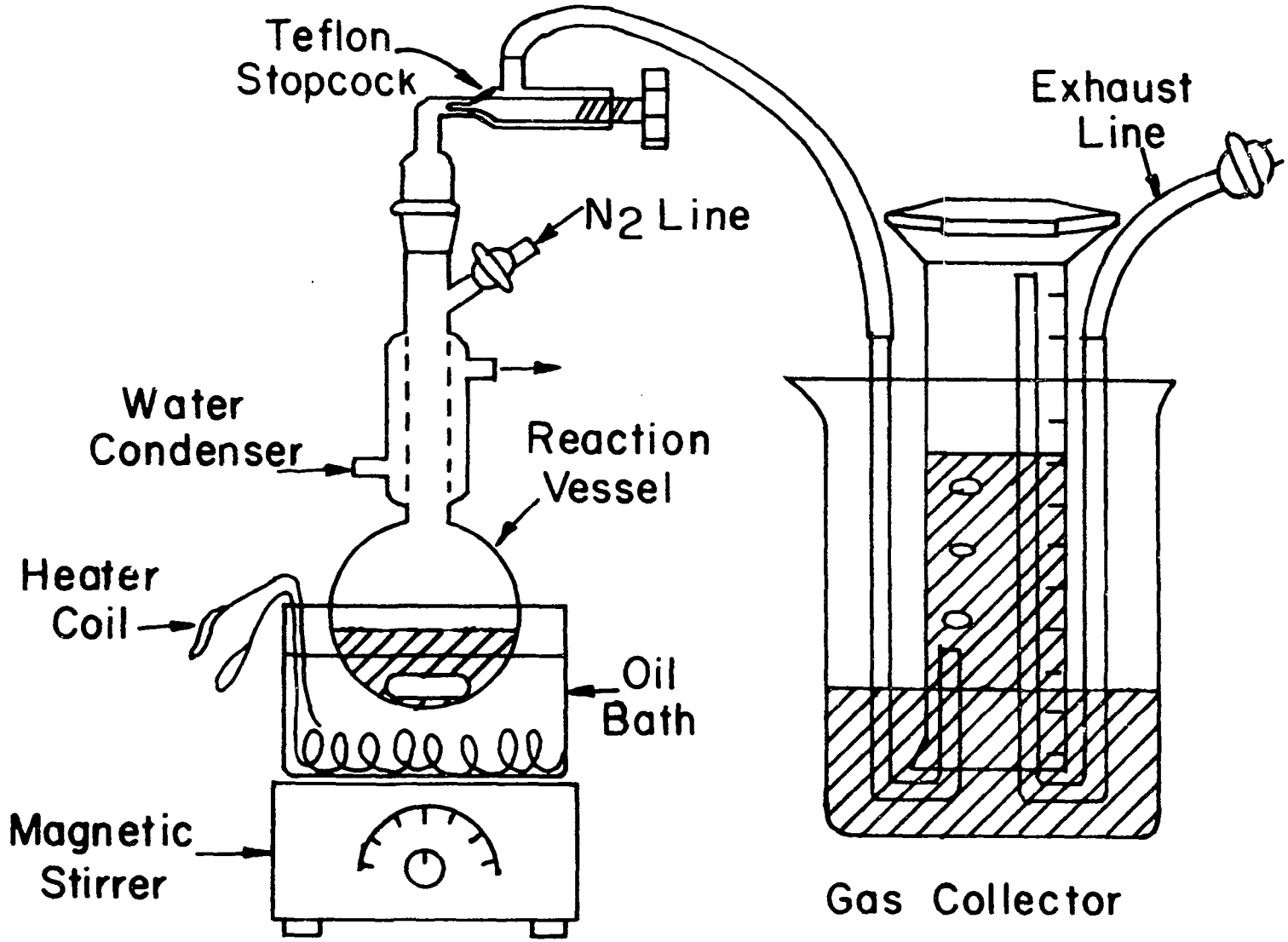

Figure 13. Schlenk reaction vessel and gas collection cylinder for preparing $[(n\text{-}C_3H_7)_4N]_2[W_2Br_9]$

room temperature.

The second and final step in the preparative sequence was initiated by adding approximately fifteen ml of 1,2-dibromoethane to the solution and heating to reflux. The solution color darkened quickly and a fine black precipitate was evident within thirty minutes. Continued reflux for six hours or more was required to expel all the carbon monoxide from the product which was isolated as an insoluble black solid and dried under dynamic vacuum.

The true color of the product was a dark forest green which was observed only after grinding a bit of the black, microcrystalline solid. The material was extremely soluble in acetonitrile, and recrystallization was accomplished by slow solvent removal under vacuum from a saturated acetonitrile solution. A double flask united with a hollow, inverted U-tube was utilized for the recrystallization to both hold the solution and trap the distilled solvent in an ice-water bath. Crystals of the product seemed stable for a period of hours when exposed to the atmosphere, but grinding the sample in air resulted in quick decomposition. Anal. Calcd. for $[(C_3H_7)_4N]_2W_2Br_9$: W, 25.19; Br, 49.27; C, 19.75; H, 3.87. Found: W, 25.14; Br, 48.99; C, 19.73; H, 4.25.

Physical Measurements

Temperature dependent magnetic susceptibility measurements were made with the Faraday balance constructed by

Converse (55). Calibration of the magnet and sample preparation were performed as described in Part I of this thesis. Temperatures within the range of 77 to 300°K were accessible in the cryostat sample chamber, with liquid nitrogen employed as a coolant offset with heat supplied by a variable resistance heater. The voltage generated by a copper-constantan thermocouple was measured to determine the temperature in the area of the sample bucket. A Cahn Electrobalance measured the force on the sample at each of five magnetic field strengths monitored for every temperature.

Infrared samples were prepared as Nujol mulls in the drybox. A Beckman IR-4250 Spectrophotometer covered the region accessible with sodium chloride windows (700 cm^{-1} to 4000 cm^{-1}) and a Beckman IR-11 instrument was employed with samples held by polyethylene sheets to record absorptions below 700 cm^{-1}.

Electronic spectra were recorded with the Cary 14 Spectrophotometer and the cell described in Part I, but solvents were syringed into the cell under a nitrogen flush rather than distilled.

A pycnometric density measurement involved careful determination of the pycnometer volume using the known density of distilled water at 25.0 °C as a standard. Next the density of a benzene sample was determined for later use as an inert solvent to fill the pycnometer space remaining after introduction of the solid. A large quantity of the solid of interest (~500 mg) was then weighed into the pycnometer and benzene was dis-

tilled into the vessel for the final weighing.

A 114.59 mm Debye-Scherrer camera with nickel-filtered Cu K_α radiation was used to obtain powder diffraction patterns. The finely ground samples were loaded in 0.2 mm thin-walled Lindemann capillaries in the drybox and temporarily sealed with silicone stopcock grease. Upon removal from the drybox the capillaries were quickly sealed permanently with a small flame while the sample remained under nitrogen.

Single crystal x-ray data were collected with Mo K_α radiation on the diffractometer described in Part I. Two distinct data sets were obtained on two separate crystals of bis(tetrapropylammonium)nonabromoditungstate and different computer controlled measurement techniques were employed in the two cases.

The first crystal of $[(C_3H_7)_4N]_2W_2Br_9$ chosen for data collection was exposed to the atmosphere during the mounting procedure. The crystal was wedged into a 0.2 mm capillary and sealed with a small flame. Preliminary alignment x-ray photographs were taken with a Weissenberg camera (Cu K_α radiation) and a Buerger precession camera (Mo K_α radiation). The orientation matrix defining the relationship of the reciprocal lattice to the angular diffractometer settings was deduced from Polaroid exposures as part of the integrated orientation procedure developed by Professor R. A. Jacobson at the Ames Laboratory (118). Intensities were measured via a stationary counting procedure following computerized peak height maximization based on the initial settings for a particular reflec-

tion as calculated from the orientation matrix. Three standards with 2θ values between 20° and 30° verified the orientation of the reciprocal lattice network after every seventy-five reflections and altered the angular settings if required. Fifteen independent reciprocal lattice points ($20° < 2\theta < 30°$) were individually optimized to obtain data which served as input for a least-squares calculation of the unit cell parameters. Data were collected to a 2θ limit of 45° in two unique octants in accord with the monoclinic symmetry displayed by the crystal. Intensity variations due to absorption were experimentally observed perpendicular to the needle axis by rotating the crystal around ∅ while X was held at 90.0° and the intensity of the same reflection was monitored every fifteen degrees. The crystal was photographed with a magnification factor of one hundred by Mr. Harlan Baker of the Ames Laboratory to allow the macroscopic crystal dimensions to be accurately measured for use in absorption correction calculations.

A second crystal was later mounted under oxygen-free conditions in the modified drybox located in Professor J. D. Corbett's laboratory. The data collection procedure was performed as above, but integrated intensities were collected by the ω-scan technique of summing counts for one-half second every one-hundredth degree in omega away from the calculated center of the peak until the counts fell below background as determined by background counts on both sides of the peak

prior to integration. Again fifteen independent high-angle reflections ($30° < 2\theta < 35°$) were optimally centered to furnish data for unit cell computations, absorption effects were monitored on a specific reflection at $\chi = 90.0°$ as a function of ϕ, and magnified pictures of the crystal were obtained for purposes of measuring the crystal dimensions.

RESULTS AND DISCUSSION

Synthesis

The majority of preparative reactions which form metal-metal bonded metal halides are either reductions of high oxidation state halides or disproportionations of intermediate oxidation state halides (1). Such synthetic approaches were discussed in the general introduction and documented for tantalum halides in the literature review of Part I. Direct oxidation of elemental metals with halogenating agents has only rarely been a method of choice for producing metal-metal bonded compounds.

Consideration of the chemical properties deemed most important in likely reactants suggested that metal carbonyl species could be profitably employed in preparing low valent metal halides and perhaps replace the more common high-temperature, sealed tube techniques in some instances. The convenient synthesis of dimolybdenum tetraacetate exemplifies the advantages one would hope to extend to other preparations, as one can simply reflux molybdenum hexacarbonyl in acetic acid and oxidation leads to the molybdenum(II) dimer which contains a quadruple metal-metal bond. The synthesis can be performed with facility since the air stable reactants can be handled with ease and Schlenk glassware is suitable for the reaction vessel. Conversion of the acetate dimer to the anionic octachlorodimolybdate(4-) dimer is easily accomplished in concen-

trated hydrochloric acid.

During the course of this work the idea of employing group VI halocarbonylmetallates as reactants was successfully implemented by R. A. D. Wentworth and co-workers. In the work published by Wentworth the oxidation-reduction reaction between a high oxidation state metal halide and a low valent carbonyl containing metal species produced intermediate oxidation state halide dimers by what could be termed a conproportionation reaction (113). The hypothetical synthetic routes we visualized differed in emphasis from those of Wentworth in that no anhydrous metal halide would be required as a reactant. If one could control the reaction of carbonyl moieties with halogenation reagents to limit the oxidation state of the metal it might be possible to eliminate the precursory anhydrous halide preparation.

R. J. Hoxmeier initiated research in the area of thermal decomposition of group VI trihalotetracarbonylmetallates in noncoordinating solvents in this laboratory. The synthetic basis for these reactions was to take advantage of the increased lability of carbon monoxide as the oxidation state of metal increased to expel the carbonyl ligands under reflux and force the low valent metal species to become ligand deficient. The unusual electronic stability imparted to low oxidation state metals by carbonyl ligands accepting metal electron density via π interactions has been well documented, and one might hope that favorable metal-metal energetics would be

necessary to overcome the loss of stability accompanying carbon monoxide loss from compounds containing oxidation state 2+ metals. The concept of producing highly reactive metal halide intermediates by thermal displacement of carbon monoxide ligands would seem to be a well-founded approach to promoting metal-metal attractions based on the above considerations. One can envision the loss of four carbonyls from $M(CO)_4X_3^-$ to produce MX_3^-, a hypothetical intermediate which has a valence and ligand ratio appropriate for forming metal clusters as ascertained by criteria presented in the general introduction. The use of a noncoordinating solvent is dictated as a means of avoiding the formation of monomeric metal halide adducts. This synthetic philosophy prompted considerable effort to be expended in hopes of isolating tractable products from reactions implementing the above concepts.

The preparation of $(R_4N)M(CO)_5X$ and subsequently $(R_4N)M(CO)_4X_3$ (M = Mo or W, X = Br or I, and R = C_2H_5, n-C_3H_7, or n-C_4H_9) was performed with a variety of solvents prior to thermal decomposition of the metal(II) species under refluxing conditions. The salts were originally prepared in oxygenated solvents such as diglyme (109), but the coordinative tendencies of ethers and other donor solvents directly conflicted with the proposed mechanistic scheme; thus the use of solvents without donor capabilities which would remain inert under vigorous reflux was required. Chlorobenzene proved to be an

excellent reaction medium with sufficient solubilizing properties to form $M(CO)_5X^-$ at reflux and $M(CO)_4X_3^-$ via elemental halogen oxidation at room temperature and still remain inert during the subsequent thermal decomposition step. Isolation and purification problems were the dominant difficulties encountered in working up products of various reactions, and insolubility of the resultant tetraalkylammonium salts in common organic solvents imposed serious limitations on characterization techniques.

Having established the general rationale which guided synthetic attempts in this study, the unsuccessful synthesis of $[(n\text{-}C_3H_7)_4N][W(CO)_5Br]$ in 1,2-dibromoethane can be presented in perspective. The boiling point and dielectric constant of $1,2\text{-}C_2H_4Br_2$ are similar to those of chlorobenzene, and a cursory exploration of the tungsten hexacarbonyl reaction with tetrapropylammonium bromide followed by elemental bromine oxidation to form $[(n\text{-}C_3H_7)_4N][W(CO)_4Br_3]$ and finally thermal decomposition was planned with 1,2-dibromoethane as a solvent. However, unlike the chlorobenzene medium which produced a golden solution of $[(n\text{-}C_3H_7)_4N][W(CO)_5Br]$ in the first step during fifteen minutes of reflux and then stabilized, the 1,2-dibromoethane solvent led to a dark solution with gas evolution proceeding far beyond the amount corresponding to the loss of one carbonyl ligand per tungsten when $[(n\text{-}C_3H_7)_4N][Br]$ and $W(CO)_6$ were refluxed in solution. The excess gas

evolution clearly indicated that the reaction had passed beyond $W(CO)_5Br^-$, and the reaction was allowed to proceed to completion at reflux overnight. The insoluble black solid which resulted ground to display a clean, but not bright, green color. The infrared spectrum from 700 to 4000 cm^{-1} indicated the presence of tetrapropylammonium cations and the absence of carbon monoxide ligands. Preliminary analyses of the product indicated the formulation $[(n\text{-}C_3H_7)_4N]_2[W_2Br_9]$ was deserving of further investigation: W, 25.12% (calcd. 25.19%); Br, 48.00% (49.27%); Br/W, 4.40 (4.50). The mass of the solid isolated was 6.4 g compared to a total mass of 4.5 g for the ten millimolar quantities of tungsten, bromide, and cation in the solid reactants. In fact, only 0.8 g of bromide had been added to the system in the form of $[(n\text{-}C_3H_7)_4N][Br]$ and 3.1 g were present in the product, so it was clear that 1,2-dibromoethane was not functioning as an inert solvent, but rather was serving as a source of bromine in this reaction.

A second preparation of this same product was carried out using chlorobenzene as a solvent to form the bromopentacarbonyltungstate anion cleanly prior to adding excess $1,2\text{-}C_2H_4Br_2$ as an oxidant in a second step as expressed in Equations 23 and 24. A red solution with lots of dark, insoluble material

$$[(n\text{-}C_3H_7)_4N][Br] + W(CO)_6 \xrightarrow[\text{reflux}\ 15\ \text{minutes}]{C_6H_5Cl} [(n\text{-}C_3H_7)_4N][W(CO)_5Br] + CO(g) \qquad (23)$$

$$[(n\text{-}C_3H_7)_4N][W(CO)_5Br] + 1,2\text{-}C_2H_4Br_2 \xrightarrow[\text{reflux}\ 9\ \text{hours}]{C_6H_5Cl} [(n\text{-}C_3H_7)_4N]_2[W_2Br_9] \quad (24)$$

was evident at reflux, but when cooled the solution assumed a light brown color similar to the appearance of weak tea. The black, microcrystalline precipitate smeared to the familiar green color observed previously, and quantitative analyses for W, Br, C and H were in excellent agreement with the values calculated for $[(n\text{-}C_3H_7)_4N]_2[W_2Br_9]$. Yields of 80 to 90% were consistently obtained when the synthesis was repeated. The product was extremely soluble in acetonitrile, and large crystals were obtained by recrystallization from dark green acetonitrile solutions via slow solvent removal under vacuum.

A possible reaction mechanism for the oxidation of the tungsten carbonyl species is suggested by the well known reaction of vicinal dihalides with metallic zinc to generate alkenes. Halogen addition across a carbon-carbon double bond is sometimes employed to protect the alkene linkage while other functional groups are manipulated, since treatment of the resultant dihalide with zinc will regenerate the original double bond by dehalogenation. The site of chemical interest in such a reaction is the organic moiety rather than the oxidized zinc halide, but in the reaction of bromopentacarbonyltungstate(1-) and 1,2-dibromoethane it is the inorganic

product which is of concern, and the only question related to the reduced organic product is its identity. Assuming ethylene results from the reduction of 1,2-$C_2H_4Br_2$ allows one to formulate a balanced equation for the redox reaction as shown in Equation 25. Identification of ethylene in the gaseous reaction products would serve to confirm the oxidative function of

$$4W(CO)_5Br^- + 7(1,2\text{-}C_2H_4Br_2) \rightarrow 2W_2Br_9^{2-} + 20\ CO(g) + 7C_2H_4(g) \quad (25)$$

the dibromoethane. Passage of the evolved gas through benzene resulted in a very dilute solution of ethylene in benzene as evidenced by the proton nuclear magnetic resonance spectrum which showed a small singlet at 5.40 δ units relative to benzene at 7.32. The gaseous species show chemical shifts of 5.18 and 7.13 δ units for ethylene and benzene (119), respectively, so the literature difference of 1.95 compares well with the experimentally observed difference of 1.92 δ units for the identification of ethylene. The very low solubility of ethylene in benzene limited the quality of the nmr spectral data, and the evidence was not considered conclusive. A definitive identification was possible via high resolution mass spectral analysis. An evacuated flask was placed in the exhaust line of the reaction vessel by means of a T-joint, and after addition of the dibromoethane and ten minutes of vigorous reflux the flask was opened to collect a sample of the evolved

gas. The reaction was performed as usual under a molecular nitrogen blanket, and hence all three of the gaseous compounds present had a mass of nearly twenty-eight amu (CO, 27.995; N_2, 28.006; and C_2H_4, 28.031), but a high resolution mass spectrum clearly indicated the presence of appreciable quantities of ethylene. Thus the proposed reaction equation was satisfactorily confirmed.

One question that poses itself is why does this reaction form the unusual odd electron dimer, $W_2Br_9^{2-}$, as opposed to some other bromotungstate, such as the more commonly encountered $M_2X_9^{3-}$ anion. In this regard it can be noted that the $[(n\text{-}C_3H_7)_4N]_2[W_2Br_9]$ salt can be isolated and then extensively refluxed with 1,2-dibromoethane again without undergoing further oxidation, indicating the average tungsten oxidation state of 3.5+ is the equilibrium product under these conditions. It seems likely that the initial cation to metal ratio of one is important in determining the stoichiometry of the final product. The retention of one negative charge per metal atom throughout the reaction sequence probably occurs as bromine oxidizes the metal by replacing carbon monoxide in the coordination sphere, and hence the resultant dimer is constrained to be a dinegative anion and an odd electron compound will result from the addition of seven bromines necessary to reach the stable M_2X_9 stoichiometry.

Several points deserve emphasis relative to the synthesis

of this dimeric compound. First of all no high oxidation state anhydrous metal halide is required as a reactant. Second, the reagents are commercially available, easily handled, and inexpensive. Third, the entire preparation can be conveniently completed in one day, and, finally, good yields are reproducibly obtained.

X-ray Powder Pattern Data

X-ray powder patterns were routinely obtained to check the identity of products. A listing of the estimated relative intensities and d-spacings based on the measured 2θ values recorded with Cu K_α radiation is presented in Table 11.

Temperature Dependent Magnetic Susceptibility Measurements

The dimeric formulation $[(n\text{-}C_3H_7)_4N]_2[W_2Br_9]$ requires the presence of at least one unpaired electron in the ground state. A temperature dependent magnetic susceptibility study was undertaken to examine the magnetic behavior between liquid nitrogen and room temperature. Eleven temperatures were selected at roughly equal intervals in terms of 1/T and forces were measured at each of five magnetic field strengths on a nonabromoditungstate sample which had been recrystallized from acetonitrile. The five data points obtained at each temperature were plotted in the Honda-Owen form (X vs 1/H), and the value of the intercept was employed in later computations to correct for the presence of any trace ferromagnetic impurities.

Table 11. X-ray powder pattern data for $[(n\text{-}C_3H_7)_4N]_2[W_2Br_9]$[a]

2θ(degrees)	d-spacing(Å)	Relative Intensity
9.15	9.66	vs
9.86	8.96	vvs
10.96	8.07	s
15.48	5.72	s
16.44	5.39	m
18.84	4.71	m
20.04	4.43	vw
21.74	4.08	vw
27.52	3.24	w
28.28	3.15	w
36.85	2.44	vw
37.90	2.37	w
46.74	1.94	vw

[a]Data obtained with Cu K_α radiation. Abbreviations: s, strong; m, moderate; w, weak; v, very.

The diamagnetic contribution due to the Teflon sample bucket was subtracted to leave only the susceptibility per gram of sample. Multiplication of the gram susceptibility by the molecular weight of $[(n\text{-}C_3H_7)_4N]_2[W_2Br_9]$, 1459.6 g/mole, led to the molar susceptibility value which was then plotted vs the inverse temperature, 1/T. The plot of χ_M vs 1/T was linear as shown in Figure 14 and indicated the simple Curie formulation was valid as expressed in Equation 26 where χ_M is the

$$\chi_M = C/T + \chi_D + \chi_{TIP} \tag{26}$$

molar susceptibility, χ_D is the diamagnetic contribution due to the paired electrons present, χ_{TIP} is the temperature independent paramagnetic contribution, and C is the Curie constant. The Curie constant is defined in terms of Avogadro's number (N), the Bohr magneton (β), the effective magnetic moment (μ_{eff}), and Boltzmann's constant (k) in Equation 27. A com-

$$C = N\beta^2\mu_{eff}^2/3k \tag{27}$$

puterized linear least-squares fit to the eleven data points confirmed the 1/T dependence as evidenced by the values shown in Equation 28. The numerical values of the slope and inter-

$$\chi_M = (.370\pm.002)\ \frac{^\circ K\ emu}{mole}\ (1/T) - (452\pm19)\times10^{-6}\ emu/mole \tag{28}$$

cept allow one to calculate the effective magnetic moment and the temperature independent paramagnetic contribution, respectively.

$$\mu_{eff} = 2.828\sqrt{C} = 1.72\ BM \tag{29}$$

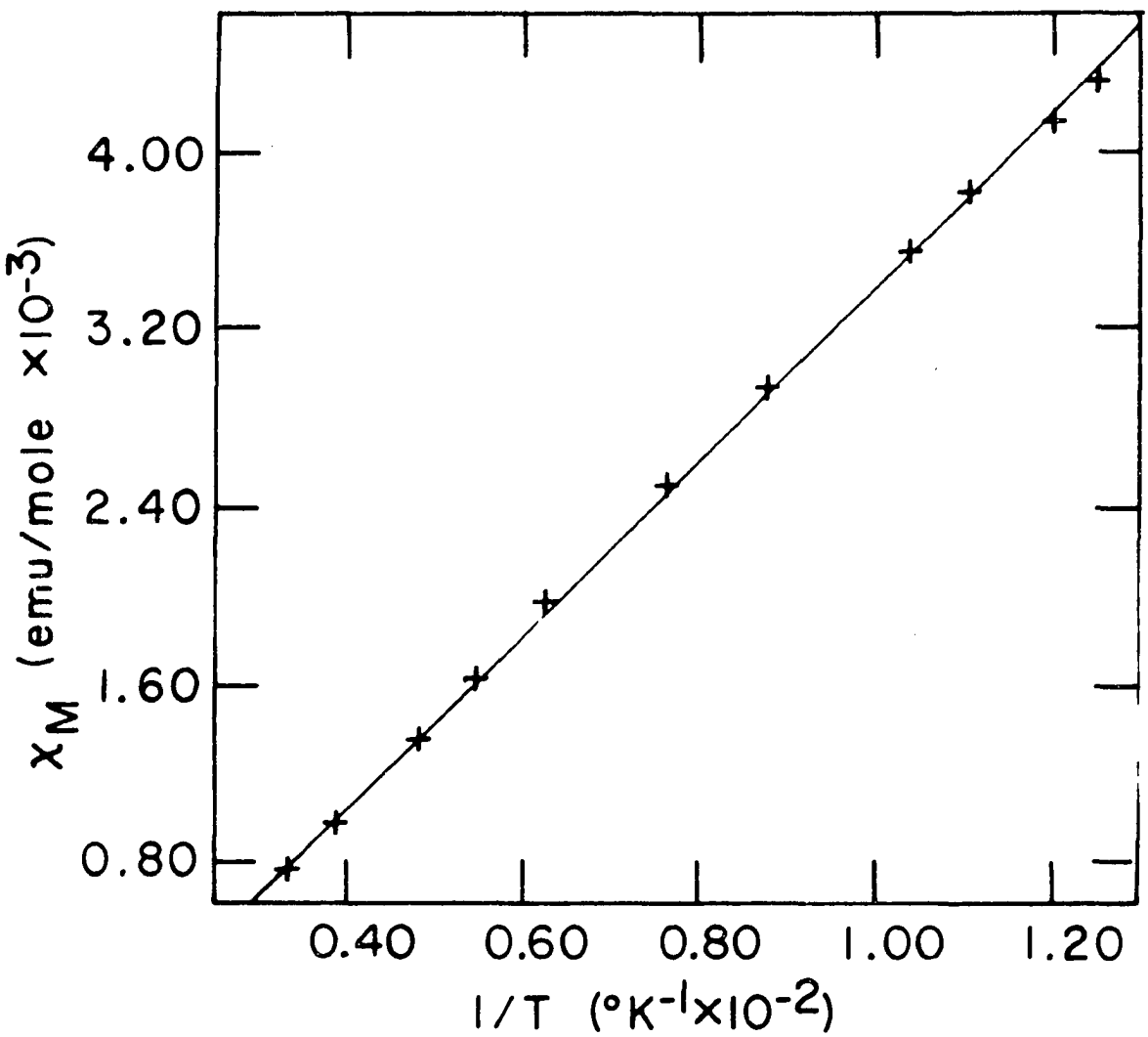

Figure 14. Curie plot (χ_M vs 1/T) for $[(n\text{-}C_3H_7)_4N]_2[W_2Br_9]$

$$\chi_{TIP} = (-452\times10^{-6}+699\times10^{-6}) \text{ emu/mole} = 247\times10^{-6} \text{ emu/mole} \quad (30)$$

The value of 1.72 BM for μ_{eff} is entirely consistent with a single unpaired electron in the ground state and compares favorably with the theoretical spin-only moment of 1.73 BM. The temperature independent paramagnetic contribution, based on a diamagnetic contribution of -699×10^{-6} emu/mole as calculated from values reported by Selwood (63), was not unexpected in view of the similarity in magnitude to those of other third row metal-metal bonded species, such as $Ta_2Br_6(SC_4H_8)_3$ where $\chi_{TIP} = 177\times10^{-6}$ emu/mole.

Electronic Spectrum

A solution spectrum of the nonabromoditungstate(2-) anion was obtained in acetonitrile. The energy of the observed band maxima and a rough estimate of the corresponding extinction coefficients based on weighing a few milligrams of sample into the cell are listed in Table 12. No interpretation of the spectrum was attempted other than to note that the extinction coefficients were very large and thus consistent with significant orbital overlap between the two metal centers which would be expected to increase the intensities of electronic transitions. A more complete discussion of absolute intensities was presented in Part I. The extinction coefficients reported here for $W_2Br_9^{2-}$ are similar in magnitude to those published for $W_2Cl_9^{2-}$ in dichloromethane: 1040 $M^{-1}cm^{-1}$ and 1700 $M^{-1}cm^{-1}$ for bands at 13,530 and 17,200 cm^{-1}, respectively (105).

Table 12. Electronic absorption band parameters for $[(n\text{-}C_3H_7)_4N]_2[W_2Br_9]$[a]

Energy($10^3 cm^{-1}$)	Extinction coefficient($M^{-1}cm^{-1}$)
13.0	1100
16.1	1300
18.2	1100
23.8	5100
27.0	6600

[a]Spectrum obtained in acetonitrile solution.

Table 13. Tetrapropylammonium infrared frequencies (700-1400 cm^{-1})[a]

$[(n\text{-}C_3H_7)_4N]_2[W_2Br_9]$	$[(n\text{-}C_3H_7)_4N][Br]$
745 s	764 vs
808 w	795 vw
841 m	847 s
867 m	908 s
912 m	936 w
962 s	970 vs
978 s	1010 s
1032 s	1030 s
1100 m	1058 s
1167 m	1101 s
1180 m	1160 s
1267 w	1260 vw,sh
1310 w,sh	1274 w
1321 w	1290 m
1348 m	1320 m
	1352 s

[a]Spectra obtained from Nujol mulls. Abbreviations: s, strong; m, moderate; w, weak; sh, shoulder.

Infrared Spectra

Infrared data in the region from 700 to 4000 cm^{-1} established two relevant facts concerning the composition of the product. The presence of tetrapropylammonium cations in the solid was confirmed by comparison with tetrapropylammonium bromide infrared data. In addition, the absence of carbonyl ligands was definitely established by the absence of absorptions between 1600 and 2600 cm^{-1}. The infrared absorptions observed in $[(n\text{-}C_3H_7)_4N]_2[W_2Br_9]$ and $[(n\text{-}C_3H_7)_4N][Br]$ are presented in Table 13 for the region from 700 to 1400 cm^{-1}.

The low frequency region of the infrared spectrum was dominated by two principle absorptions at 232 and 208 cm^{-1}. These very strong bands were assigned to terminal metal-halogen stretching vibrational modes of symmetries A_2'' and E' due to obvious parallels with similar assignments in a normal coordinate analysis of $M_2X_9^{3-}$ compounds by Ziegler and Risen (120). The above two symmetry modes are infrared allowed while the remaining terminal vibrations of A_1' and E'' symmetry are not allowed. Some comparable metal-chloride terminal vibrational frequencies in $M_2X_9^{n-}$ (n = 2,3) anions are listed in Table 14. Particularly noteworthy is the dependence of the observed intensity of the $W_2Cl_9^{3-}$ anion vibrations on the cation present in the lattice. Only the tetraalkylammonium cation resulted in very strong intensities for both the A_2'' and E' terminal modes. Furthermore, the other low frequency

Table 14. Low frequency metal-halogen vibrations in $M_2X_9^{n-}$ anions

Compound	Terminal metal-halogen vibrational modes[a] (cm^{-1})	
	A_2''	E'
$[(n\text{-}C_3H_7)_4N]_3Mo_2Cl_9$[b]	318s	290s
$[(n\text{-}C_4H_9)_4N]_2Mo_2Cl_9$[b]	345s	305s
$Cs_3W_2Cl_9$[c]	313vs	282w
$K_3W_2Cl_9$[c]	313vs	285w
$[(n\text{-}C_4H_9)_4N]_3W_2Cl_9$[c]	311vs	289vs
$[(n\text{-}C_3H_7)_4N]_2W_2Br_9$[d]	232vs	208vs

[a]All data obtained on Nujol mulls. Abbreviations: s, strong; w, weak; v, very.

[b]Data from reference 113.

[c]Data from reference 120.

[d]This work.

bands in $[(n\text{-}C_4H_9)_4N]_3[W_2Cl_9]$ were of only moderate intensity or less relative to the two very intense absorptions mentioned above; such a spectrum is consistent with the present observation of only two strong bands in $[(n\text{-}C_3H_7)_4N]_2[W_2Br_9]$. The frequencies of these two bands are in good agreement with the expected vibrational absorptions based on the following logic. One can legitimately compare $M_2Cl_9^{n-}$ vibrational frequencies with those of $M_2Br_9^{n-}$ as a function of the ratio of the halide masses. It is known that metal-halogen stretching frequencies generally increase as the oxidation state of the metal increases, and this trend is reflected in the data for $Mo_2Cl_9^{3-}$ and $Mo_2Cl_9^{2-}$ in Table 14. The sensitivity of infrared bands to the oxidation state of the metal invalidates a comparison of $W_2Br_9^{2-}$ and $W_2Cl_9^{3-}$ metal-halogen frequencies on a mass basis alone. A better gauge is to note the similarity between the frequencies in $W_2Cl_9^{3-}$ and $Mo_2Cl_9^{3-}$; it is common for isoelectronic compounds of second and third row group VI metals to display metal-halogen stretching vibrations of nearly identical frequencies. One can then predict that $W_2Br_9^{2-}$ would probably have metal-halogen force constants producing frequencies related to those of $Mo_2Cl_9^{2-}$ by the square root of the halogen mass ratio. The square root of the mass ratio of bromine to chlorine is 1.50 and division of the $Mo_2Cl_9^{2-}$ A_2'' and E' vibrational energies by this factor leads to predicted values of 230 and 203 cm^{-1}, respectively, for similar modes in $W_2Br_9^{2-}$.

These predicted energy values agree well with the frequencies observed for tungsten-bromine terminal vibrational modes in the nonabromoditungstate(2-) anion which were located at 232 and 208 cm^{-1}.

X-ray Structural Determination of $[(n\text{-}C_3H_7)_4N]_2[W_2Br_9]$

In order to firmly establish the exact structure of the dimeric anion in $[(N\text{-}C_3H_7)_4N]_2[W_2Br_9]$ an x-ray structural determination was undertaken. Although a confacial bioctahedral structure was postulated, the drastic structural reorganization accompanying the one-electron oxidation of $Mo_2Cl_8^{4-}$ to $Mo_2Cl_8^{3-}$ offered some support for bizarre structural possibilities in the case of the $W_2Br_9^{2-}$ anion. Previous x-ray data had determined confacial bioctahedral structures for many $M_2X_9^{3-}$ dimers of group VI metals (77), but no structural data had been published on the extant odd-electron dimeric anions, $Mo_2Cl_9^{2-}$ or $W_2Cl_9^{2-}$, nor had the structure of $W_2Br_9^{3-}$ been reported. Our initial expectations were realized when a confacial bioctahedral nonabromoditungstate(2-) anion was successfully located and refined after collecting data on two separate crystals and processing the combined data in the manner described below.

Crystals suitable for x-ray studies were chosen from among those recrystallized from acetonitrile. Preliminary photographs indicated a monoclinic space group, and needle shaped crystals proved to have the unique b axis parallel to the

needle axis. After characterizing the space group and unit cell with several crystals a crystal of dimensions 0.05x0.16x 0.35 mm was chosen for diffractometer data collection. Absorption corrections were based on photographs taken by Harlan Baker of the Ames Laboratory with a magnification factor of 100. The orientation and shape of the crystal were input to the TALABS (121) absorption program to generate a corrected data set. The calculated transmission factors varied from 0.4 to 0.1.

Location of fourteen random reciprocal lattice points via Polaroid film techniques followed by computer calculation of the orientation matrix confirmed the 2/m reciprocal lattice symmetry. Data collection was initiated assuming a primitive unit cell, but after several hundred reflections had been monitored it was concluded that a C-centered cell was appropriate as indicated by the absence of all reflections with h+k odd. Two octants of data were collected to a 2θ limit of 45° using Mo Kα radiation. A magnetic tape flaw prohibited transfer of the final 1410 data points so it was necessary to recollect data for those reflections. A scaling procedure was used to normalize the data based on the intensity of the three standards which were checked after every fifty reflections. A total of 2693 data points were retained with $I > 3\sigma(I)$.

Solution of the structure was based on location of the two independent tungsten atoms per asymmetric unit in the

Patterson map. A c-glide plane was present as evidenced by the absence of h0ℓ reflections for ℓ odd. The possible space groups were thus narrowed to Cc or C2/c, and the density of peaks in the Harker planes corresponding to a two-fold rotation axis dictated the centrosymmetric space group, C2/c, be chosen for refinement. Location of the nine bromine atoms proceeded from the electron density map phased by the tungsten atoms. From the eleven heavy atom positions a confacial bioctahedral anionic dimer was confirmed, and a discrepancy factor of 16.3% accompanied the refinement at this point.

Difficulties were encountered in refining the light atom parameters of the two independent tetrapropylammonium cations in the unit cell. Although the basic structural conformation of the four propyl groups tetrahedrally coordinated to each of the two central nitrogen atoms was evident, the thermal parameters and interatomic distances within each cation were disturbingly variant, and the discrepancy factor leveled off at 10.0%. The eleven heavy atoms present in $[(n\text{-}C_3H_7)_4N]_2[W_2Br_9]$ clearly dominated the refinement and the positional coordinates and thermal parameters of these atoms were insensitive to the location and refinement of the light atoms present in the two cations. Attempts to introduce statistical disorder into the light atom positions uniformly failed to improve the refinement.

In hopes of resolving the difficulties encountered in refining the parameters describing the twenty-six light atoms

a second crystal was selected for data collection. Drybox techniques were used to mount the crystal to assure the complete absence of oxygen and moisture. The crystal dimensions were 0.21x0.32x0.66 mm as measured on magnified photographs obtained in the same manner as for the first crystal. The TALABS absorption program was again employed to generate a set of corrected intensities from the raw data. The calculated transmission factors varied from 0.03 to 0.12 in accord with the experimentally observed variation as a function of $\emptyset$ at $\chi = 90.0°$. Data were collected to a 2θ limit of 50.0°. A total of 3285 reflections were stored based on a sorting criterion of $I > 3\sigma(I)$.

Refinement of the heavy atom positions proceeded as with the first data set and location of the light atoms from an electron density difference map produced results similar to those of the first data set as well. The light atom thermal parameters were abnormally large and the carbon-carbon single-bond distances varied considerably. Although the two data sets were collected on different size crystals selected from different preparations with different counting techniques employed, and in addition a time lag of six months separated the two procedures, the results of the two independent refinements were basically the same. This observation indicated that a data averaging procedure might aid the refinement and would be justified as a means of eliminating any systematic errors present in either the collection techniques or the absorption

computations.

The two independent data sets were normalized by comparing the two scale factors from the best refinement cycle of each set and scaling all of the data from one crystal by this factor. Averaging of equivalent data was then performed, and data points with symmetry equivalent indices that deviated by more than 20% of the average intensity of the two data points were discarded. Of the 2370 equivalent reflections averaged 2255 agreed sufficiently well for use in the final refinement.

Lattice constants were determined by a least-squares fitting procedure which restricted α and γ to 90.0° as required by monoclinic symmetry. Thirty high angle 2θ values that had been individually centered, fifteen from each crystal, were input for the calculation. The following lattice parameters and associated errors resulted: $a = 36.420 \pm .025$Å, $b = 12.067 \pm .008$Å, $c = 19.624 \pm .012$Å, and $\beta = 95.90 \pm .02°$.

A satisfactory discrepancy factor was obtained with the averaged data set. Anisotropic refinement of all nonhydrogen atoms led to $R = \Sigma||F_o|-|F_c||/\Sigma|F_o| = 5.0\%$ and $R_w = [\Sigma w(|F_o|-|F_c|)^2/\Sigma w(F_o)^2]^{1/2} = 6.3\%$. The scattering factors were those of Hanson et al. (73), with tungsten and bromine modified for the real and imaginary parts of anomalous dispersion (74). The final positional and thermal parameters are listed in the Appendix along with their standard deviations as derived from the inverse matrix of the final least-squares cycle (75).

Interatomic distances within the cations and a tabulation of F_o and F_c are also found in the Appendix.

The confacial bioctahedral structure of the nonabromoditungstate(2-) anion is illustrated in Figure 15, and the two independent cation conformations are shown in Figure 16. Bond distances, nonbonded distances, and angles of interest for the anion are listed in Tables 15, 16, and 17, respectively. The structure is best described as two octahedra sharing a common trigonal face such as has been observed for $M_2X_9^{3-}$ salts structurally characterized by various workers (77).

The tungsten-tungsten distance of 2.601(2)Å in $W_2Br_9^{2-}$ is definitely in the range indicative of strong metal-metal attractive forces, even though it is 0.19Å longer than the corresponding distance in $W_2Cl_9^{3-}$. Again one must turn to the distortional moduli derived for confacial bioctahedral structures to correctly assess the extent of the metal-metal interaction. A comparison of the generalized parameter values for $W_2Br_9^{2-}$ ($d'/d'' = 0.90$, $90.0° - \alpha' = -7.1°$, and $\beta - 70.5° = -10.5°$) with those of the other confacial bioctahedral dimers is available in Table 18. The two tungsten dimers, $K_3W_2Cl_9$ and $[(n\text{-}C_3H_7)_4N]_2[W_2Br_9]$, are clearly separated from the other confacial bioctahedral structures by greater axial distortions as reflected in the numerical values of the moduli proposed by Cotton and Ucko (77).

Data for the $Mo_2Cl_8^{3-}$ anion has been included in Table 18,

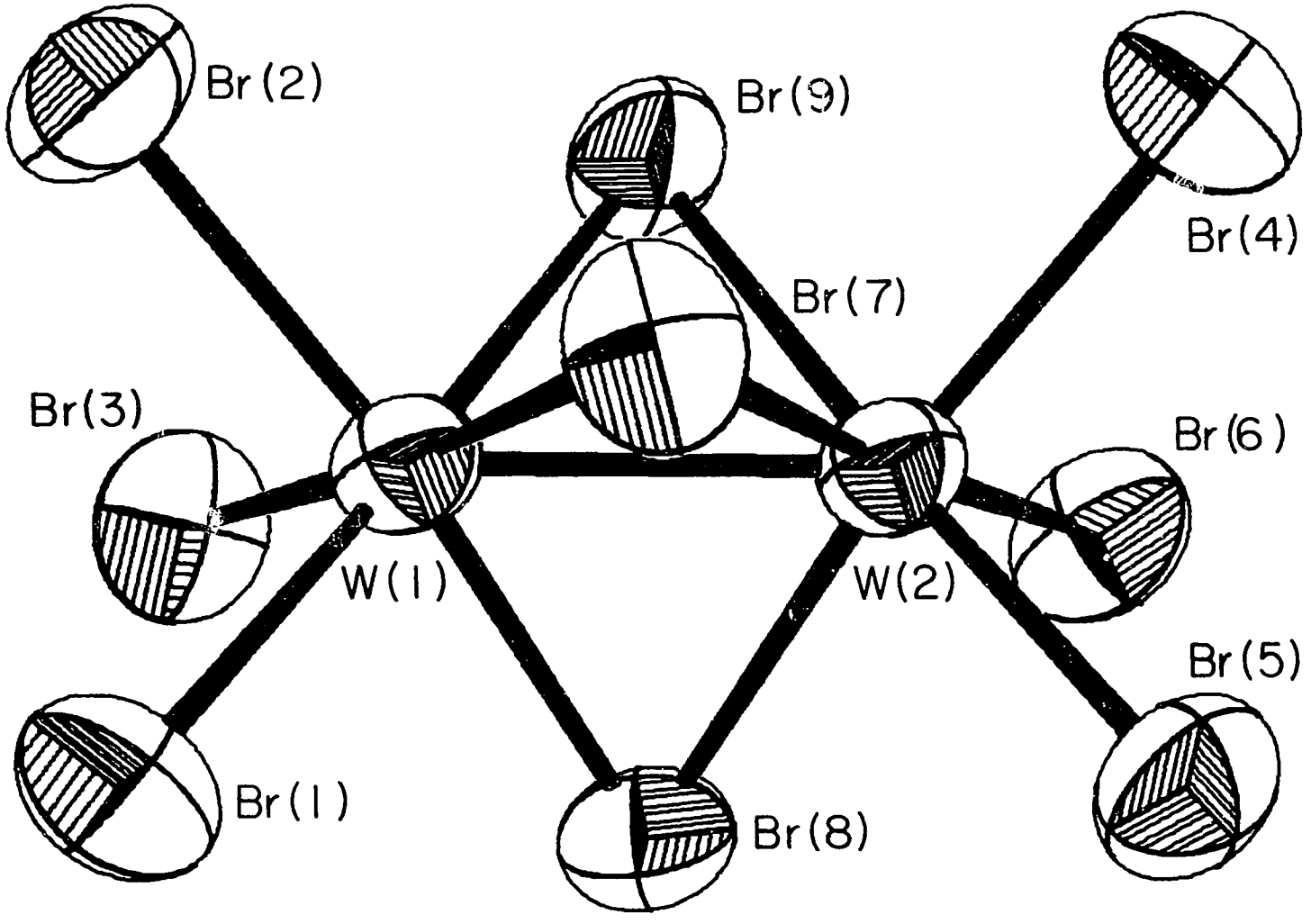

Figure 15. A perspective view of the 50% probability thermal ellipsoids of the $W_2Br_9^{2-}$ anion

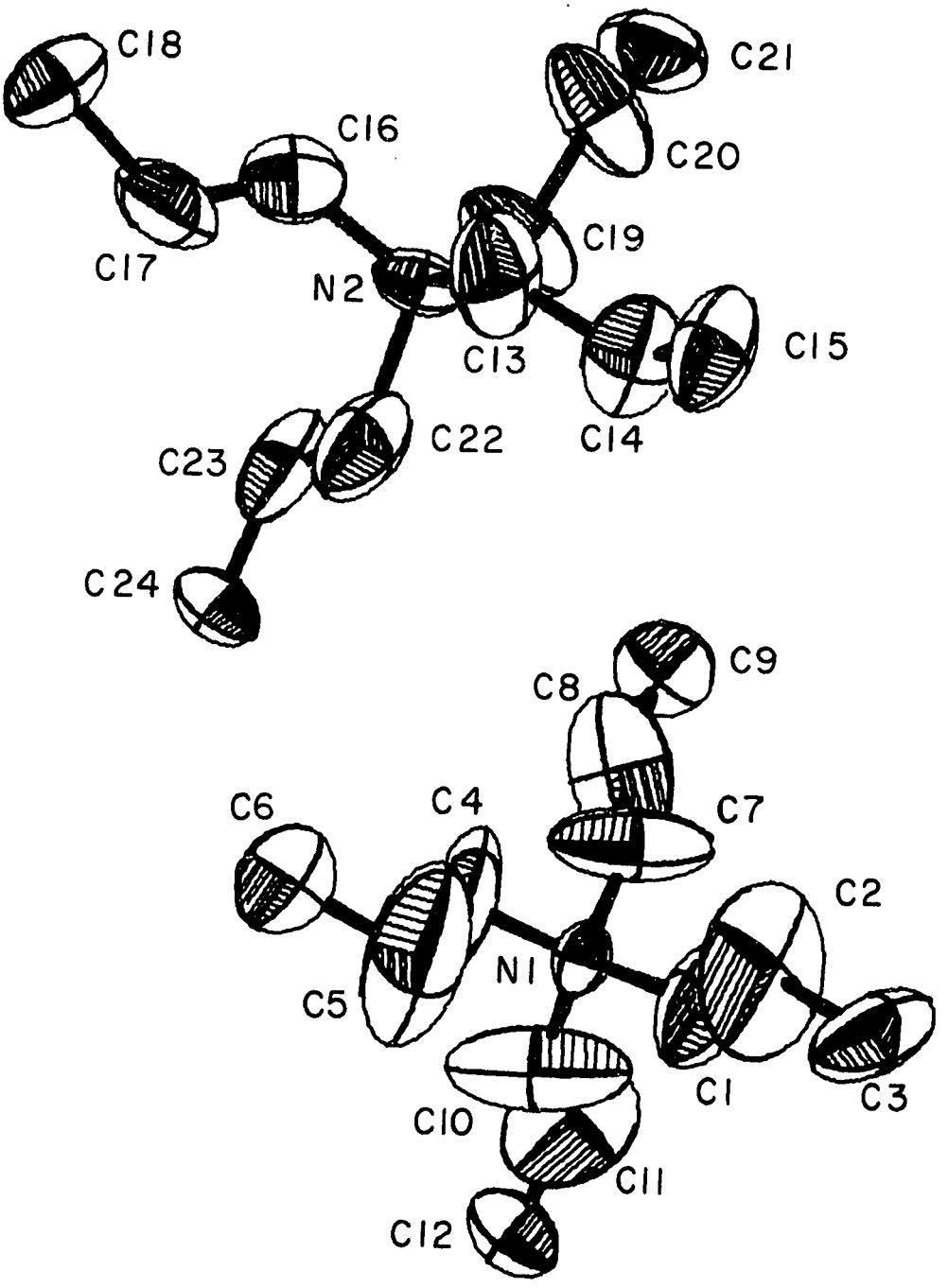

Figure 16. A perspective view of the 33% probability thermal ellipsoids of the two independent $[(n\text{-}C_3H_7)_4N]^+$ cations

Table 15. Bond distances in $W_2Br_9^{2-}$, Å

W(1)-W(2)	2.601(2)
W(1)-Br(1)	2.535(4)
W(1)-Br(2)	2.538(4)
W(1)-Br(3)	2.544(4)
W(2)-Br(4)	2.547(4)
W(2)-Br(5)	2.525(4)
W(2)-Br(6)	2.514(4)
Average $W\text{-}Br_{terminal}$	2.534
W(1)-Br(7)	2.600(3)
W(1)-Br(8)	2.597(4)
W(1)-Br(9)	2.602(4)
W(2)-Br(7)	2.608(4)
W(2)-Br(8)	2.597(4)
W(2)-Br(9)	2.599(4)
Average $W\text{-}Br_{bridge}$	2.601

Table 16. Nonbonded distances in $W_2Br_9^{2-}$, Å

Br(1)-Br(2)	3.588(5)
Br(1)-Br(3)	3.671(5)
Br(2)-Br(3)	3.574(6)
Br(4)-Br(5)	3.579(5)
Br(4)-Br(6)	3.558(6)
Br(5)-Br(6)	3.643(5)
Average $Br_{terminal}\text{-}Br_{terminal}$	3.602
Br(1)-Br(7)	3.535(5)
Br(1)-Br(8)	3.494(6)
Br(2)-Br(7)	3.472(5)
Br(2)-Br(9)	3.542(5)
Br(3)-Br(8)	3.456(5)
Br(3)-Br(9)	3.531(6)
Br(4)-Br(7)	3.515(6)
Br(4)-Br(9)	3.537(5)
Br(5)-Br(7)	3.535(5)
Br(5)-Br(8)	3.504(5)
Br(6)-Br(8)	3.416(6)
Br(6)-Br(9)	3.509(5)
Average $Br_{terminal}\text{-}Br_{bridge}$	3.504
Br(7)-Br(8)	4.011(5)
Br(7)-Br(9)	3.788(5)
Br(8)-Br(9)	3.891(5)
Average $Br_{bridge}\text{-}Br_{bridge}$	3.897

Table 17. Angles (degrees) within $W_2Br_9^{2-}$

W(1)-Br(7)-W(2)	59.93(8)
W(1)-Br(8)-W(2)	60.10(9)
W(1)-Br(9)-W(2)	60.02(8)
Average W-Br_{bridge}-W	60.02
Br(7)-W(1)-Br(8)	101.1(1)
Br(7)-W(1)-Br(9)	93.5(1)
Br(8)-W(1)-Br(9)	96.9(1)
Br(7)-W(2)-Br(8)	100.8(1)
Br(7)-W(2)-Br(9)	93.4(1)
Br(8)-W(2)-Br(9)	97.0(1)
Average Br_{bridge}-W-Br_{bridge}	97.1
Br(1)-W(1)-Br(2)	90.0(1)
Br(1)-W(1)-Br(3)	92.6(1)
Br(2)-W(1)-Br(3)	89.4(1)
Br(4)-W(2)-Br(5)	89.8(1)
Br(4)-W(2)-Br(6)	89.3(1)
Br(5)-W(2)-Br(6)	92.6(1)
Average $Br_{terminal}$-W-$Br_{terminal}$	90.6
Br(1)-W(1)-Br(7)	87.0(1)
Br(1)-W(1)-Br(8)	85.8(1)
Br(2)-W(1)-Br(7)	85.0(1)
Br(2)-W(1)-Br(9)	87.1(1)
Br(3)-W(1)-Br(8)	84.5(1)
Br(3)-W(1)-Br(9)	86.7(1)
Br(4)-W(2)-Br(7)	86.0(1)
Br(4)-W(2)-Br(9)	86.8(1)
Br(5)-W(2)-Br(7)	87.0(1)
Br(5)-W(2)-Br(8)	86.3(1)
Br(6)-W(2)-Br(8)	83.9(1)
Br(6)-W(2)-Br(9)	86.7(1)
Average ($Br_{terminal}$-W-Br_{bridge})$_{cis}$	86.1
Br(1)-W(1)-Br(9)	177.1(1)
Br(2)-W(1)-Br(8)	172.4(1)
Br(3)-W(1)-Br(7)	174.4(1)
Br(4)-W(2)-Br(8)	172.0(1)
Br(5)-W(2)-Br(9)	176.5(1)
Br(6)-W(2)-Br(7)	175.3(1)
Average ($Br_{terminal}$-W-Br_{bridge})$_{trans}$	174.6

Table 18. Selected confacial bioctahedral structural comparisons[a]

Modulus	$W_2Br_9^{2-}$[b]	$W_2Cl_9^{3-}$	$Mo_2Br_9^{3-}$	$Mo_2Cl_9^{3-}$	$Cr_2Br_9^{3-}$	$Cr_2Cl_9^{3-}$	$Mo_2Cl_8^{3-}$
M-M,D(Å)	2.60	2.41	2.82	2.66	3.32	3.12	2.38
$\angle X_{br}\text{-}M\text{-}X_{br}, \alpha'$(°)	97.1	98	93.9	94.2	83.0	85.8	99.2
$\angle M\text{-}X_{br}\text{-}M, \beta$(°)	60.0	58	64.9	64.5	80.0	76.4	56.8
d'/d"	0.90	0.90	0.97	0.98	1.28	1.23	0.89
90.0°-α'(°)	-7.1	-8	-3.9	-4.2	7.0	4.2	-9.2
β-70.5°(°)	-10.5	-12.5	-5.6	-6.0	9.5	5.9	-13.7

[a]Data taken from reference 77 unless otherwise noted.

[b]This work.

but, as was emphasized in the literature review of Part II, the statistical absence of one bridging chlorine invalidates quantitative moduli comparisons between this unusual ion and true confacial bioctahedral structures. Nonetheless, the $Mo_2Cl_8^{3-}$ data is important in that the strength and structural influence of repulsions due to the presence of bridging ligands is firmly established by noting the distortional parameters calculated for the $Mo_2Cl_8^{3-}$ anion are consistently indicative of a greater degree of contraction than in any case involving a true triply-bridged dimer of D_{3h} symmetry. Only the two tungsten confacial bioctahedral structures have sufficient metal-metal bond strengths to display distortions similar to those of the unorthodox octachlorodimolybdate(3-) dimer.

The similarity in the distortional parameter values calculated for $W_2Cl_9^{3-}$ and $W_2Br_9^{2-}$ lends credence to the exceptionally short W-W distance of 2.41Å in the nonachloroditungstate(3-). The comparison of $Mo_2Cl_9^{3-}$ and $Mo_2Br_9^{3-}$ detailed earlier in the literature review revealed the advantages of considering factors other than the metal-metal distance in these structures. Even though the Mo-Mo separation increased by 0.16Å when bromines replaced chlorines in these molybdenum dimers the deviations from the idealized confacial bioctahedron were nearly identical for the two compounds. In the case of the $W_2Br_9^{2-}$ and $W_2Cl_9^{3-}$ dimers a difference in oxidation states exists in addition to the difference in the halogen atoms. The

W-W distance differs by almost 0.19Å between these two compounds, and yet the distortional parameters indicate that the degree of contraction is nearly the same in both anions, so the variance in the metal-metal bond length can be attributed almost entirely to the steric and electronic requirements of bridging bromine atoms as compared to chlorine atoms.

The conclusion that steric requirements of the halide ligands dominate the metal-metal separation neglects the electron configuration difference between $W_2Cl_9^{3-}$ and $W_2Br_9^{2-}$. The six valence d-electrons available from the two metal atoms in $W_2Cl_9^{3-}$ are predicted to nicely fill the a_1' σ-bonding molecular orbital and the degenerate e' π-bonding orbitals, hence producing a formal bond order of three. The $W_2Br_9^{2-}$ anion has only five valence electrons available for metal-metal bonding, and consequently the a_1' molecular orbital is filled but only three electrons occupy the e' orbitals. This leads to a calculated bond order of 2 1/2 and a corresponding difference of 1/2 in the formal bond orders between the two tungsten dimers, which is a somewhat misleading indicator of the actual physical difference in the attractive force between the metal atoms. An electron in the σ-bonding orbital doubtlessly contributes more stability to the metal-metal bond than an electron in the π-bonding orbital, but the bond order is functionally independent of which bonding orbital is occupied or empty; i.e. it is only the number of electrons present in bonding orbitals which establishes the bond order and not

which bonding orbitals are involved. The contribution of a single electron in the π-bonding metal-metal molecular orbitals may be a relatively minor force in determining the actual metal atom separation. Certainly examining the results of comparing $Mo_2Cl_9^{3-}$ and $Mo_2Br_9^{3-}$ in light of a similar comparison between $W_2Cl_9^{3-}$ and $W_2Br_9^{2-}$ guides one toward such an evaluation of the impact of altering the bond order by removal of one π-bonding electron. The 0.19Å elongation observed in the nonabromoditungstate(2-) relative to the nonachloroditungstate(3-) metal-metal distance is only 0.03Å longer than the difference in the two $Mo_2X_9^{3-}$ (X = Cl, Br) dimers where the electron configuration remains unchanged.

One aspect of the electronic structure predicted for a confacial bioctahedron with five electrons in metal-metal bonding molecular orbitals such as those depicted in Figure 9 is the existence of an orbitally degenerate $^2E'$ ground state. This orbital degeneracy theoretically requires some distortion to occur in order to break the degeneracy in accord with the theorem of Jahn and Teller (122). The Jahn-Teller theorem states that if a nonlinear molecule gives rise to an orbitally degenerate ground state as first presented, it will be found that a reduction to lower symmetry will occur as a means of removing that degeneracy. These distortions may be either static or dynamic in nature. Examples of observed Jahn-Teller distortions in octahedral complexes are largest when the e_g σ-antibonding orbitals have an odd number of electrons present

(refer to Figure 7 for the octahedral molecular orbital diagram). Axial ligand displacements of up to 0.3Å in $Cu^{2+}(d^9)$ octahedral complexes have been attributed to such Jahn-Teller effects (123). On the other hand static Jahn-Teller distortions resulting from degeneracies within the t_{2g} manifold of molecular orbitals which are nonbonding relative to the metal-ligand σ-bonds lack experimental confirmation (124). The t_{2g} orbital energies are not greatly influenced by metal-ligand distortions and as a result the driving force for Jahn-Teller stabilization is too small to effect observable changes in the ligand dispositions.

The nonabromoditungstate(2-) dimer molecular orbital scheme (Figure 9) reveals the situation with respect to metal-ligand bond distortions to be the same as in monomeric octahedral compounds with orbital degeneracies due to electron occupancy of the t_{2g} orbitals. A Jahn-Teller distortion is theoretically predicted, but the nonbonding nature of the degenerate e' orbitals involved with respect to the metal-ligand σ-bond framework precludes any significant metal-ligand bond length dependence on the occupancy or location of these energy levels. The dimeric case differs substantially from the monomeric case in that the e' orbitals of D_{3h} symmetry derived from the O_h t_{2g} orbitals are potentially bonding orbitals for the metal-metal interaction, albeit the energy of this contribution is of uncertain magnitude. Thus a distortion

of the metal-metal bonding description would be anticipated to break the ground state orbital degeneracy while metal-ligand bonding remains virtually undistorted in the sense that bonds that were equivalent in D_{3h} symmetry would retain similar bond lengths in the distorted structure.

The task of distorting the confacial bioctahedral structure to remove the e' degeneracy cannot be completed by varying the metal-metal separation, however. Even though contraction and elongation along the three-fold axis will drastically alter the orbital overlap, and therefore the absolute energy, of the a_1' and e' bonding orbitals, the D_{3h} symmetry would be retained and the e' degeneracy would remain unbroken. The only remaining distortions are angular in nature, and one can envision several possibilities for preferentially lowering the energy of one of the two π-bonding molecular orbitals which are energetically equivalent in rigorous D_{3h} symmetry.

It is conceivable that an angular distortion in the disposition of the three bridging bromides could favor one of the two π-orbitals at the expense of the other in a manner reminiscent of that detailed in the discussion of the structure of $Ta_2Br_6(SC_4H_8)_3$. In the tantalum dimer an additional and very important constraint was the Ta-S_{br} bond length of 2.39Å which forced large angular displacements of the two bridging bromines in order to favorably accommodate the b_1 symmetry π-orbital between the bridging sulfur and bromine atom separations of 3.86 and 3.90Å while the bridging bromines closed to

within 3.30Å of one another. The Ta-Br_{br} average bond length of 2.63Å is similar to the 2.60Å distance from tungsten to the bridging bromines in the tungsten dimer, but the presence of three such bridging bromines in $W_2Br_9^{2-}$, rather than only two with the third bridging atom almost 0.2Å closer to the two metal atoms as in $Ta_2Br_6(SC_4H_8)_3$, allows the nonbonded separations among the bridging atoms in the tungsten dimer to vary from a minimum value of 3.79Å through 3.89Å to 4.01Å. These separations average 3.90Å while the corresponding average in the tantalum dimer is 3.69Å due to the additional constraints imposed by the Ta-S_{br} bond distances. Since the average bridging nonbonding separation in $W_2Br_9^{2-}$ is nearly equal to the two larger bridging separations in $Ta_2Br_6(SC_4H_8)_3$, it seems plausible that angular distortions of the bridging bromides would not be required nor would they be likely to promote a lower energy for either π-orbital in the tungsten dimer. It appears that the nonbonded bridging distances in $W_2Br_9^{2-}$ are inherently large enough to support the intervening π-electron density as a result of the contraction of the two metal centers which couples with the inflexible length of the tungsten-bromine bridge bonds to enlarge the bridging atom triangle. While an angular displacement of the bridging bromides might possibly break the degeneracy of the π-levels by raising the energy of one of the two π-molecular orbitals depicted in Figure 10 by collapsing toward the occupied lobes of the orbital, it seems doubtful that the increased space

available to the other π-orbital would cause a correspondingly large decrease in energy, and hence the overall result would be energetically unfavorable.

The search for a small angular distortion in the structure of $[(n\text{-}C_3H_7)_4N]_2W_2Br_9$ consistent with the relative importance of the e' molecular orbital occupancy was rewarded by the following apparently picayune observation to which chemical significance may be attached. The three planes used to define d' and d'' in Part I (see Figure 6) were assumed to be perpendicular to the metal-metal axis, and in the D_{3h} case these planes are necessarily parallel to one another and perpendicular to the three-fold axis by symmetry. Crystallographic three-fold symmetry is not imposed on the $W_2Br_9^{2-}$ anion, however, and, in fact, the location of each of the eleven heavy atoms is independent of any symmetry restrictions. The distortion which is experimentally observed in $W_2Br_9^{2-}$ is a slight canting of the two planes defined by the two sets of three terminal bromine atoms toward the bridgehead position occupied by Br(8). Distances and angles relevant to this distortion are presented in Figure 17. This angular rotation of the terminal trigonal face of ligands on each tungsten atom may appear unrelated to the metal-metal π-bonding interaction, but a strong link exists between the orientation of the metal d-orbital lobes used for metal-metal overlap and the spatial disposition of the remaining metal atom orbitals which form σ-bonds to the ligands. If one attempts to break the π-orbital

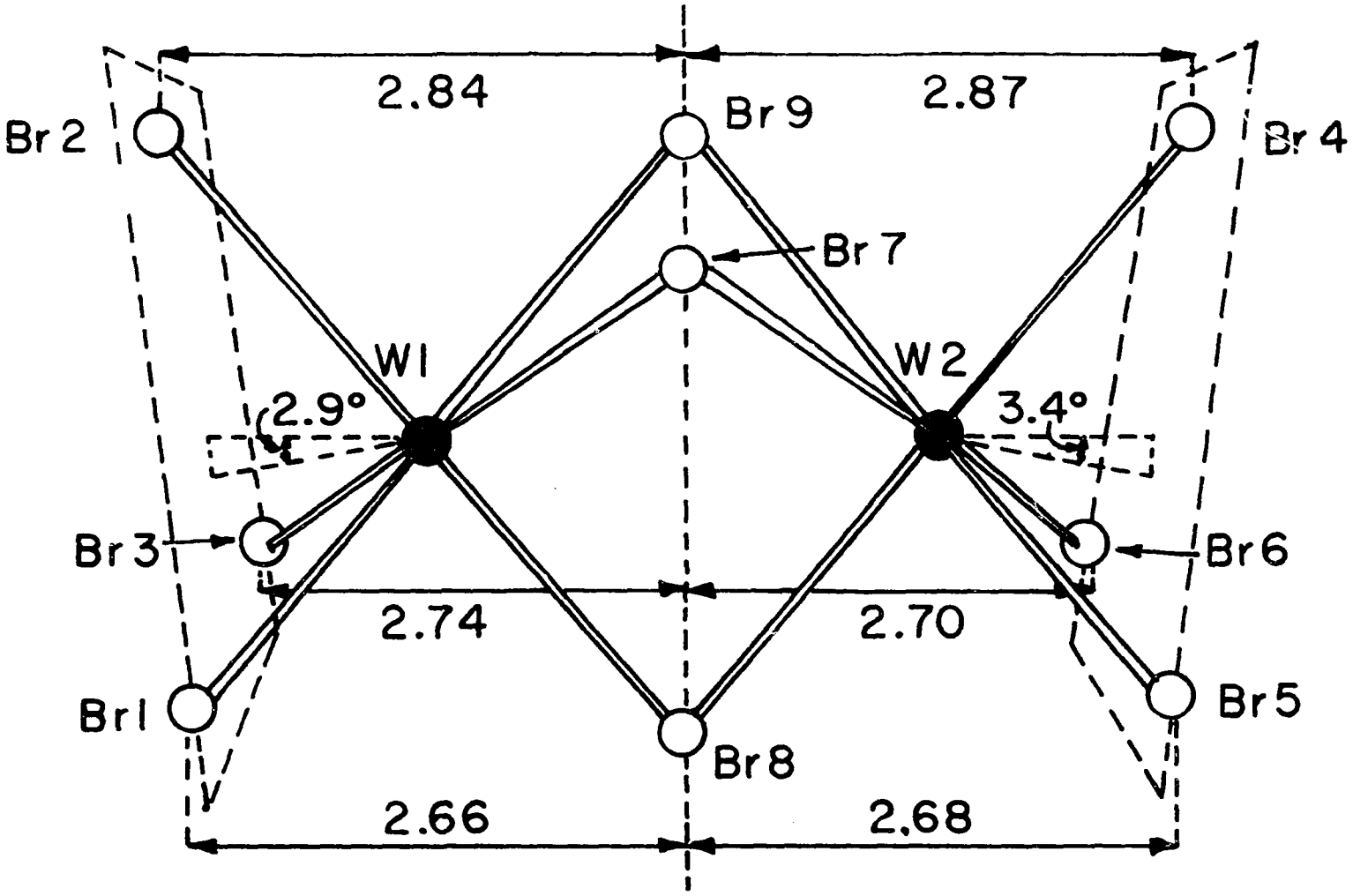

Figure 17. Schematic diagram of the canted terminal ligand planes in $W_2Br_9^{2-}$

degeneracy by some means other than raising the energy of one of the two orbitals via an angular displacement of the three bridging ligands such as discussed and rejected above for $W_2Br_9^{2-}$, it becomes evident upon examining the overlap considerations depicted in Figure 18 that a small rotation of the atomic orbitals on both tungsten atoms around axes perpendicular to the plane of the paper will effect the desired energy separation. The orbital rotation illustrated would increase the overlap of the b_1 π-orbital where the b_1 representation is appropriate after tilting the terminal ligand planes reduces the effective symmetry of the dimer by eliminating the C_3 axis. In the case where both terminal planes tilt towards one another, as observed in the $W_2Br_9^{2-}$ structure, the symmetry elements retained consist of the identity element, two mirror planes and one two-fold axis perpendicular to the metal-metal axis. In other words, an effective symmetry of C_{2v} pertains to the distorted structure observed for $W_2Br_9^{2-}$, and the molecular orbital representations derived in Part I for $Ta_2Br_6(SC_4H_8)_3$ are valid in the discussion of the symmetry reduction apparent in $[(n\text{-}C_3H_7)_4N]_2W_2Br_9$.

Before pursuing any interpretation of the tilted planes further the validity of examining the structure in terms of such a small deviation from D_{3h} symmetry should be firmly established. The theoretical prediction of a Jahn-Teller distortion was couched in terms of the relative effects apparent in octahedral complexes of different configurations. The

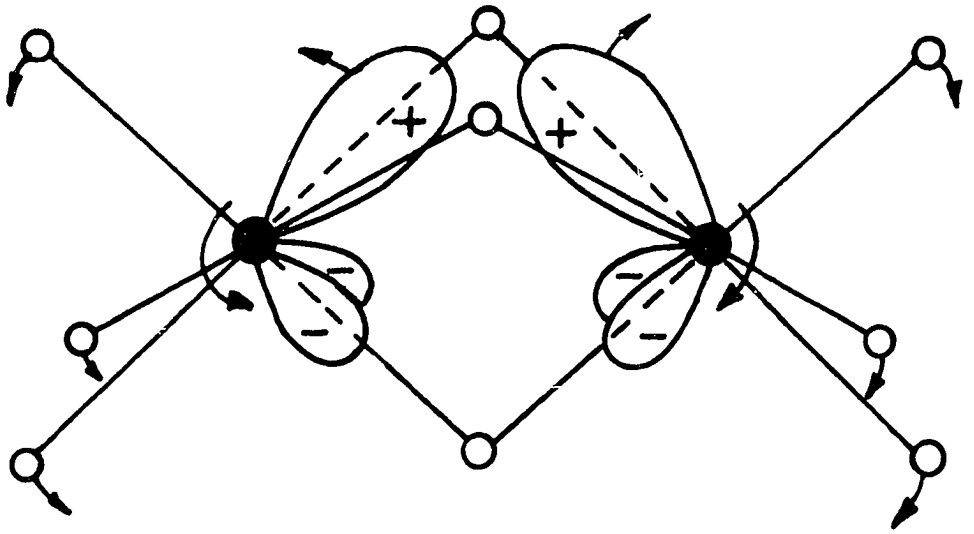

a_1 π-orbital in C_{2V} symmetry

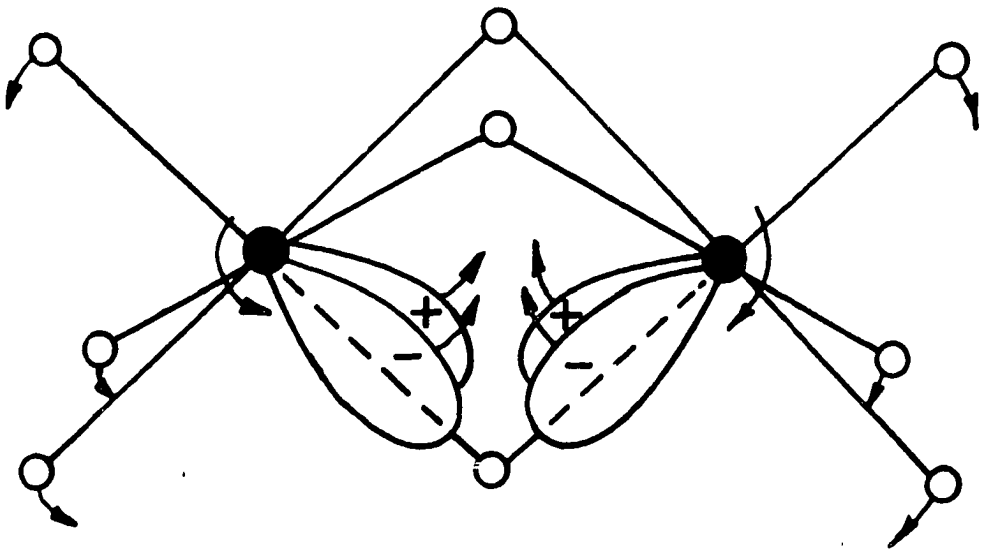

b_1 π-orbital in C_{2V} symmetry

Figure 18. Metal orbital rotation proposed to influence the energy of the metal-metal π-bonds

existence of large distortions resulting from the involvement of antibonding e_g orbitals was contrasted with the negligible distortions due to t_{2g} nonbonding orbital occupancy. The union of two octahedra to form the dimeric $W_2Br_9^{2-}$ anion should then fit in the latter category of negligible distortions since the odd electron is found in a "modified t_{2g} orbital" where an unknown perturbation is introduced by the possibilities of metal-metal bonding. This redundant summary of the Jahn-Teller background material is intended to clarify the type of structural deformation one might expect in the paramagnetic tungsten dimer. A subtle distortion that will favorably influence one of the two π-orbitals without altering any metal-ligand bond strengths seems most likely to result as a compromise among the contributing factors. The use of the word subtle is to be emphasized since a complete absence of any detectable distortion could have been rationalized on the basis of comparisons with certain octahedral species for which Jahn-Teller distortions are predicted but not observed in crystal structures.

The point to be stressed is that there does exist a very significant deviation from D_{3h} symmetry relative to the standard deviations of the parameters involved in the structure of $W_2Br_9^{2-}$. The distortion observed is a real one even though it is small in magnitude, and a chemical explanation can justifiably be sought. Packing forces within the crystal and van der Waals interactions should be investigated before searching for

more sophisticated and perhaps less reliable rationalizations, but nonetheless a rationalization of some sort is in order.

A survey of the nearest neighbor distances between the cations and the anion reveals only seven heavy atom-light atom separations of less than 4.0Å: Br(6)-C(8), 3.99(7); Br(6)-C(11), 3.88(6); Br(6)-C(21), 3.84(4); Br(1)-C(23), 3.81(5); Br(4)-C(17), 3.80(5); Br(5)-C(7), 3.98(4); Br(8)-C(2), 3.94(7). These distances are acceptable nonbonding separations with no systematic structural implications and in no way account for the distortions observed in the dianion.

Examination of nonbonded contacts within the $W_2Br_9^{2-}$ anion are not suggestive of any gross violation of van der Waals radii boundaries similar to that encountered in the bridging bromines of $Ta_2Br_6(SC_4H_8)_3$. However, a close inspection does reveal some trends which are small but significant in that they oppose the observed canted deformation rather than promoting any tilt of the terminal ligand planes.

As mentioned previously the bridging ligands are well separated from one another, and in fact they exceed the remaining cis-bromine nonbonded distances by an average of 0.37Å. Examination of the Br_{term}-Br_{term} nonbonded contacts indicates two classifications can be derived from the six distances. Four distances are between 3.56 and 3.59Å while the remaining two are 3.64 and 3.67Å with the associated standard deviations near .005Å for each of the distances. The two longer distances are related in that both are between terminal atoms cis

to bridging Br(8); more concisely the two longer separations are related by the C_2-axis of C_{2v} symmetry even though no such relationship is crystallographically imposed.

Continued scrutiny of the nonbonded terminal-bridging bromine contacts supplements the previous data by again singling out $Br_{br}(8)$ as slightly unique in the array of cis-bromine distances: $Br_{br}(8)$-Br_t average 3.47Å; $Br_{br}(9)$-Br_t average 3.53Å; $Br_{br}(7)$-Br_t average 3.51Å. The differences in the average Br_{br}-Br_t distances are small but statistically significant since the standard deviations are near 0.005Å for these heavy atoms as was mentioned previously. Particularly when one considers that the larger separations observed between Br(1)-Br(3) and Br(5)-Br(6) would tend to increase the nonbonded separations of $Br_{br}(8)$ with all four adjacent terminal cis-bromines and yet the $Br_{br}(8)$ contacts still remain significantly less than those of $Br_{br}(7)$ and $Br_{br}(9)$, it seems logical to discount steric hindrance among the bromines as a possible contributor to the observed canted structure. Quite the opposite conclusion can be reached in relating the steric interactions to the observed structure deformation: to the extent that nonbonded contacts are important they oppose the observed small rotation of the terminal trigonal faces since greater repulsions result as four of the terminal atoms approach bridging atom Br(8) more closely. Figure 19 illustrates the nonbonding distances discussed above.

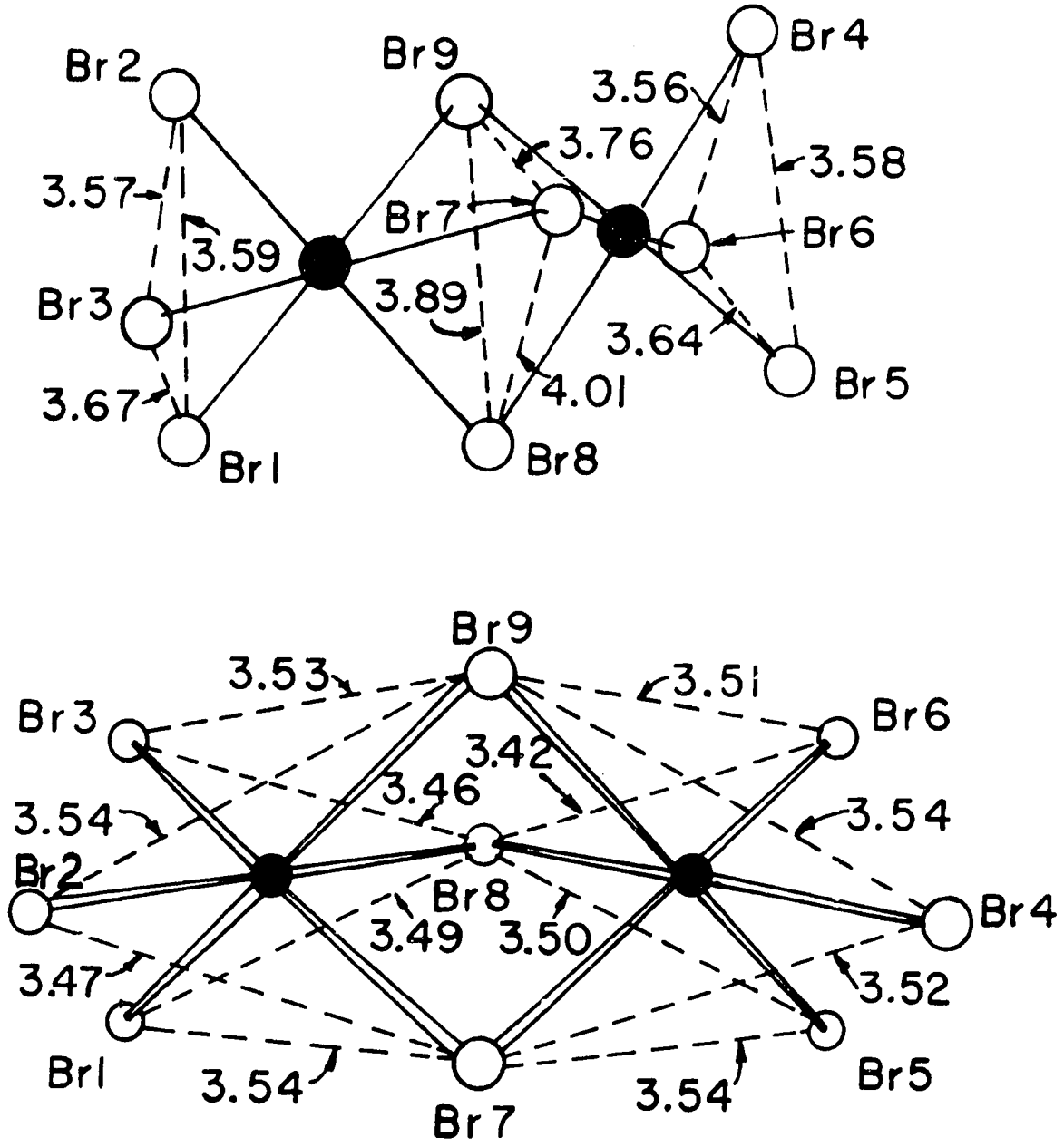

Figure 19. Schematic diagram of nonbonded distances in $W_2Br_9^{2-}$ which identify $Br_{br}(8)$ as unique

The excursion to consider packing forces and steric repulsions which might influence the structure was a fruitful exercise even though no rationalization for the small structural deformation was found. The question of what factors cause the terminal ligand planes to tip as evidenced by the angles of approximately 3° between the metal-metal axis and the normals to the two planes remains, and an electronic explanation now seems appropriate. Metal-ligand σ-bonds are not expected to favor any deviation from the idealized confacial bioctahedral structure. The a_1' metal-metal sigma bonding molecular orbital is axially symmetric and not influenced by angular distortions. As in the case of $Ta_2Br_6(SC_4H_8)_3$ a process of elimination leads one to the metal-metal π-orbital arena to explain the structural details of the nonabromoditungstate(2-) anion.

The positions of the bridging bromines in $W_2Br_9^{2-}$ are not indicative of a systematic distortion even though certain parameters, such as the Br_{br}-W-Br_{br} angles and the nonbonded separations, do vary considerably. The lack of any systematic distortion in the bridging positions in view of the canted orientation of the terminal ligand planes can be explained as a result of the fixed constraints inherent in bridging positions. The triangle formed by the two metal atoms and a bridging ligand has three sides which are effectively fixed in length by bonding interactions and thus no degree of freedom is left. For terminal atoms the bond length can remain unchanged during a rotation of the halide ligand around an axis

passing through the metal atom, but this mode of distortion is not available to the three bridging ligands with the one exception of an axis coincident with the metal-metal axis which has already been discounted.

That a slight rotation of the atomic orbitals on each of the tungsten atoms around an axis bisecting Br(7) and Br(1) on W(1) and bisecting Br(7) and Br(5) on W(2) would increase the overlap of the b_1 π-orbital and decrease the overlap of the a_1 π-orbital is clear from Figures 17 and 18.

A quantitative description of the overlap dependence on an angular rotation of the orbitals is not possible in this thesis, but a crude geometrical argument offers some insight into the overlap variations which accompany a small rotation. The d_{xy}, d_{xz}, and d_{yz} orbitals of each metal atom will be mutually perpendicular and the angle between two corresponding orbitals, one from each metal atom, will be 70.5° in a confacial bioctahedron of D_{3h} symmetry. A small rotation of $\Delta\theta$ causes the orbital lobe to shift by a distance $r\Delta\theta$, where r is a length describing the orbital and $\Delta\theta$ is the rotation angle in radians, either towards or away from the adjacent metal atom depending on the sense of the rotation relative to the orbital lobe in question. Figure 20 graphically illustrates the orbital motion of one lobe of a metal d_{xy}-orbital in a D_{3h} dimer upon descending to C_{2v} symmetry via a rotation of $\Delta\theta$. For a rotation angle of 3.3° the lobe shifts by 0.058r or

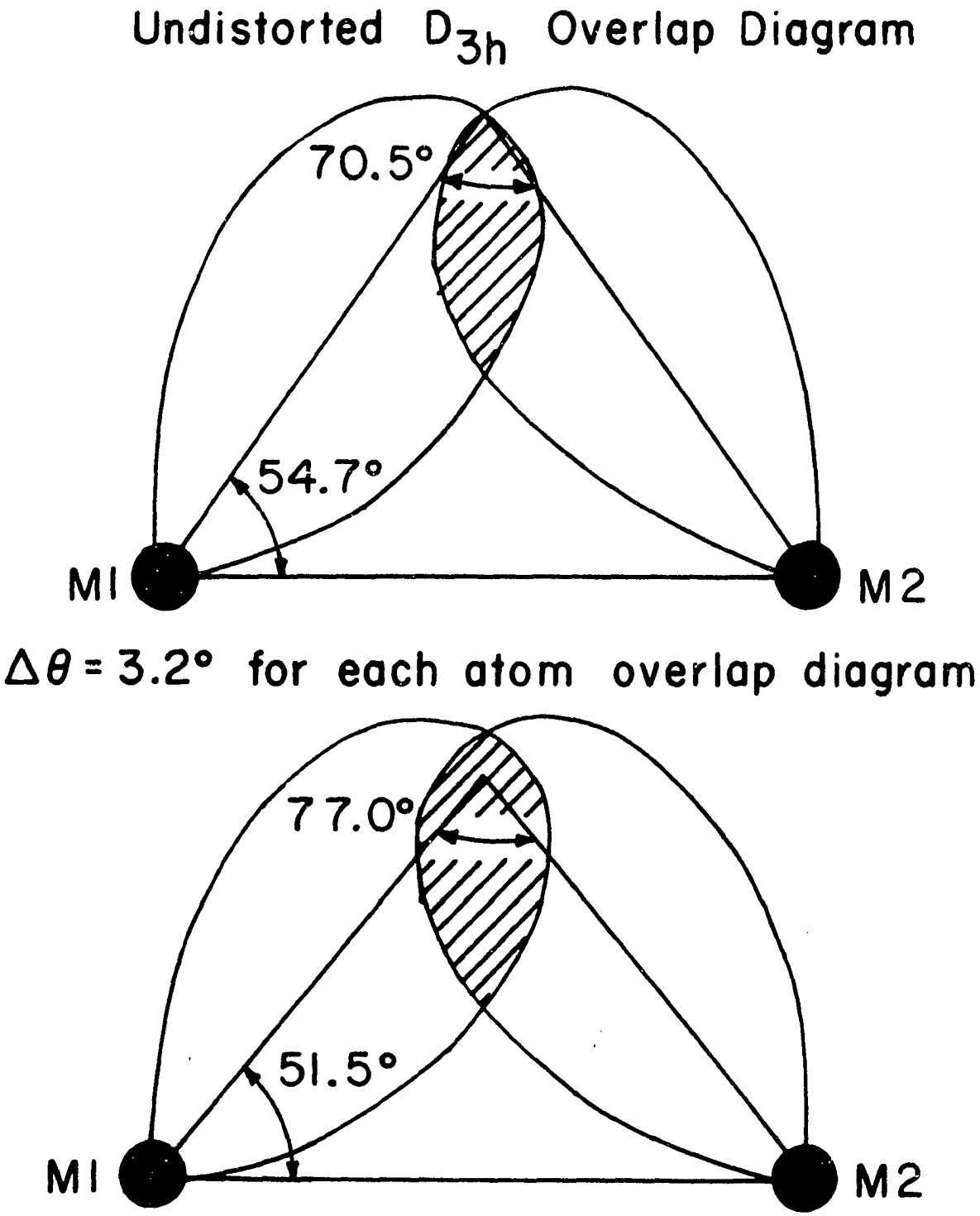

Figure 20. Orbital motion of a metal d-orbital upon rotation by an angle of $\Delta\theta$

nearly 0.06Å per Å of orbital lobe length. A combination of two such angular displacements, with each tungsten rotated slightly as shown in Figure 20, leads to an energy separation of the two π-bonding orbitals since the a_1 overlap decreases as the b_1 overlap increases. This mechanism is postulated as the route by which the e' orbital degeneracy is broken in accord with the Jahn-Teller theorem. The actual orbital rotation which affects the metal-metal π-bonding orbitals is not directly observable, but the canted terminal ligand planes testify to the existence of this static angular deformation.

SUMMARY

The union of monomeric metal moieties to produce metal-metal bonded dimers was promoted by two diametrically opposite preparative routes for tantalum and tungsten: reduction of Ta(V) and oxidation of W(0). Reduction of TaX_5, (X = Cl or Br), with two equivalents of sodium amalgam occurred at room temperature in the presence of excess tetrahydrothiophene to form $Ta_2X_6(SC_4H_8)_3$, a highly-colored dimer which was soluble in the aromatic reaction medium and could be purified via extraction. Oxidation of $[(n\text{-}C_3H_7)_4N][W(CO)_5Br]$ occurred in refluxing chlorobenzene with excess 1,2-dibromoethane as the oxidant to expel carbon monoxide and produce a dark green precipitate of $[(n\text{-}C_3H_7)_4N]_2[W_2Br_9]$.

Magnetic susceptibility measurements indicated that the tantalum dimer had no unpaired electrons in the ground state (spin-pairing of the two d^2 configurations through metal-metal bonding offers a satisfactory explanation for this diamagnetic behavior) and the tungsten anion exhibited Curie behavior consistent with one unpaired electron per dimer over a wide temperature range (a total of five valence electrons are distributed between the two tungsten atoms and hence four are paired). The observed magnetic properties were consistent with metal-metal bond orders of 2.0 and 2.5 for $Ta_2X_6(SC_4H_8)_3$ and $W_2Br_9^{2-}$, respectively.

The presence of tetrahydrothiophene ligands in two differ-

ent molecular environments in a ratio of 1:2 was indicated by proton magnetic resonance spectra of $Ta_2X_6(SC_4H_8)_3$. Nuclear quadrupole resonances of chlorine and bromine isotopes in $Ta_2X_6(SC_4H_8)_3$ were also divisible into two types for each isotope, and interpretation in terms of a confacial bioctahedral dimer with two bridging halides and one bridging tetrahydrothiophene ligand accounted for the observation of both terminal and bridging halogen nqr frequencies as well as agreeing with the pmr data mentioned previously. Further spectral data obtained for both $Ta_2X_6(SC_4H_8)_3$ and $[(n\text{-}C_3H_7)_4N]_2[W_2Br_9]$ included Nujol mull infrared spectra and solution electronic spectra.

Confacial bioctahedral structures were determined for both $Ta_2Br_6(SC_4H_8)_3$ and $[(n\text{-}C_3H_7)_4N]_2[W_2Br_9]$ via single crystal x-ray techniques. The tantalum dimer contained a unique bridging tetrahydrothiophene trans to terminal tetrahydrothiophene ligands on each of the metal octahedra, and bromines occupied the remaining six ligand positions. A Ta-Ta distance of 2.710(2)Å was found and considered appropriate for a metal-metal double bond. The $W_2Br_9^{2-}$ anion exhibited d(W-W) = 2.601 (2) Å and axial contraction of the two metal atoms was evident in the distortions present in the confacial bioctahedral structure.

An examination of the electron configurations present in each of the dimers structurally chracterized (four electrons

for $Ta_2Br_6(SC_4H_8)_3$ and five electrons for $W_2Br_9^{2-}$) in conjunction with a qualitative description of the metal-metal molecular orbitals resulting from overlap of metal atomic orbitals offered considerable insight into the unusual distortions present in the dimers. Occupation of only one of the two available metal-metal π-bonding orbitals in the tantalum dimer was reflected in the disposition of the three bridging ligands due to the stereochemical requirements of the two π-bonding electrons. The distortion present in the $W_2Br_9^{2-}$ anion was a slightly more subtle deviation involving canted terminal ligand planes as a result of a Jahn-Teller effect which splits the degeneracy of $^2E'$ ground state appropriate for D_{3h} symmetry by a static rotation of the metal orbital components of the π-bonding molecular orbitals.

BIBLIOGRAPHY

1. J. E. Fergusson in "Preparative Inorganic Reactions," W. L. Jolly, Ed., Vol. 7, Wiley-Interscience, New York, N.Y., 1971, pp 93-163.

2. M. C. Baird in "Progress in Inorganic Chemistry," F. A. Cotton, Ed., Vol. 9, Interscience Publishers, New York, N.Y., 1968, pp 1-159.

3. F. A. Cotton, Accounts Chem. Res., 2, 240 (1969).

4. J. C. Sheldon, Australian J. Chem., 17, 1191 (1964).

5. H. Schäfer and H. G. von Schnering, Angew. Chem., 76, 833 (1964).

6. D. Brown in "Comprehensive Inorganic Chemistry," Vol. 3, Pergamon Press, Rushcutters Bay, Australia, 1973, pp 553-622.

7. D. Cozzi and S. Vivarelli, Z. Electrochem., 57, 406 (1953).

8. D. Cozzi and S. Vivarelli, Z. Electrochem., 58, 177 (1954).

9. V. P. Gladyshev and Ya. Rakmatulin, Izv. Akad. Nauk Kaz. SSR, Serkhim., 19, 30 (1969).

10. B. O. Marinder, Acta Chem. Scand., 15, 707 (1961).

11. F. P. Gortsema and R. Didchenko, Inorg. Chem., 4, 182 (1965).

12. H. Schäfer and F. Kahlenberg, Z. Anorg. Allg. Chem., 275, 198 (1954).

13. R. E. McCarley and J. C. Boatman, Inorg. Chem., 2, 547 (1963).

14. J. D. Corbett and P. W. Seabaugh, J. Inorg. Nucl. Chem., 6, 207 (1958).

15. L. F. Dahl and D. L. Wampler, Acta Crystallogr., 15, 903 (1962).

16. G. W. A. Fowles, D. J. Tidmarsh and R. A. Walton, Inorg. Chem., 8, 631 (1969).

17. G. W. A. Fowles and K. F. Gadd, J. Chem. Soc. A, 2232 (1970).

18. M. Allbutt, K. Feenan and G. W. A. Fowles, J. Less-Common Metals, 6, 299 (1964).

19. R. E. McCarley, B. G. Hughes, J. C. Boatman and B. A. Torp, Adv. Chem. Series, 37, 243 (1963).

20. F. Fairbrother and J. F. Nixon, J. Chem. Soc., 150 (1962).

21. A. H. Cowley, F. Fairbrother and N. Scott, J. Chem. Soc., 3133 (1958).

22. K. Feenan and G. W. A. Fowles, J. Chem. Soc., 2449 (1965).

23. S. E. Livingston, Quart. Rev. (London), 19, 386 (1965).

24. J. B. Hamilton and R. E. McCarley, Inorg. Chem., 9, 1333 (1970).

25. G. W. A. Fowles, D. J. Tidmarsh and R. A. Walton, J. Inorg. Nucl. Chem., 31, 2373 (1969).

26. D. C. Bradley and I. M. Thomas, Canadian J. Chem., 40, 1355 (1962).

27. D. C. Bradley and I. M. Thomas, Canadian J. Chem., 40, 449 (1962).

28. A. Broll, H. G. von Schnering and H. Schäfer, J. Less-Common Metals, 22, 243 (1970).

29. D. G. Blight, R. L. Deutscher and D. L. Kepert, J. Chem. Soc., Dalton Trans., 87 (1972).

30. W. E. Streib and R. B. Jackson, Inorg. Chem., 10, 1760 (1971).

31. P. A. Finn, M. S. King, P. A. Kilty and R. E. McCarley, J. Amer. Chem. Soc., 97, 220 (1975).

32. R. Gut and W. Perron, J. Less-Common Metals, 26, 369 (1972).

33. H. Schäfer, R. Gerken and H. Scholz, Z. Anorg. Allg. Chem., 335, 96 (1965).

34. H. Schäfer and K. D. Dohmann, Z. Anorg. Allg. Chem., 311, 134 (1961).

35. H. G. von Schnering, H. Wöhrle and H. Schäfer, Naturwissenschaften, 48, 159 (1959).

36. H. Schäfer and K. D. Dohmann, Z. Anorg. Allg. Chem., 311, 134 (1961).

37. A. Simon and H. G. von Schnering, J. Less-Common Metals, 11, 31 (1966).

38. W. H. Chapin, J. Amer. Chem. Soc., 32, 323 (1910).

39. D. L. Kepert and K. Vrieze in "Halogen Chemistry," V. Gutmann, Ed., Vol. 3, Academic Press, Inc., New York, N.Y., 1967, pp 1-26.

40. H. Schäfer, H. Scholtz and R. Gerken, Z. Anorg. Allg. Chem., 331, 154 (1964).

41. D. Bauer, H. G. von Schnering and H. Schäfer, J. Less-Common Metals, 8, 388 (1965).

42. P. J. Kuhn and R. E. McCarley, Inorg. Chem., 4, 1482 (1965).

43. P. A. Vaughan, J. H. Sturdivant and L. Pauling, J. Amer. Chem. Soc., 72, 5477 (1950).

44. J. H. Espenson and R. E. McCarley, J. Amer. Chem. Soc., 88, 1063 (1966).

45. F. A. Cotton and T. E. Haas, Inorg. Chem., 3, 10 (1964).

46. E. K. Barefield, G. W. Parshall and F. N. Tebbe, J. Amer. Chem. Soc., 92, 5234 (1970).

47. A. N. Nesmeyanov, A. I. Gusev, A. A. Pasynskii, K. N. Anisimov, N. E. Kolobova and Yu. T. Struchkov, Chem. Commun., 1365 (1968).

48. F. W. Siegert and H. J. DeLiefde Meijer, J. Organometal. Chem., 23, 177 (1970).

49. H. J. DeLiefde Meijer and F. Jellinek, Inorg. Chim. Acta, 4, 651 (1970).

50. E. O. Fischer and F. Röhrscheid, J. Organometal. Chem., 6, 53 (1966).

51. M. R. Churchill and S. W. Y. Chang, Chem. Commun., 248 (1974).

52. R. B. King , D. M. Braitsch and P. N. Kapoor, J. Amer. Chem. Soc., 97, 60 (1975).

53. E. T. Maas, Jr. and R. E. McCarley, Inorg. Chem., 12, 1096 (1973).

54. R. E. McCarley, Iowa State University of Science and Technology, private communication, 1973.

55. J. G. Converse, Ph.D. Thesis, Iowa State University of Science and Technology, Ames, Iowa, 1968.

56. P. A. Edwards, Ph.D. Thesis, Iowa State University of Science and Technology, Ames, Iowa, 1972.

57. P. A. Edwards, R. E. McCarley and D. R. Torgeson, Inorg. Chem., 11, 1185 (1972).

58. E. T. Strom, B. S. Snowden, Jr., H. C. Custard, D. E. Woessner and J. R. Norton, J. Org. Chem., 33, 2555 (1968).

59. E. T. Maas, Jr., Ph.D. Thesis, Iowa State University of Science and Technology, Ames, Iowa, 1972.

60. H. P. Fritz and K. E. Schwarzhans, J. Organometal. Chem., 5, 283 (1966).

61. E. F. Paulus, H. P. Fritz and K. E. Schwarzhans, J. Organometal. Chem., 11, 647 (1968).

62. C. J. Pouchert and J. R. Campbell, "The Aldrich Library of NMR Spectra," Vol. 1, Aldrich Chemical Company, Inc., Milwaukee, Wisconsin, 1974, p 50.

63. P. W. Selwood, "Magnetochemistry," 2nd ed., Interscience Publishers, Inc., New York, N.Y., 1956.

64. E. A. C. Lucken, "Nuclear Quadrupole Coupling Constants," Academic Press, New York, N.Y., 1969.

65. T. P. Das and E. L. Hahn, Solid State Phys., Suppl., No. 1, (1958).

66. S. L. Segel and R. G. Barnes, Catalog of Nuclear Quadrupole Interactions and Resonance Frequencies in Solids. Part I. Elements and Inorganic Compounds, USAEC, IS-520 (revised) (1968).

67. T. L. Brown, W. G. McDugle, Jr. and L. G. Kent, J. Amer. Chem. Soc., 92, 3645 (1970).

68. G. K. Semin, S. I. Kuznetsov, I. M. Alimov, T. L. Khotsianova, E. V. Bryukhova, L. A. Nisselson and K. V. Tretyakova, Inorg. Chim. Acta, 13, 181 (1974).

69. J. B. Hamilton, Ph.D. Thesis, Iowa State University of Science and Technology, Ames, Iowa, 1968.

70. J. Lewis, J. R. Miller, R. L. Richards and A. Thompson, J. Chem. Soc., 5850 (1965).

71. S. L. Lawton and R. A. Jacobson, Inorg. Chem., 7, 2124 (1968).

72. W. R. Busing, K. O. Martin and H. A. Levy, "ORELS, a Fortran Crystallographic Least Squares Program," U.S. Atomic Energy Commission Report ORNL-TM-305, Oak Ridge National Laboratory, Oak Ridge, Tenn., 1962.

73. H. P. Hanson, F. Herman, J. D. Lea and S. Skillman, Acta Crystallogr., 17, 1040 (1964).

74. D. H. Templeton in "International Tables for X-ray Crystallography," Vol. III, Kynoch Press, Birmingham, England, 1962, pp 215-216.

75. W. R. Busing, K. O. Martin and H. A. Levy, "ORFFE, a Fortran Crystallographic Function and Error Program," U.S. Atomic Energy Commission Report ORNL-TM-306, Oak Ridge National Laboratory, Oak Ridge, Tenn., 1964.

76. C. B. Thaxton and R. A. Jacobson, Inorg. Chem., 10, 1460 (1971).

77. F. A. Cotton and D. A. Ucko, Inorg. Chim. Acta, 6, 161 (1972).

78. R. Saillant, R. B. Jackson, W. E. Streib, K. Folting and R. A. D. Wentworth, Inorg. Chem., 10, 1453 (1971).

79. A. Zalkin and D. E. Sands, Acta Crystallogr., 11, 615 (1958).

80. J. E. Huheey, "Inorganic Chemistry: Principles of Structure and Reactivity," Harper & Row, Publishers, New York, N.Y., 1972, pp 183-185.

81. A. Bondi, J. Phys. Chem., 68, 441 (1964).

82. F. A. Cotton, "Chemical Applications of Group Theory," Interscience Publishers, New York, N.Y., 1967, p 225.

83. W. H. Watson and J. Waser, Acta Crystallogr., 11, 689 (1958).

84. G. J. Wessel and D. J. W. Ijdo, Acta Crystallogr., 10, 466 (1957).

85. M. H. Lietzke and M. L. Holt, Inorg. Syn., 3, 163 (1950).

86. T. M. Brown and E. L. McCann, Inorg. Chem., 7, 1227 (1968).

87. R. E. McCarley and T. M. Brown, Inorg. Chem., 3, 1232 (1964).

88. R. Siepmann, H. G. von Schnering and H. Schäfer, Angew. Chem. Internat. Edit., 6, 637 (1967).

89. R. Siepmann and H. G. von Schnering, Z. Anorg. Allg. Chem., 357, 289 (1968).

90. E. Bannister and G. Wilkinson, Chem. Ind. (London), 319 (1960).

91. F. A. Cotton and M. Jeremic, Syn. Inorg. Metal-Organic Chem., 1, 265 (1971).

92. O. Olsson, Z. Anorg. Allg. Chem., 88, 49 (1914).

93. R. C. Young, J. Amer. Chem. Soc., 54, 4515 (1932).

94. R. A. Laudise and R. C. Young, Inorg. Syn., 6, 149 (1960).

95. R. Saillant, J. L. Hayden and R. A. D. Wentworth, Inorg. Chem., 6, 1497 (1967).

96. E. Konig, Inorg. Chem., 2, 1238 (1963).

97. E. A. Heintz, Inorg. Syn., 7, 142 (1963).

98. J. L. Hayden and R. A. D. Wentworth, J. Amer. Chem. Soc., 90, 5291 (1968).

99. G. L. Hawkins and C. S. Garner, J. Amer. Chem. Soc., 80, 2946 (1958).

100. R. Saillant and R. A. D. Wentworth, Inorg. Chem., 7, 1606 (1968).

101. W. E. Streib and R. B. Jackson, Inorg. Chem., 10, 1760 (1971).

102. R. Saillant and R. A. D. Wentworth, Inorg. Chem., 8, 1226 (1969).

103. M. J. Bennett, J. V. Brencic and F. A. Cotton, Inorg. Chem., 8, 1060 (1969).

104. F. S. Cotton, Z. C. Mester and T. R. Webb, Acta Crystallogr., B30, 2768 (1974).

105. R. Saillant and R. A. D. Wentworth, J. Amer. Chem. Soc., 91, 2174 (1969).

106. W. H. Delphin and R. A. D. Wentworth, J. Amer. Chem. Soc., 95, 7920 (1973).

107. B. Moore and G. Wilkinson, Proc. Chem. Soc., 61 (1959).

108. E. O. Fischer and K. Öfele, Z. Naturforsch., 14b, 736 (1959).

109. E. W. Abel, I. S. Butler and J. G. Reid, J. Chem. Soc., 2068 (1963).

110. R. B. King, Inorg. Chem., 3, 1039 (1964).

111. M. C. Ganorkar and M. H. B. Stiddard, J. Chem. Soc., 3494 (1965).

112. J. A. Bowden and R. Colton, Australian J. Chem., 21, 2657 (1968).

113. W. H. Delphin, R. A. D. Wentworth and M. C. Matson, Inorg. Chem., 13, 2552 (1974).

114. W. H. Delphin and R. A. D. Wentworth, Inorg. Chem., 12, 1914 (1973).

115. H. D. Murdoch, J. Organometal. Chem., 4, 119 (1965).

116. J. F. White and M. F. Farona, J. Organomet. Chem., 37, 119 (1972).

117. G. Schmid, R. Boese and E. Welz, Chem. Ber., 108, 260 (1975).

118. R. A. Jacobson, "An Algorithm for Automatic Indexing and Bravais Lattice Selection," prepared under USAEC contract W-7405-eng-82, Ames, Iowa, 1974.

119. J. A. Pople, W. G. Schneider and H. J. Bernstein, "High-resolution Nuclear Magnetic Resonance," McGraw-Hill Book Co., Inc., New York, N.Y., 1959, p 90.

120. R. J. Ziegler and W. M. Risen, Inorg. Chem., 11, 2796 (1972).

121. (a) N. W. Alcock, presented in part at the International Summer School on Crystallographic Computing, Ottawa, Canada, Aug. 1969; (b) J. D. Scott, Queen's University, Kingston, Ontario, Canada, personal communication, 1971.

122. H. Jahn and E. Teller, Phys. Rev., 49, 874 (1937).

123. B. N. Figgis, "Introduction to Ligand Fields," Wiley, London, 1966, p 212.

124. F. A. Cotton and G. Wilkinson, "Advanced Inorganic Chemistry," 2nd ed., Interscience Publishers, New York, N.Y., 1966, p 686.

APPENDIX

Table 19. Final positional parameters for $Ta_2Br_6(SC_4H_8)_3$[a]

Atom	x	y	z
Ta(1)	-0.3118(1)	0.2873(1)	0.2651(2)
Ta(2)	-0.1428(1)	0.2090(1)	0.2111(2)
Br(1)	-0.3144(4)	0.2954(3)	0.5429(5)
Br(2)	-0.5401(3)	0.2196(3)	0.1092(6)
Br(3)	0.0271(4)	0.1494(3)	0.4425(5)
Br(4)	-0.2066(4)	0.0622(3)	0.0082(6)
Br(5)	-0.0807(3)	0.3958(3)	0.3578(5)
Br(6)	-0.2767(4)	0.3255(3)	-0.0111(5)
S(1)	-0.2897(9)	0.1044(8)	0.3215(13)
S(2)	-0.3515(9)	0.4828(7)	0.2177(14)
S(3)	0.0430(9)	0.3060(8)	0.1216(13)
C(1)	-0.2448(31)	0.0426(29)	0.5276(47)
C(2)	-0.3607(53)	-0.0617(48)	0.4967(80)
C(3)	-0.3940(50)	-0.1043(47)	0.3479(77)
C(4)	-0.4207(34)	-0.0147(32)	0.2130(51)
C(5)	-0.2434(37)	0.5744(33)	0.3956(55)
C(6)	-0.3364(36)	0.6061(32)	0.4494(53)
C(7)	-0.4600(35)	0.5960(32)	0.3287(53)
C(8)	-0.4967(33)	0.4826(30)	0.2403(50)
C(9)	0.1164(35)	0.2022(33)	0.0971(54)
C(10)	0.1018(50)	0.2217(47)	-0.0767(78)
C(11)	0.0382(70)	0.2881(66)	-0.1695(102)
C(12)	-0.0159(45)	0.3493(42)	-0.0884(68)

[a]Numbers in parentheses are the estimated standard deviations of the coordinates and refer to the last significant digit of the preceding number.

Table 20. Final thermal parameters ($\times 10^4$) for $Ta_2Br_6(SC_4H_8)_3$

Atom	β_{11}	β_{22}	β_{33}	β_{12}	β_{13}	β_{23}
Ta(1)[a]	81(1)	47(1)	116(3)	7(1)	44(2)	-12(2)
Ta(2)	83(2)	48(2)	135(3)	7(1)	48(2)	-17(2)
Br(1)	142(5)	80(3)	120(8)	37(3)	74(5)	0(4)
Br(2)	76(4)	73(3)	230(10)	0(3)	45(5)	41(5)
Br(3)	109(4)	65(3)	183(9)	29(3)	52(5)	16(5)
Br(4)	138(5)	73(3)	236(10)	-2(3)	95(6)	-69(5)
Br(5)	80(4)	50(3)	145(8)	4(3)	40(4)	26(4)
Br(6)	108(4)	80(3)	116(8)	24(3)	53(5)	0(4)
S(1)	117(11)	52(7)	187(22)	5(7)	66(13)	-30(11)
S(2)	130(11)	43(7)	207(24)	22(7)	95(14)	2(11)
S(3)	95(10)	86(9)	175(22)	10(8)	66(13)	-19(12)
C(1)[b]	4.3(8)					
C(2)	10.2(16)					
C(3)	9.5(15)					
C(4)	5.1(9)					
C(5)	5.9(10)					
C(6)	5.5(9)					
C(7)	5.4(9)					
C(8)	4.7(8)					
C(9)	5.6(9)					
C(10)	8.9(14)					
C(11)	14.1(23)					
C(12)	8.4(13)					

[a]The form of the anisotropic temperature factor expression is $\exp[-(\beta_{11}h^2+\beta_{22}k^2+\beta_{33}\ell^2+2\beta_{12}hk+2\beta_{13}h\ell+2\beta_{23}k\ell)]$.

[b]The form of the isotropic temperature factor expression is $\exp[-\beta(\sin^2\theta/\lambda^2)]$.

Table 21. Observed and calculated structure factors for $Ta_2Br_6(SC_4H_8)_3$

Table 21. (Continued)

K	L	FO	FC
-12	1	42	49
-11	2	64	-55
-11	4	72	69
-10	1	87	-96
-10	2	32	-26
-10	3	58	59
-10	4	55	59
-10	5	51	-56
-9	1	50	48
-9	2	66	74
-9	3	120	115
-9	4	72	-68
-9	6	60	55
-8	1	133	138
-8	3	87	81
-8	4	78	-78
-8	5	87	86
-7	1	32	41
-7	2	107	-103
-7	3	125	-120
-7	4	57	50
-7	6	60	-67
-6	1	190	-191
-6	2	103	-96
-6	3	116	118
-6	1	134	-132
-5	2	108	106
-5	3	62	53
-5	4	50	-46
-4	1	128	123
-4	2	29	28
-4	3	138	-139
-4	4	29	31
-4	5	102	-108
-4	7	94	-94
-3	1	91	91
-3	2	35	-29
-3	3	91	-95
-3	4	70	-75
-3	5	57	-58
-2	2	182	-173
-2	4	70	-71
-2	5	97	99
-2	0	47	-42
-1	1	145	-136
-1	2	249	-243
-1	3	50	-47
-1	6	56	-57
-1	7	125	-126
0	1	191	-200
0	2	83	81
0	3	54	58
0	4	131	124
0	5	80	-74
0	6	163	-154
0	7	54	54
0	8	55	62
0	9	42	-32
1	0	45	42
1	2	160	172
1	3	141	144
1	4	100	-98
1	5	146	-140
1	6	83	82
1	7	155	171
1	8	77	-81
2	1	33	30
2	2	42	37
2	3	191	-189
2	4	212	-196
2	5	63	57
2	6	145	140
2	7	141	-139
2	8	55	-55
3	0	120	126
3	1	58	58
3	2	66	-67
3	3	243	-216
3	4	272	239
3	5	99	87
3	6	37	-27
3	7	91	-90
3	8	67	74
3	9	38	43
4	0	127	132
4	1	131	-131
4	2	164	-159
4	3	210	203
4	4	221	206
4	7	93	88
4	8	81	77
5	0	279	-276
5	1	87	-88
5	2	210	194
5	3	246	226
5	4	184	-170
5	7	58	51
5	8	57	-51
6	0	26	-30
6	1	308	301
6	2	185	177
6	3	117	-108
6	4	37	-36
6	5	91	92
6	6	49	53
7	0	291	306
7	1	76	74
7	2	36	-35
7	3	80	-76
7	4	91	85
7	5	102	99

K	L	FO	FC
7	7	36	39
7	8	39	45
8	0	39	36
8	1	153	-150
8	2	97	-93
8	4	80	77
8	7	47	47
8	8	30	-35
9	0	111	-122
9	1	33	-29
9	2	91	86
9	3	92	88
9	4	38	44
9	5	48	-49
9	7	56	-52
10	1	63	64
10	2	89	89
10	4	34	21
11	1	37	30
11	2	65	-64
11	4	59	-54
11	6	74	-70
12	2	44	-48
12	4	88	-91
12	5	27	36
13	3	45	-43

H = -2

K	L	FO	FC
-10	4	40	53
-9	1	36	-33
-9	2	61	-53
-9	4	36	41
-9	5	89	-92
-9	6	58	-69
-8	2	76	73
-8	3	118	119
-8	4	105	-108
-8	6	66	66
-8	7	55	59
-7	1	151	154
-7	2	76	83
-7	3	93	-87
-7	5	105	114
-6	1	40	45
-6	2	118	-113
-6	3	109	-99
-6	4	145	143
-6	6	46	-51
-6	7	62	-52
-5	1	214	-207
-5	2	94	88
-5	3	187	185
-5	4	92	80
-5	5	56	-53
-5	7	63	56
-4	1	49	41
-4	2	152	141
-4	3	48	42
-4	4	90	-83
-4	5	56	-50
-4	6	79	77
-3	1	102	103
-3	2	25	-22
-3	3	141	-125
-3	4	115	-109
-3	6	42	51
-3	7	86	-84
-3	8	34	32
-2	1	85	86
-2	2	60	-54
-2	3	39	-40
-2	4	78	77
-2	5	114	100
-1	2	155	-132
-1	3	203	178
-1	4	88	-83
-1	5	56	42
-1	8	51	-60
-1	9	35	46
0	1	60	-69
0	2	51	-39
0	3	187	-172
0	4	167	-144
0	5	31	-27
0	6	123	-119
0	7	97	-101
1	1	62	-75
1	3	170	-159
1	4	174	155
1	5	124	-126
1	6	67	-65
1	7	100	103
1	8	61	63
1	9	32	-32
2	0	60	-64
2	1	79	-83
2	2	79	109
2	4	110	-99
2	5	60	-56
2	6	115	114
2	7	81	79
2	8	82	-82
3	0	255	-246
3	1	131	121
3	2	25	-22
3	3	184	-179
3	4	131	-118
3	5	48	39
3	7	140	-135
3	8	84	-80
4	0	123	130
4	1	179	174
4	2	195	-190
4	3	120	-111
4	4	134	128
4	6	44	-33
4	7	106	-107

K	L	FO	FC
4	8	62	62
4	9	51	60
5	0	137	133
5	1	235	-226
5	2	121	-115
5	3	202	213
5	4	41	41
5	6	90	-88
5	7	93	101
5	8	83	83
6	0	253	-261
6	1	65	-65
6	2	126	121
6	3	115	111
6	4	184	-174
6	5	62	-59
6	6	55	53
6	7	91	91
6	8	64	-63
7	0	29	32
7	1	138	133
7	2	149	147
7	3	83	-80
7	4	57	44
7	5	106	114
7	6	109	121
7	7	76	-68
8	0	195	200
8	1	64	65
8	2	42	41
8	3	114	-104
8	4	162	158
8	5	106	107
8	6	40	-35
9	0	52	51
9	1	64	-69
9	2	90	-87
9	3	83	84
9	4	76	72
9	5	59	-64
9	6	98	-108
10	2	87	92
10	4	39	-44
10	6	36	46
10	8	44	-43
11	1	97	103
11	2	44	40
11	3	36	-35
11	4	52	62
12	0	50	57
12	3	35	41

H = -1

K	L	FO	FC
-12	2	39	32
-12	3	68	-60
-11	2	49	-54
-10	1	49	-26
-10	5	62	48
-9	2	63	-63
-9	3	33	-31
-9	4	49	54
-8	5	36	26
-8	1	76	-68
-8	3	98	94
-8	6	46	-47
-7	2	186	178
-7	4	110	-103
-7	6	30	32
-7	7	87	77
-6	1	157	157
-6	3	163	-159
-6	5	65	70
-6	6	68	75
-5	1	90	-88
-5	2	137	-132
-5	3	122	-116
-5	4	221	214
-5	5	50	37
-5	6	62	-53
-5	7	92	-78
-4	1	99	-93
-4	2	95	90
-4	3	293	280
-4	4	184	167
-4	5	111	-106
-4	6	43	-35
-4	7	93	93
-3	1	232	211
-3	2	118	111
-3	3	216	200
-3	4	211	-197
-3	5	61	-57
-3	6	104	101
-2	2	93	78
-2	3	210	-191
-2	5	80	80
-2	7	33	-48
-1	2	259	-207
-1	4	183	165
-1	5	97	97
-1	7	37	48
0	0	308	-313
0	2	97	44
0	3	229	212
0	4	66	-56
0	5	57	53
1	0	286	-305
1	1	65	-65
1	2	181	169
1	3	117	-114
1	5	49	-48
1	6	66	-70
1	7	64	-73
2	1	65	64
2	2	112	106
2	3	28	-25
2	4	70	68

H = 0

K	L	FO	FC
-13	1	63	-65
-12	2	61	67
-11	1	75	93
-11	3	68	-67
-10	2	70	-71
-9	4	57	-44
-8	1	65	-64
-8	2	95	-97
-7	1	143	-143
-7	2	38	52
-7	5	62	-48
-6	2	88	64
-6	7	71	59
-5	1	96	89
-5	2	39	36
-5	3	141	-139
-5	4	98	-68
-5	5	82	73
-5	6	64	48
-5	7	147	-107
-4	1	43	35
-4	2	182	-171
-4	3	198	-176
-4	4	237	205
-4	7	55	-64
-3	1	132	-121
-3	2	59	-42
-3	3	279	253
-3	4	93	74
-3	5	72	67
-3	6	75	67
-3	7	435	375
-2	1	28	-25
-2	2	170	140
-2	3	199	171
-2	4	198	-174
-2	5	72	74
-2	6	75	67
-1	1	435	375
-1	2	195	191
-1	5	200	-173
-1	7	80	-69
0	1	33	34
0	2	56	-62
0	4	152	164
0	5	57	61
0	6	25	-28
0	8	27	33
1	1	308	-307
1	3	101	117

K	L	FO	FC
1	4	32	36
1	5	26	-26
1	7	71	76
2	0	331	-311
2	1	88	-77
2	2	78	74
2	3	28	31
2	5	38	-42
2	6	71	74
2	7	68	-72
3	0	59	51
3	1	176	176
3	2	229	220
3	4	92	47
3	8	51	60
4	0	93	93
4	1	173	159
4	2	87	87
4	3	81	-83
4	4	63	66
4	5	84	77
4	6	73	72
4	7	56	52
5	0	210	195
5	1	38	-36
5	2	128	-128
5	3	113	111
5	4	25	20
5	5	57	61
6	0	20	-24
6	1	82	-80
6	2	99	96
6	3	43	38
6	4	51	-55
6	5	44	41
6	6	46	-39
6	7	52	-65
7	0	28	28
7	1	47	47
7	2	34	38
7	3	51	-49
7	4	89	86
7	6	21	-28
7	7	31	-18
8	1	100	-102
8	2	22	17
8	5	67	-67
9	0	95	-99
9	3	41	-35
9	4	60	-61
9	5	36	-37
9	6	38	30
10	0	33	-31
10	1	82	88
10	3	36	-40
10	4	27	-22
10	5	46	43
11	0	53	57
11	2	76	-81
11	3	44	-42
11	4	56	56
12	1	73	-75
12	2	51	-54

H = 1

K	L	FO	FC
-12	1	74	-78
-12	3	69	56
-11	1	78	86
-11	2	84	89
-10	2	120	124
-10	3	50	-40
-10	3	99	-90
-9	1	44	-48
-9	2	85	-92
-8	3	121	126
-7	2	55	51
-7	4	49	-53
-6	3	134	-132
-6	5	117	-96
-5	1	110	-102
-5	3	65	58
-5	4	68	-57
-5	6	104	93
-4	3	152	-139
-4	4	84	-80
-4	5	87	84
-4	7	123	-105
-3	1	34	37
-3	2	211	-197
-3	4	145	137
-3	5	66	-46
-3	6	112	-95
-3	7	81	-63
-2	1	141	-137
-2	2	93	80
-2	3	235	222
-2	4	57	-48
-2	5	67	-54
-2	7	113	108
-1	2	71	82
-1	4	197	-199
-1	7	89	68
-1	8	85	-68
-1	8	85	-68
0	0	94	64
0	1	229	259
0	3	224	-231
0	5	102	108
0	6	70	75
0	7	79	-84
1	0	372	383
1	1	58	-61
1	4	316	344
1	5	70	77
1	6	58	-62

K	L	FO	FC
1	8	35	42
2	0	95	-81
2	1	103	-106
2	3	252	256
2	5	136	-147
2	7	45	49
3	0	178	-184
3	1	93	88
3	2	148	145
3	3	45	45
3	4	160	-163
3	5	22	-27
3	6	56	63
3	7	33	-30
3	8	42	40
4	0	43	46
4	1	227	226
4	2	87	87
4	3	81	-83
4	4	63	66
4	5	84	77
4	6	73	72
4	7	56	52
5	0	210	195
5	1	38	-36
5	2	128	-128
5	3	113	111
5	4	25	20
5	5	57	61
6	0	20	-24
6	1	82	-80
6	2	99	96
6	3	43	38
6	4	51	-55
6	5	44	41
6	6	46	-39
6	7	52	-65
7	0	28	28
7	1	47	47
7	2	34	38
7	3	51	-49
7	4	89	86
7	6	21	-28
7	7	31	-18
8	1	100	-102
8	2	22	17
8	5	67	-67
9	0	95	-99
9	3	41	-35
9	4	60	-61
9	5	36	-37
9	6	38	30
10	0	33	-31
10	1	82	88
10	3	36	-40
10	4	27	-22
10	5	46	43
11	0	53	57
11	2	76	-81
11	3	44	-42
11	4	56	56
12	1	73	-75
12	2	51	-54

H = 2

K	L	FO	FC
-13	1	48	51
-12	1	79	-78
-11	2	55	44
-10	1	82	97
-10	2	90	90
-10	4	91	-84
-9	1	132	131
-9	3	127	-118
-9	5	82	61
-8	1	36	-27
-8	2	91	-91
-8	4	86	83
-7	1	143	-147
-7	3	110	109
-6	2	97	88
-6	3	49	-63
-5	1	134	134
-5	4	96	96
-5	5	54	-72
-4	3	36	30
-4	4	72	-61
-3	2	268	-263
-3	3	91	-83
-3	4	112	-96
-3	7	69	-70
-2	1	188	-203
-2	2	107	-113
-2	4	82	-83
-1	1	107	-112
-1	2	138	150
-1	3	120	122
-1	5	65	-64
-1	6	79	-68
-1	7	127	108
0	0	104	-118
0	2	49	61
0	3	31	-36
0	4	224	-246
0	5	66	-69
0	6	55	63
0	8	68	-68
1	1	76	91
1	3	296	-325
1	5	118	127
1	6	24	27
1	7	93	-91
2	0	147	139
2	1	39	-45
2	2	204	-216
2	4	264	292
2	6	53	-50

K	L	FO	FC
2	8	51	52
3	0	86	-89
3	1	200	-195
3	3	214	235
3	4	38	-40
3	5	84	-90
3	7	46	36
4	0	271	-258
4	1	164	159
4	2	169	170
4	3	53	49
4	4	89	-92
5	0	210	196
5	1	266	267
5	2	37	32
5	3	39	-57
5	4	23	27
5	5	57	50
5	6	53	58
6	0	276	270
6	1	115	-113
6	2	104	-100
6	3	17	-14
6	4	42	36
6	5	46	47
6	7	33	30
7	0	59	-60
7	1	86	-89
7	3	58	60
7	4	41	41
7	6	37	33
8	0	21	-20
8	2	121	122
8	3	65	61
8	4	56	58
9	1	56	59
9	2	65	68
9	3	18	-21
9	5	46	-44
10	2	37	-45
10	4	67	-65
11	3	39	-46

H = 3

K	L	FO	FC
-11	2	50	-42
-10	1	47	-43
-10	3	84	95
-9	1	36	32
-9	2	92	86
-9	4	127	-109
-9	5	61	60
-8	2	124	122
-8	3	101	-109
-8	4	58	63
-7	1	61	-65
-7	4	79	89
-6	1	111	-112
-6	2	100	97
-6	3	56	61
-5	1	98	97
-5	2	70	66
-4	3	59	-54
-4	5	55	-40
-4	1	123	137
-4	4	54	55
-3	2	73	-76
-2	2	93	-94
-2	3	65	54
-2	4	104	-109
-2	7	53	-69
-1	1	46	-53
-1	3	62	-62
-1	4	47	44
0	0	100	110
0	1	131	-142
0	4	22	20
0	5	78	-84
0	6	25	32
0	7	85	91
1	0	229	-240
1	1	144	-156
1	2	67	73
1	4	156	-169
1	6	54	59
1	7	28	-25
2	0	99	-95
2	1	223	231
2	3	176	-186
2	4	38	45
2	5	49	50
2	7	101	-101
3	0	199	203
3	1	32	-26
3	2	154	-163
3	4	79	79
3	6	74	-74
4	0	206	-198
4	1	205	-206
4	2	61	-64
4	3	71	78
4	4	77	-80
4	5	66	-65
4	6	42	-43
4	7	71	73
5	0	267	-252
5	1	69	69
5	2	93	90
5	4	93	-92
5	6	64	65
6	0	130	140
6	1	147	145
6	2	62	80
6	3	91	-95
6	4	31	26
6	5	100	95
7	0	149	152
7	1	32	-32

Table 21. (Continued)

7	2	87	-96
7	4	95	94
7	5	33	-29
7	6	47	-48
8	1	70	-71
8	3	105	98
8	5	33	-10
9	0	86	-89
9	1	20	28
9	[illegible]	89	92
10	1	65	63
11	0	44	52

H = 4

K	L	FO	FC
-10	2	89	-75
-10	4	61	39
-9	1	56	-68
-9	2	42	48
-9	3	106	102
-8	1	81	76
-8	2	59	70
-8	3	48	-41
-8	4	89	-93
-7	2	86	-90
-7	3	131	-122
-6	1	139	-149
-6	4	158	146
-5	1	82	-82
-5	2	88	87
-5	3	169	175
-5	5	74	-67
-4	2	116	121
-4	4	149	-138
-3	1	202	219
-3	3	125	-123
-3	4	73	68
-2	1	52	-72
-2	2	109	-125
-2	3	106	115
-1	1	115	-128
-1	2	58	59
0	1	107	118
0	2	103	110
0	4	73	80
0	5	53	-50
1	0	156	161
1	1	39	-50
1	2	33	38
1	5	58	-61
1	7	48	44
2	0	134	-131
2	2	34	-33
2	3	71	-72
2	4	105	-108
2	6	35	40
3	1	68	72
3	2	124	-120
3	3	23	-30
3	5	75	74
3	6	22	29
4	0	29	29
4	1	106	-107
4	2	34	-36
4	3	35	37
4	4	87	91
4	5	18	13
4	6	94	-93
5	0	74	-79
5	1	106	-113
5	3	86	88
5	4	73	-73
5	5	111	-116
5	6	45	-41
6	0	79	-77
6	2	97	98
6	3	54	-55
6	4	151	-149
7	0	23	22
7	1	65	66
7	3	166	-166
7	4	68	62
7	5	77	77
8	0	58	61
8	1	66	-66
8	2	122	-122
8	3	36	35
8	4	84	81
9	0	39	-45
9	1	47	-52
9	2	47	43
9	3	75	76
10	0	79	-77
10	1	69	74
10	2	48	42
11	0	44	54

H = 5

K	L	FO	FC
-10	2	47	-49
-9	1	51	-47
-9	2	42	-51
-8	1	92	-44
-8	2	71	68
-7	1	90	93
-7	4	86	-69
-6	2	36	-54
-6	3	133	-124
-5	2	107	-101
-5	4	141	131
-4	1	160	-156
-4	3	150	155
-4	4	94	-86
-3	1	133	144
-3	2	87	89
-3	3	45	-53
-3	4	108	-105
-2	1	176	199
-1	1	121	-132
-1	2	32	-33
0	0	165	-171
1	0	60	-65
1	1	72	79
1	2	123	133
1	3	24	19
1	4	56	57
1	6	30	33
2	0	73	79
2	1	101	110
2	2	50	56
2	4	48	46
2	5	34	-27
3	0	66	68
3	1	85	87
3	2	75	-77
3	4	78	-76
3	6	38	36
4	0	33	35
4	3	27	-21
4	5	78	79
5	1	45	-49
5	2	50	-51
5	4	93	90
6	1	142	-135
6	2	23	25
6	3	79	79
6	4	55	-55
6	5	67	-66
7	0	77	-78
7	1	49	51
7	2	113	116
7	3	51	-52
7	4	71	-74
8	0	39	43
8	1	77	77
8	2	54	-54
8	3	101	-98
9	0	40	42
9	1	80	-85
9	2	96	-91
10	0	86	-92
10	1	48	-51

H = 6

K	L	FO	FC
-12	1	62	60
-9	1	38	-23
-6	1	35	-48
-6	3	52	-47
-6	4	67	-65
-6	5	48	33
-5	1	78	79
-5	3	42	-62
-4	2	79	-79
-4	3	77	85
-4	4	76	59
-4	5	66	-91
-3	1	95	-118
-3	3	64	65
-3	4	117	-106
-3	5	54	-47
-2	3	65	-57
-2	4	98	-91
-1	3	72	-63
-1	4	57	65
-1	5	68	73
0	0	103	102
0	1	112	-117
0	2	49	-49
0	4	84	89
0	6	48	-39
1	0	126	-128
1	1	65	-66
1	2	62	62
1	3	95	96
1	4	67	-60
1	5	55	-54
2	0	78	-82
2	1	135	141
2	2	110	111
2	3	59	-60
3	0	50	48
3	1	69	73
3	2	70	-72
3	4	43	35
4	0	43	47
4	1	37	-33
4	3	64	57
4	5	43	38
5	1	55	54
5	2	60	60
5	4	42	39
6	0	80	82
6	4	29	24
7	0	24	-15
7	1	79	-79
8	0	41	-48
8	1	49	50
8	2	30	31
9	0	33	32
9	1	24	27

H = 7

K	L	FO	FC
-11	1	79	63
-10	1	77	64
-10	2	52	-41
-9	1	96	-75
-9	3	79	57
-8	1	68	-65
-8	2	36	48
-7	4	49	36
-6	2	50	53
-4	1	35	37
-4	2	86	-87
-3	1	77	-78
-3	3	57	56
-3	4	73	64
-2	3	68	58
-2	4	60	-55
-1	3	65	-72
-1	4	85	-93
0	0	93	92
0	1	34	40
0	2	62	-61
0	3	116	-118
0	4	79	75
0	5	36	40
1	0	41	43
1	1	155	-153
1	2	133	-124
1	3	69	64
1	4	66	61
1	5	49	-39
2	0	166	-166
2	1	73	-74
2	2	84	82
2	3	83	83
2	4	69	-63
2	5	21	-25
3	0	68	-63
3	1	161	161
3	2	59	57
3	3	26	-31
3	4	20	-21
4	0	125	119
4	1	30	23
4	2	52	-48
4	3	24	-29
5	0	42	43
5	1	53	-52
5	2	33	-34
6	0	43	-37
6	2	32	29
6	3	39	35
7	2	38	42
8	1	37	38

H = 8

K	L	FO	FC
-9	1	48	44
-9	2	42	-44
-8	1	65	-78
-8	3	72	42
-5	1	42	45
-4	2	48	-47
-4	3	53	31
-1	1	73	-75
-1	4	55	-51
0	0	68	-64
0	1	48	45
0	2	55	58
0	3	64	-63
0	4	26	-19
1	0	75	75
1	1	97	93
1	3	41	-38
1	4	64	60
2	0	56	48
2	1	119	-113
2	2	86	-79
2	3	31	30
3	0	150	-148
3	1	49	-50
3	3	39	33
4	0	40	-42
4	1	53	56
4	2	39	35
5	0	79	75
6	0	60	61
6	1	56	-61
6	2	46	-40
7	1	44	-37

H = 9

K	L	FO	FC
-7	1	80	-77
-7	3	55	34
-5	1	103	100
-4	1	46	42
-4	2	73	-71
-2	2	56	53
0	1	31	-36
0	2	36	24
0	3	28	-23
1	0	53	-51
1	1	55	50
2	0	39	33
2	2	39	-33
3	1	52	-49
3	2	38	-31
4	0	39	-35
4	2	33	33
5	1	35	33
6	0	40	38

H = 10

K	L	FO	FC
-6	1	79	-66
-5	2	38	33
-4	1	109	106
0	2	42	34
1	1	28	31
2	0	33	30

H = 11

K	L	FO	FC
-5	1	58	-65
-1	1	47	-41
0	0	39	-37
1	0	25	-20
2	0	33	31

Table 22. Bond distances in the tetrapropylammonium cations of $[(n\text{-}C_3H_7)_4N]_2[W_2Br_9]$, Å

Cation #1		
N(1)-C(1)	1.57(5)	
N(1)-C(4)	1.54(7)	
N(1)-C(7)	1.47(5)	
N(1)-C(10)	1.47(6)	
Average N(1)-C		1.51
C(1)-C(2)	1.16(6)	
C(2)-C(3)	1.41(7)	
C(4)-C(5)	1.33(9)	
C(5)-C(6)	1.57(8)	
C(7)-C(8)	1.40(7)	
C(8)-C(9)	1.25(8)	
C(10)-C(11)	1.13(6)	
C(11)-C(12)	1.43(6)	
Average C-C		1.34
Cation #2		
N(2)-C(13)	1.56(4)	
N(2)-C(16)	1.52(5)	
N(2)-C(19)	1.52(4)	
N(2)-C(22)	1.61(5)	
Average N(2)-C		1.55
C(13)-C(14)	1.45(6)	
C(14)-C(15)	1.43(5)	
C(16)-C(17)	1.28(6)	
C(17)-C(18)	1.52(5)	
C(19)-C(20)	1.41(6)	
C(20)-C(21)	1.45(5)	
C(22)-C(23)	1.46(6)	
C(23)-C(24)	1.52(6)	
Average C-C		1.44

Table 23. Final positional parameters for $[(n\text{-}C_3H_7)_4N]_2[W_2Br_9]$[a]

Atom	x	y	z
W(1)	0.38141(3)	0.3262(1)	0.3840(1)
W(2)	0.36504(3)	0.1425(1)	0.3184(1)
Br(1)	0.3906(1)	0.5079(3)	0.3232(1)
Br(2)	0.3437(1)	0.4255(3)	0.4671(1)
Br(3)	0.4389(1)	0.3544(3)	0.4670(1)
Br(4)	0.3082(1)	0.0211(3)	0.3241(2)
Br(5)	0.3566(1)	0.1305(3)	0.1893(1)
Br(6)	0.4047(1)	-0.0281(3)	0.3290(1)
Br(7)	0.3191(1)	0.3089(2)	0.3072(1)
Br(8)	0.4269(1)	0.2429(3)	0.3041(1)
Br(9)	0.3707(1)	0.1455(2)	0.4515(1)
N(1)	0.4374(8)	0.247(2)	0.032(1)
N(2)	0.1861(6)	0.206(2)	0.330(1)
C(1)	0.444(1)	0.355(3)	0.076(2)
C(2)	0.449(2)	0.385(5)	0.132(2)
C(3)	0.458(1)	0.482(3)	0.170(2)
C(4)	0.447(2)	0.143(4)	0.074(5)
C(5)	0.480(2)	0.131(5)	0.110(6)
C(6)	0.486(1)	0.023(4)	0.154(3)
C(7)	0.396(1)	0.239(5)	0.020(2)
C(8)	0.365(2)	0.199(6)	-0.020(3)
C(9)	0.331(1)	0.195(3)	-0.022(2)
C(10)	0.453(1)	0.256(7)	-0.033(3)
C(11)	0.452(2)	0.289(6)	-0.087(2)
C(12)	0.475(1)	0.287(3)	-0.141(2)
C(13)	0.205(1)	0.265(4)	0.395(2)

[a]Numbers in parentheses are the estimated standard deviations of the coordinates and refer to the last significant digit of the preceding number.

Table 23. (Continued)

Atom	x	y	z
C(14)	0.210(1)	0.384(4)	0.397(2)
C(15)	0.228(1)	0.435(2)	0.457(2)
C(16)	0.185(1)	0.088(3)	0.356(2)
C(17)	0.207(1)	0.005(4)	0.357(2)
C(18)	0.205(1)	-0.103(3)	0.395(1)
C(19)	0.149(1)	0.259(4)	0.306(2)
C(20)	0.124(1)	0.277(4)	0.356(2)
C(21)	0.086(1)	0.295(4)	0.331(2)
C(22)	0.212(1)	0.216(3)	0.269(2)
C(23)	0.201(1)	0.158(3)	0.205(2)
C(24)	0.231(1)	0.157(3)	0.157(1)

Table 24. Final thermal parameters ($x10^3$) for $[(n\text{-}C_3H_7)_4N]_2[W_2Br_9]$[a]

Atom	β_{11}	β_{22}	β_{33}	β_{12}	β_{13}	β_{23}
W(1)	1.04(1)	9.3(1)	2.96(4)	0.10(3)	0.32(1)	0.12(5)
W(2)	1.12(1)	8.6(1)	2.97(3)	0.08(3)	0.40(1)	0.17(5)
Br(1)	1.58(3)	11.7(3)	5.4(1)	-0.44(9)	0.21(5)	2.2(1)
Br(2)	1.97(4)	13.2(3)	4.7(1)	0.9(1)	1.19(6)	-0.8(1)
Br(3)	1.46(3)	16.7(4)	5.1(1)	0.2(1)	-0.59(5)	-0.4(2)
Br(4)	1.43(3)	12.4(3)	6.1(1)	-0.80(9)	0.38(6)	1.3(1)
Br(5)	1.92(4)	14.2(3)	3.2(1)	-0.2(1)	0.13(5)	-0.1(1)
Br(6)	1.84(4)	12.5(3)	5.3(1)	1.6(1)	0.55(6)	0.4(1)
Br(7)	1.12(3)	10.6(3)	5.5(1)	0.35(8)	-0.23(5)	-0.1(1)
Br(8)	1.25(3)	14.9(3)	5.1(1)	-0.21(9)	1.00(5)	-0.8(1)
Br(9)	2.27(4)	11.0(3)	3.0(1)	-0.2(1)	0.67(5)	0.5(1)
N(1)	1.8(2)	6.7	8.8	-1.0	1.7	-3.9
N(2)	1.0(2)	17.2	2.3	-0.6	0.3	-0.5
C(1)	4.3(9)	15(4)	7(2)	-1.8	0.1	-2.3
C(2)	10(2)	30(8)	6(1)	1.6	4.1	-7.6
C(3)	3.1(6)	18(4)	8(2)	-4.1	1.6	-3.7
C(4)	3(1)	8(4)	26(6)	2.4	0.5	-1.0
C(5)	4(1)	21(8)	27(8)	1.9	-1.2	4.9
C(6)	3.3(8)	19(5)	15(3)	1.2	2.6	6.5
C(7)	2.8(6)	5(1)	4(1)	-6.7	1.4	-0.8
C(8)	4(1)	4(1)	7(2)	4.9	-2.2	-3.7
C(9)	1.3(3)	23(6)	7(1)	-0.8	-1.5	-0.4
C(10)	2.5(6)	8(1)	8(2)	-6.5	0.6	10.0
C(11)	5(1)	4(1)	3(1)	-4.9	2.5	-1.2
C(12)	1.7(4)	24(5)	6(1)	0.7	0.7	0.1
C(13)	1.8(5)	20(5)	9(2)	-0.3	-0.3	-7.0

[a]The form of the anisotropic temperature factor expression is $\exp[-(\beta_{11}h^2+\beta_{22}k^2+\beta_{33}\ell^2+2\beta_{12}hk+2\beta_{13}h\ell+2\beta_{23}k\ell]$.

Table 24. (Continued)

Atom	β_{11}	β_{22}	β_{33}	β_{12}	β_{13}	β_{23}
C(14)	2.3(6)	15(5)	10(2)	0.2	-0.1	-2.1
C(15)	2.8(5)	10(3)	6(1)	-0.7	-0.3	-1.9
C(16)	5.6(9)	17(5)	5(1)	2.7	4.5	4.5
C(17)	3.7(7)	20(6)	8(1)	3.0	3.7	2.9
C(18)	2.2(4)	14(3)	4(1)	-1.9	-0.2	1.9
C(19)	0.9(3)	37(7)	8(2)	-0.1	0.0	-5.8
C(20)	1.1(3)	38(7)	10(2)	3.2	0.2	-6.1
C(21)	1.8(4)	26(5)	10(2)	2.1	2.6	5.5
C(22)	3.8(7)	12(3)	7(1)	-2.7	0.2	-1.5
C(23)	3.7(8)	9(4)	10(2)	-0.4	0.0	2.9
C(24)	2.2(4)	19(5)	5(1)	0.3	2.0	-1.3

Table 25. Observed and calculated structure factors for $[(n\text{-}C_3H_7)_4N]_2[W_2Br_9]$

Table 25. (Continued)

4 10	46	-48
4 8	67	66
4 3	174	-161
4 0	126	-124
4 -1	287	261
4 -2	70	-70
4 -4	98	87
4 -9	94	91
4-10	125	129
4-11	131	127
4-13	71	-68
2 14	57	60
2 12	55	48
2 11	60	60
2 10	48	-56
2 9	57	56
2 7	147	-147
2 4	49	-43
2 3	209	211
2 1	166	-167
2 0	250	-252
2 -1	144	-147
2 -3	96	104
2 -4	147	150
2 -6	142	-147
2 -7	217	216
2-11	158	-163
2-12	59	57
2-13	147	149
2-16	40	70
2-17	83	-90
0 14	111	-121
0 10	159	184
0 8	99	-109
0 6	54	-59
0 4	48	-40
0 0	374	378
0 -2	174	-184
0 -4	154	-152
0 -8	210	217
0-12	84	-88
0-14	106	-102
0-16	114	117
0-18	80	99

H = 15

K	L	FO	FC
9	7	130	120
9	6	50	48
9	1	122	128
9 -1		127	-128
9 -7		149	-154
9 -9		78	79
9-13		84	-89
7 14		55	56
7 8		138	136
7 6		96	-93
7 3		130	138
7 2		113	122
7 1		60	-73
7 0		128	-122
7 -1		110	-121
7 -2		63	63
7 -3		71	66
7 -6		69	64
7 -8		72	-73
7 -9		98	87
7-11		111	-109
7-12		63	-59
5 15		90	86
5 14		87	-84
5 13		116	-111
5 11		87	-86
5 7		98	-97
5 5		90	-92
5 3		73	-81
5 2		168	182
5 -1		216	230
5 -2		143	-132
5 -3		14	30
5 -6		53	62
5 -7		89	98
5 -9		70	68
5-10		88	-90
5-12		86	-85
5-15		100	-89
3 16		83	78
3 15		84	-86
3 13		87	-80
3 8		87	-88
3 7		114	120
3 6		164	162
3 5		88	-90
3 4		47	-49
3 2		278	-284
3 1		112	116
3 0		132	124
3 -1		78	-76
3 -3		44	42
3 -7		40	-40
3 -8		280	-289
3 -9		61	59
3-10		118	138
3-12		118	124
3-14		120	-122
1 15		83	-82
1 13		161	148
1 9		130	-131
1 8		120	119
1 7		171	168
1 6		198	-192
1 3		148	157
1 2		187	201
1 1		106	107
1 0		201	-200
1 -1		393	-416
1 -3		124	136
1 -6		49	41

1 -8	169	161
1 -7	290	-294
1 -8	256	254
1-12	54	-50
1-13	55	57
1-14	118	110
1-15	127	119
1-17	89	-96

H = 14

K	L	FO	FC
10	6	81	-78
10	0	103	-102
10 -2		88	82
10 -3		125	-121
10 -8		95	103
8 9		58	-63
8 6		127	118
8 5		140	133
8 3		86	-97
8 0		127	138
8 -1		57	70
8 -2		41	-45
8 -3		75	-68
8 -5		64	60
8 -6		68	-66
8 -8		104	-104
8 -9		134	-134
8-10		122	118
8-11		77	71
6 7		96	98
6 2		231	233
6 0		113	-121
6 -1		81	-64
6 -2		144	-148
6 -3		57	56
6 -7		58	-54
6-10		130	-128
6-14		72	79
6-16		51	49
4 15		88	-80
4 14		112	110
4 12		96	-93
4 8		109	118
4 6		220	-225
4 5		116	-114
4 1		109	123
4 0		237	-238
4 -2		247	231
4 -3		121	-118
4 -6		129	-131
4 -7		57	44
4 -8		219	227
4 -9		124	118
4-11		109	-107
4-13		94	-91
4-14		84	82
4-16		101	-103
2 15		107	108
2 12		87	-94
2 10		87	-83
2 8		118	121
2 7		154	-170
2 6		97	-99
2 5		318	334
2 4		66	-73
2 1		280	-270
2 0		138	-138
2 -1		311	329
2 -2		284	261
2 -3		70	-85
2 -5		68	60
2 -6		187	-184
2 -8		193	196
2 -9		410	-396
2-10		82	83
2-11		124	131
2-15		179	-181
0 14		118	-118
0 12		98	103
0 8		131	-137
0 6		78	78
0 4		108	118
0 2		277	292
0 0		93	92
0 -2		266	-288
0 -6		238	258
0 -8		85	88
0 -8		166	-173
0-10		46	45
0-12		165	-159
0-14		77	84
0-16		136	146
0-18		134	-149

H = 13

K	L	FO	FC
11 -4		64	61
9 8		84	89
9 5		124	-120
9 4		68	-77
9 3		74	71
9 -1		121	-122
9 -3		110	98
9 -4		75	-70
9 -6		71	-70
9 -8		72	64
9 -9		112	118
9-11		76	-83
7 12		74	-74
7 8		76	75
7 4		75	81
7 1		181	-197
7 0		38	-40
7 -1		90	98
7 -3		68	71
7 -4		84	-82
7 -8		50	-49

7 -7	68	-70
7-10	102	-93
7-11	97	104
5 13	86	-81
5 7	58	-63
5 6	102	118
5 1	211	218
5 0	189	-188
5 -3	92	-89
5 -9	113	-110
5-11	92	-92
5-12	84	82
5-14	49	51
5-17	70	73
3 14	76	-73
3 9	112	114
3 8	109	98
3 6	101	103
3 4	317	-344
3 3	73	88
3 1	82	-81
3 0	236	234
3 -1	81	-83
3 -2	192	-185
3 -5	118	-118
3 -6	158	-164
3-10	303	308
3-11	67	-77
3-12	124	-128
3-16	123	117
1 15	100	103
1 13	81	80
1 7	141	140
1 6	186	203
1 3	91	-100
1 2	73	73
1 1	214	-230
1 0	78	-83
1 -1	151	-145
1 -2	192	181
1 -3	216	226
1 -6	87	84
1 -5	130	-134
1 -6	91	82
1 -7	213	-230
1 -9	147	143
1-10	176	-172
1-13	68	65
1-15	46	39
1-16	90	-90
1-17	103	-108
1-19	78	82

H = 12

K	L	FO	FC
10 0		60	66
10 -1		88	-88
10 -5		76	79
10 -6		93	91
8 8		64	69
8 7		111	112
8 6		87	-86
8 3		89	-83
8 -7		118	-123
8 -8		138	137
8-11		86	88
6 4		149	158
6 2		111	-122
6 0		266	-258
6 -1		69	67
6 -2		129	118
6-12		137	133
6-14		64	70
4 16		88	89
4 14		98	-95
4 12		73	-66
4 10		120	119
4 9		67	67
4 8		248	-249
4 7		118	-117
4 5		89	-92
4 3		277	284
4 2		200	-214
4 1		70	-79
4 0		278	284
4 -1		170	-171
4 -2		77	70
4 -6		186	-180
4 -8		190	188
4 -7		139	139
4 -9		105	-100
4-11		124	-137
2 17		90	84
2 16		68	-76
2 10		105	107
2 9		89	-86
2 7		320	317
2 6		146	-149
2 5		95	102
2 3		332	-362
2 1		138	144
2 0		105	103
2 -1		83	-90
2 -2		287	289
2 -3		120	-128
2 -4		326	-329
2 -5		113	-110
2 -7		374	-388
2 -8		198	209
2 -9		87	88
2-10		196	-217
2-11		164	169
2-13		86	-94
0 18		88	-73
0 14		188	188
0 8		72	72
0 6		148	149
0 4		443	484

0 2	185	-179
0 0	372	-379
0 -2	185	183
0 -6	123	-123
0 -8	181	-186
0-10	106	-109
0-14	94	106
0-16	127	-138
0-20	61	74

H = 11

K	L	FO	FC
11 0		51	-58
11 -2		77	76
9 7		138	-137
9 6		93	-93
9 1		107	-117
9 -1		121	118
9 -5		70	69
9 -7		111	117
9 -8		91	88
9 -9		101	-99
7 13		65	-64
7 8		85	-81
7 7		57	61
7 6		86	98
7 5		81	-84
7 3		118	-122
7 1		82	83
7 0		107	111
7 -1		71	76
7 -5		72	-75
7 -8		116	-118
7 -9		133	132
7-13		72	-71
5 15		85	-102
5 14		67	67
5 13		103	106
5 12		78	-78
5 10		57	-56
5 9		101	-105
5 7		150	150
5 3		145	167
5 2		128	-131
5 0		123	-117
5 -1		342	-387
5 -2		207	196
5 -3		115	116
5 -4		95	88
5 -6		82	-78
5 -7		185	-186
5 -9		66	60
5-10		62	63
5-13		65	71
5-15		116	124
5-16		87	-84
3 16		95	-96
3 15		84	93
3 9		78	78
3 8		198	202
3 7		233	-234
3 6		814	-801
3 5		73	87
3 3		77	-87
3 2		364	371
3 1		277	-290
3 0		378	-382
3 -1		127	122
3 -2		128	134
3 -3		192	-188
3 -6		46	43
3 -7		109	106
3 -8		478	478
3 -9		92	-98
3-10		161	-156
3-11		107	102
3-12		108	-107
3-16		166	166
1 17		78	78
1 15		93	105
1 13		110	-108
1 9		108	109
1 7		74	-66
1 6		236	224
1 5		178	-191
1 4		110	107
1 3		213	-214
1 2		71	-81
1 1		90	-91
1 0		56	56
1 -1		219	248
1 -2		88	-89
1 -5		298	-320
1 -6		200	-201
1 -7		223	226
1 -8		297	-307
1-18		148	-146
1-17		97	104

H = 10

K	L	FO	FC
10 6		77	74
10 5		66	64
10 0		72	64
10 -2		79	-80
10 -3		70	62
10 -7		78	-77
8 9		70	73
8 6		113	-115
8 5		330	-329
8 0		96	-81
8 -1		62	-69
8 -6		88	100
8 -8		63	67
8 -9		121	117
8-10		103	-116
8 16		60	58

6 13	77	-69
6 12	80	-77
6 7	72	-74
6 6	70	69
6 2	175	-230
6 0	108	109
6 -1	170	174
6 -2	101	101
6 -3	67	-61
6 -4	61	-60
6 -7	91	91
6 -9	88	-93
6-12	65	63
6-14	108	-111
6-16	70	-73
6-17	58	60
4 15	54	58
4 14	104	-104
4 12	101	101
4 9	139	-137
4 8	219	-220
4 7	116	-114
4 6	298	284
4 5	262	261
4 4	137	-143
4 3	63	-67
4 2	74	77
4 1	163	-168
4 0	397	387
4 -1	82	89
4 -2	381	-364
4 -3	59	59
4 -4	173	170
4 -5	218	204
4 -6	202	198
4 -8	228	-238
4 -9	178	-169
4-10	101	99
4-11	129	129
4-13	71	62
4-16	100	106
2 12	96	86
2 9	66	58
2 8	110	-109
2 7	113	101
2 5	818	-808
2 4	69	83
2 3	73	-76
2 0	191	200
2 -1	398	-388
2 -2	291	-272
2 -4	187	-188
2 -5	130	-122
2 -6	388	389
2 -7	85	86
2 -8	244	-246
2 -9	479	498
2-10	66	-71
2-11	70	-68
2-12	103	118
2-15	170	169
2-16	97	101
0 16	119	118
0 14	69	84
0 8	128	117
0 6	221	228
0 4	332	-367
0 2	388	-408
0 -2	86	-69
0 -4	258	-256
0 -6	236	-290
0 -8	188	181
0-12	136	138
0-16	168	-160
0-18	181	198

H = 9

K	L	FO	FC
11 1		68	-73
11 0		60	64
9 9		80	-74
9 8		108	-100
9 5		91	88
9 4		119	118
9 3		83	-80
9 -6		121	112
9 -8		78	-79
9 -9		88	-81
9-10		73	-68
7 11		78	72
7 9		83	88
7 8		83	86
7 7		98	-107
7 6		113	107
7 -2		118	-103
7 -3		148	-138
7 -7		63	-70
7 -7		117	118
7 -8		82	-88
7-11		108	-109
5 15		78	76
5 11		98	-93
5 7		52	54
5 6		83	89
5 3		100	97
5 1		249	-263
5 0		178	182
5 -2		168	155
5 -3		303	293
5 -5		128	-123
5 -8		148	-146
5 -9		73	-83
5 -8		83	87
5 -9		68	66
5-13		95	98
5-14		76	-66
5-15		85	-91
0-17		87	-100

3 18	63	-65
3 13	72	-69
3 10	104	100
3 9	147	-140
3 8	394	-382
3 7	94	-91
3 6	116	-118
3 5	79	81
3 4	395	389
3 3	168	-173
3 2	191	-205
3 1	107	118
3 -1	128	118
3 -2	193	188
3 -5	180	182
3 -6	631	612
3 -8	70	-81
3-10	267	-260
3-12	131	132
3-16	98	-90
1 15	123	-117
1 8	63	67
1 7	180	-177
1 5	200	-219
1 4	106	-109
1 3	206	208
1 2	256	-288
1 0	73	-80
1 -1	109	112
1 -3	97	-108
1 -4	286	-280
1 -6	139	-133
1 -7	309	316
1 -8	135	130
1 -9	92	-86
1-10	340	338
1-11	93	-81
1-13	86	-48
1-16	61	62
1-17	118	123
1-19	67	-74

H = 8

K	L	FO	FC
10 8		61	72
10 3		88	-87
10 1		68	-82
10 0		84	-80
10 -5		89	-88
8 8		105	-107
8 7		144	-144
8 6		148	148
8 5		66	-63
8 3		68	74
8 2		48	-60
8 1		89	-94
8 -2		105	-98
8 -4		93	93
8 -7		129	140
8 -8		180	-187
6 15		76	-81
6 10		98	92
6 9		81	-84
6 7		127	128
6 4		83	-98
6 3		76	79
6 1		181	188
6 0		284	262
6 -1		180	-168
6 -2		188	-181
6 -4		197	-192
6 -5		63	60
6 -8		34	38
6 -7		149	-158
6-12		86	-88
6-13		61	-60
6-14		109	-112
6-15		83	86
6-16		86	94
4 16		122	-122
4 14		97	96
4 11		101	-102
4 10		181	-179
4 9		99	-85
4 8		269	262
4 7		332	316
4 6		64	-68
4 3		79	-84
4 2		337	330
4 1		148	167
4 0		344	-358
4 -2		63	65
4 -3		228	213
4 -4		234	228
4 -5		101	-110
4 -6		267	-268
4 -7		304	-299
4 -8		120	119
4 -9		105	106
4-11		61	68
4-13		101	-91
2 14		103	101
2 11		91	112
2 10		74	-63
2 7		86	-88
2 10		105	-100
2 9		126	119
2 8		82	-58
2 7		480	-473
2 6		75	77
2 5		80	-61
2 3		191	206
2 2		64	67
2 1		131	-142
2 -1		272	256
2 -2		208	-191
2 -4		404	387
2 -5		188	195
2 -7		440	481

2 -8	223	-233
2 -9	135	-137
2-10	188	187
2-11	106	-98
2-13	91	97
2-15	84	-69
2-18	71	-80
0 18	88	88
0 16	92	108
0 14	161	-149
0 6	114	-108
0 4	574	-576
0 2	95	106
0 0	183	180
0 -2	176	-162
0 -4	55	48
0 -6	123	114
0 -8	122	126
0-10	135	141
0-12	88	-87
0-14	132	-135
0-16	150	149
0-18	67	73
0-20	62	-73

H = 7

K	L	FO	FC
11 3		86	-84
11 0		102	98
11 -2		92	-87
9 10		70	-74
9 7		114	118
9 6		123	119
9 5		102	-96
9 -6		94	91
9 -8		88	-87
9 -9		86	91
9-10		60	53
7 14		73	76
7 11		87	91
7 9		103	-110
7 8		116	119
7 7		70	-78
7 6		162	-131
7 5		181	162
7 4		89	-97
7 0		283	-283
7 -1		97	-94
7 -2		36	-36
7 -3		112	-109
7 -5		193	188
7 -6		89	-100
7 -8		168	176
7 -9		138	-146
7-13		69	69
7-14		91	89
5 16		86	98
5 14		89	-63
5 13		91	-91
5 10		83	81
5 9		168	166
5 7		87	-89
5 6		137	142
5 4		92	-85
5 3		94	-104
5 2		44	43
5 1		102	-121
5 0		154	162
5 -1		824	806
5 -2		287	-286
5 -3		268	-269
5 -4		123	-123
5 -5		184	-179
5 -6		106	116
5 -7		194	193
5 -8		82	-98
5 -9		238	-238
5-11		76	72
5-15		198	-188
3-16		120	122
3-17		110	118
3 15		95	-86
3 14		99	-107
3 12		74	77
3 10		198	-197
3 9		104	-104
3 8		232	-222
3 7		292	301
3 6		614	609
3 3		83	-67
3 2		49	-60
3 1		293	316
3 0		441	493
3 -1		164	-168
3 -2		154	-133
3 -4		381	384
3 -7		189	-197
3 -8		813	-464
3 -9		88	82
3-10		178	174
3-11		97	-97
3-14		128	-135
1 17		67	-63
1 16		134	-134
1 13		120	121
1 9		189	-182
1 8		105	98
1 6		233	-238
1 5		122	116
1 4		163	-168
1 3		133	138
1 2		174	171
1 1		76	81
1 0		134	-137
1 -1		436	-469
1 -4		89	88
1 -5		390	377
1 -6		128	127

Table 25. (Continued)

1 -7	118	-110	9 9	94	99	8 3	41	-46	7-14	91	-90	6 -3	138	-124	8 3	48	-49	2-12	171	168
1 -6	228	224	9 8	106	107	8 2	107	120	8 15	56	-61	6 -5	91	86	8 2	172	-169	2-10	78	-76
1-15	186	182	9 7	55	-46	8 1	320	-316	8 14	61	67	6 -6	84	-82	8 1	361	-372	2-16	70	-62
1-17	86	-90	9 6	80	-78	8 0	336	-347	8 13	111	109	6 -8	99	90	8 0	133	136	0 -2	293	-281
			9 4	96	-99	8 -1	702	703	8 10	114	-114	6 -9	73	-65	8 -1	116	123	0 -4	303	-303
H = 6			9 1	87	87	8 -4	338	340	8 9	70	-87	6-10	82	-76	8 -3	244	230	0 -6	716	679
K L	FO	FC	9 -6	115	-111	8 -6	109	-111	8 8	75	72	6-11	73	66	8 -4	127	-137	0 -8	506	-499
10 -1	127	112	9 -8	89	97	8 -8	102	-97	8 6	52	59	6-12	106	106	8 -9	88	-47	0-10	178	174
10 -2	71	66	9-10	56	57	8 -7	211	210	8 5	133	-140	6-13	70	-75	8 -8	83	-94	0-12	181	-117
10 -7	108	90	7 13	98	93	8 -8	103	107	8 4	91	86	6-14	76	-76	8 -7	79	77	0-14	393	-402
8 10	88	-82	7 12	63	-67	8 -9	90	-83	8 3	76	78	6-16	122	-133	8 -8	87	-85	0-16	178	189
8 9	72	-73	7 11	99	-96	8-13	81	76	8 0	163	-189	6-17	69	71	5-10	102	101			
8 8	64	63	7 9	124	-117	8-14	140	142	8 -1	886	-936	4 10	138	141	5-13	136	132			
8 7	118	-113	7 8	119	-116	8-15	108	-107	8 -2	271	273	4 9	292	-285	5-14	93	-97			
8 6	85	80	7 7	213	199	8-16	100	-103	8 -3	111	111	4 6	71	64	5-15	85	-93			
8 5	116	109	7 6	188	-187	8-18	88	-89	8 -6	87	81	4 5	95	99	5-17	73	-83			
8 4	116	-117	7 5	45	-42	4 16	68	80	8 -5	146	138	4 4	226	232	3 16	43	53			
8 0	49	-55	7 2	77	-83	4 14	84	-92	8 -8	99	-108	4 2	59	-60	3 15	59	-71			
8 -1	131	133	7 -1	156	-153	4 11	194	196	8 -7	185	-182	4 0	61	54	3 12	141	140			
8 -3	54	56	7 -2	148	138	4 10	104	109	8 -9	218	218	4 -1	109	-106	3 10	95	89			
8 -5	72	76	7 -3	267	259	4 8	75	-71	8-10	71	-65	4 -2	127	-120	3 8	373	-367			
8 -6	120	-114	7 -5	151	149	4 7	357	-340	8-11	50	-47	4 -3	189	187	3 7	143	139			
8 -9	112	-113	7 -7	164	-173	4 6	95	96	8-12	69	67	4 -4	260	-262	3 6	94	88			
8-10	102	109	7 -8	77	73	4 5	78	-78	8-16	219	217	4 -5	308	285	3 5	350	330			
8 12	73	76	7 -9	60	48	4 2	58	-69	8-18	107	-112	4 -7	72	-73	3 2	77	80			
8 10	46	46	7-10	58	-55	4 0	257	261	8-17	98	-106	4 -8	128	-124	3 1	157	149			
8 8	110	-110	7-11	51	57	4 -1	68	-69	3 11	67	-69	4 -9	151	-145	3 0	37	-40			
8 7	74	72	7-12	62	62	4 -2	63	67	3 10	283	282	4-10	64	-60	3 -1	65	75			
8 6	62	-65	5 16	59	-61	4 -3	342	-335	3 8	156	155	4-13	66	64	3 -2	344	-317			
8 3	41	31	5 15	78	-81	4 -4	140	-141	3 7	190	-184	4-16	85	90	3 -3	122	119			
8 2	101	102	5 12	46	52	4 -5	208	211	3 6	342	-342	4-17	50	-60	3 -4	247	233			
8 1	77	-80	5 11	87	86	4 -6	66	67	3 5	79	-85	2 14	111	-109	3 -5	69	-66			
6 -1	226	-229	5 8	82	-88	4 -7	278	269	3 3	251	234	2 13	67	-75	3 -6	293	287			
6 -2	368	-367	5 6	48	-46	4 -8	157	-145	3 1	110	-117	2 12	81	78	3 -8	175	-176			
6 -3	80	78	5 5	114	-113	4 -9	89	-99	3 0	101	-96	2 11	90	-89	3 -9	132	-124			
6 -4	102	93	5 3	111	-119	4-12	62	-60	3 -1	172	185	2 10	164	150	3-10	141	-137			
6 -8	100	-98	5 2	61	78	4-13	73	74	3 -2	118	-119	2 9	286	283	1 17	103	103			
6 -6	98	106	5 1	295	304	4-14	126	-118	3 -3	223	223	2 8	169	-162	1 16	81	-77			
6 -7	91	-98	5 0	116	-131	4-16	88	90	3 -4	384	-368	2 7	164	178	1 15	185	-189			
6 -8	80	-72	5 -1	164	-161	2 17	63	66	3 -6	82	88	2 6	84	-80	1 13	149	-153			
6 -9	128	129	5 -2	134	-128	2 16	84	81	3 -7	209	214	2 5	181	-152	1 12	129	-133			
6-10	75	72	5 -3	384	-373	2 15	122	-121	3 -8	322	298	2 4	114	94	1 11	244	231			
6-11	74	-78	5 -4	184	185	2 12	79	-78	3 -9	63	-67	2 2	63	-67	1 10	179	-176			
6-12	84	-86	5 -5	120	124	2 11	138	-138	3-10	149	-146	2 1	223	238	1 9	86	-91			
6-13	67	69	5 -7	142	-146	2 10	132	122	3-12	60	-65	2 0	100	-97	1 8	273	265			
6-14	90	87	5 -9	68	-61	2 9	740	-833	3-13	89	87	2 -1	87	93	1 7	170	165			
6-15	63	67	5-11	73	68	2 8	86	84	3-15	94	-87	2 -2	186	-188	1 6	136	-117			
6-18	112	121	5-13	132	-132	2 7	448	437	1 16	80	82	2 -3	102	78	1 5	103	102			
6-17	78	-91	5-14	110	104	2 6	84	-80	1 15	181	185	2 -4	140	-137	1 4	187	-172			
6-18	88	-80	5-16	126	128	2 4	88	-78	1 13	213	-212	2 -8	86	-86	1 3	187	-149			
4 14	98	100	5-17	105	114	2 3	141	-183	1 11	134	-133	2 -6	81	76	1 2	235	228			
4 12	69	-76	5-18	80	-80	2 2	112	101	1 10	94	-102	2 -8	196	196	1 1	811	811			
4 9	322	313	3 16	60	-64	2 1	204	214	1 9	186	173	2 -9	260	269	1 0	73	-18			
4 8	174	171	3 14	67	64	2 0	132	120	1 8	213	-209	2-10	161	-147	1 -1	98	-98			
4 7	86	81	3 12	86	-88	2 -1	85	-87	1 7	182	-188	2-11	71	-71	1 -2	173	171			
4 6	142	-148	3 10	94	-81	2 -3	267	262	1 6	236	228	2-13	118	-116	1 -3	816	-838			
4 5	221	-219	3 9	69	82	2 -4	114	-111	1 5	128	136	2-14	163	153	1 -4	198	178			
4 3	84	96	3 8	867	866	2 -6	66	-92	1 3	268	-288	0 10	86	-78	1 -5	78	79			
4 1	80	-80	3 6	136	-146	2 -8	138	-133	1 2	238	-238	0 14	185	181	1 -6	120	-123			
4 0	808	-822	3 4	101	-117	2 -7	380	-378	1 1	100	-100	0 14	138	140	1 -7	284	-286			
4 -2	363	361	3 2	281	297	2 -8	119	118	1 0	117	127	0 12	316	-314	1 -8	148	142			
4 -3	183	-188	3 0	181	-178	2 -9	209	213	1 -1	429	596	0 8	162	-184	1 -9	61	87			
4 -4	408	-389	3 -1	206	-193	2-11	123	118	1 -2	93	-88	0 6	362	-387	1-10	188	178			
4 -6	143	-139	3 -2	184	186	2-12	183	-163	1 -3	168	-133	0 4	238	284	1-11	201	-182			
4 -7	113	117	3 -4	187	-202	2-13	81	-82	1 -4	98	87	0 2	632	-661	1-13	220	-214			
4 -8	173	165	3 -6	476	-487	0 18	183	-180	1 -5	84	-70	0 -2	988	985	1-15	180	148			
4 -9	133	137	3 -8	132	141	0 16	287	277	1 -6	79	86	0 -4	256	-249						
4-10	110	-112	3-10	121	123	0 12	66	68	1 -7	179	168	0 -6	269	259						
4-11	103	-103	3-12	98	-101	0 10	210	-201	1 -8	286	-275	0 -8	291	298	H = 0					
4-12	118	-112	1 17	77	-80	0 8	581	592	1 -9	84	-96	0-10	63	-73	K L	FO	FC			
4-17	49	48	1 15	139	133	0 6	298	-296	1-10	138	123	0-12	283	289	10 0	106	-101			
4-18	86	87	1 13	81	88	0 4	117	130	1-11	113	118	0-14	102	-106	10 -1	144	137			
2 12	92	-90	1 11	189	-189	0 2	97	103	1-12	138	138	0-16	215	-219	10 -6	86	96			
2 10	81	-86	1 8	178	-176	0 0	869	-1036	1-13	167	-160	0-18	81	78	10-11	68	59			
2 9	234	-228	1 6	105	101	0 -2	279	286	1-14	54	-59				8 0	103	99			
2 8	142	136	1 4	66	74	0 -4	186	176	1-16	199	-191	H = 1			8 -1	86	86			
2 7	177	-171	1 1	840	-819	0 -6	446	-434	1-16	73	67	K L	FO	FC	8 -2	109	-104			
2 6	80	76	1 -2	88	-85	0 -8	241	240	1-17	101	101	11 2	112	-122	8 -3	81	-84			
2 5	363	391	1 -3	426	391	0-10	96	-100				11 1	86	-94	8 -4	89	48			
2 4	78	-81	1 -4	94	102	0-12	104	102	H = 2			11 0	121	121	8 -6	128	122			
2 3	67	68	1 -6	77	73	0-14	206	201	K L	FO	FC	11 -4	88	-82	8 -7	169	167			
2 2	103	102	1 -7	119	124	0-16	185	-163	12 2	44	-50	9 12	83	83	8 -8	197	-186			
2 1	172	-158	1 -8	48	-43	0-20	82	60	12 -3	81	-85	9 9	86	-94	8 -9	82	-58			
2 -1	177	188	1 -9	90	79				10 13	67	65	9 8	82	-77	8-11	48	-47			
2 -2	120	130	1-10	188	-167	H = 3			10 3	88	92	9 7	62	70	8-12	87	64			
2 -3	108	112	1-11	127	120	K L	FO	FC	10 2	84	94	9 4	77	77	8 0	509	629			
2 -4	178	183	1-15	90	-82	11 4	57	88	10 1	60	-65	9 1	48	54	8 -1	264	-237			
2 -5	192	187	1-17	98	-98	11 3	97	97	10 -1	130	-128	9 -1	49	-54	8 -2	161	-129			
2 -6	228	-216				11 0	126	-134	10 -2	58	-56	9 -2	88	-86	8 -4	222	-207			
2 -9	369	-389	H = 4			11 -1	70	-68	10 -3	67	73	9 -5	88	79	8 -5	56	64			
2-10	88	83	K L	FO	FC	11 -2	108	109	10 -6	52	-42	9 -7	123	-115	8 -6	130	133			
2-12	86	-71	10 6	62	60	9 10	97	92	10 -7	68	-61	9 -9	88	-86	8 -7	178	-164			
2-13	86	48	10 5	48	36	9 7	132	-126	8 10	131	117	7 13	89	-86	8 -8	77	-73			
2-15	99	-108	10 1	112	128	9 6	94	-98	8 9	109	114	7 11	63	64	8 -9	126	121			
2-16	78	-79	10 0	94	89	9 5	100	99	8 7	98	101	7 10	60	-63	8-10	48	85			
0 16	130	-128	8 12	80	-83	9 3	83	87	8 6	97	-83	7 9	97	95	8-14	127	-136			
0 14	90	-97	8 9	71	-78	9 -1	60	54	8 5	142	-140	7 8	175	178	8-16	106	118			
0 12	101	98	8 8	177	168	9 -4	101	-91	8 4	130	132	7 7	124	-114	8-18	77	84			
0 8	106	-94	8 7	161	147	9 -5	69	78	8 1	82	83	7 6	48	38	4 0	229	-180			
0 6	144	139	8 6	193	-183	9 -9	83	-83	8 -1	88	-90	7 5	84	-62	4 -1	88	85			
0 2	481	473	8 5	128	118	7 14	93	-82	8 -4	61	-67	7 2	129	138	4 -2	224	-200			
0 0	96	60	8 3	99	-110	7 11	113	-109	8 -5	108	-114	7 1	91	84	4 -3	89	91			
0 -2	824	-868	8 2	86	83	7 9	116	119	8 -6	128	124	7 0	114	-118	4 -4	139	-142			
0 -4	749	782	8 1	119	110	7 8	148	-158	8 -8	136	130	7 -1	81	82	4 -6	67	68			
0 -8	198	-177	8 -1	88	84	7 7	87	82	8-10	127	-127	7 -3	193	-173	4 -7	298	-283			
0-12	94	-106	8 -2	181	186	7 6	161	186	8-11	49	-46	7 -6	180	-178	4-11	141	129			
0-14	92	98	8 -4	114	-110	7 5	171	-111	6 16	77	79	7 -7	132	128	4-12	110	106			
0-16	225	219	8 -7	147	-149	7 4	60	48	6 13	49	-80	7-10	82	69	4-14	107	104			
0-18	118	-119	8 -8	177	180	7 0	270	271	6 12	119	-118	7-11	67	-68	4-16	63	-62			
			8-11	62	68	7 -1	188	189	6 8	41	34	7-13	84	-88	2 0	334	-333			
H = 5			8-13	57	-57	7 -3	110	118	6 7	76	-73	8 17	68	-71	2 -1	188	180			
K L	FO	FC	8 16	53	-59	7 -4	71	68	6 4	111	112	8 16	84	73	2 -3	388	-384			
11 2	98	94	8 15	101	102	7 -5	214	-208	6 3	97	-103	8 14	138	143	2 -6	142	-138			
11 1	116	118	8 14	87	84	7 -6	118	113	6 2	236	-227	8 11	86	-87	2 -7	384	364			
11 0	88	-82	8 10	142	-139	7 -8	208	-209	6 1	90	97	8 8	82	88	2 -8	94	-88			
11 -2	87	-86	4 9	76	76	7 -9	116	114	6 -1	141	144	8 7	124	-127	2 -9	293	-289			
11 -4	87	80	8 8	67	-61	7-10	88	83	6 -2	488	462	8 6	84	80	2-10	163	-162			
9 11	49	-58	8 7	138	-132	7-13	60	-61	6 -3	98	-97	8 5	116	107	2-11	210	-211			